SYNTHESIS AND CHARACTERIZATION OF N-ALKYLTHIOUREA AND N, N'-DIALKYLTHIOUREA COMPLEXES OF Cu, Cd AND Pb, AND THEIR USE AS SINGLE SOURCE PRECURSORS FOR THE SYNTHESIS OF METAL SULFIDE NANOPARTICLES.

This is submitted to the Faculty of Science and Agriculture in fulfillment for the award of the degree, Doctor of Philosophy, in the Department of Chemistry

University of Zululand

BY

MAKWENA JUSTICE MOLOTO

The work was promoted by Prof. N. Revaprasadu and co-promoted by Prof. G. A. Kolawole both from the University of Zululand, Department of Chemistry in collaboration with Prof. P. O'Brien from the University of Manchester.

Department of Chemistry
University of Zululand
Private Bag X1001
KwaDlangezwa, 3886

Academic year 2005

ACKNOWLEDGEMENTS

I am grateful to my promoter, Prof. N. Revaprasadu and co-promoter, Prof. G. A. Kolawole for their constant and unwavering support throughout my study. Their invaluable advice, motivation and guidance have helped me through even at times when it seemed impossible. My special gratitude goes to Prof. P. O'Brien, Chair of the Department of Chemistry at the University of Manchester and research leader of the team I was given an opportunity to work and learn from their expertise. His support towards the outcomes of my visits and some of the international conferences has been invaluable.

I am grateful to the following people for their advice and assistance, Mr. P. Kenway for good quality results from TEM, HRTEM, SAED and EDAX, Ms. J. Shackleton for the running and analysis of XRD data (both from Manchester Materials Science Center). Mr. M. Motevalli from Imperial College in London, is also thanked for X-ray structures. I would also like to thank the members of Paul O'Brien's group for making my visits profitable. Special mention goes to Dr. M. A. Malik and Dr. P. Christian for their constant support and advice throughout the UK visits.

This work has been dedicated to my family who have stood by me and endured the strain of being away from them. To my beloved wife, Nosipho and son Tumisho, they have been constant reminder of the hard work I put to make this work successful in order to make up for the time lost for family bonding. My son was born when I was away for the first time to the UK and that made it a very difficult time, though encouraging, spending

fruitful time for our long-term benefits. To my other family, mother, Phillipine, brothers Geoffrey and Stanley, and sisters, Geneva and Jenny, I would like to thank you for moral support, encouragement and patience throughout my studies. It will be so unfair to forget my late grandfather, Joseph and grandmother, Welhelminah, who even though uneducated has been a pillar of strength during my studies.

Thanks are due to all staff support of the Department of Chemistry, the research team and the University of Zululand for making it possible to undertake research project under impossible conditions. All members of our research team have been so inspirational and motivational to me as staff member and senior students to assist in their respective projects.

I would like to acknowledge National Research Foundation (NRF) for their constant financial support, which has made it possible through the Royal Society (RS) in the UK for my visits to the University of Manchester to be fruitful.

TABLE OF CONTENTS

LIST OF TABLES

LIST OF FIGURES

LIST OF ABBREVIATIONS

Chemical reagents

tu	thiourea
mtu	methylthiourea
dmit	1,3-dimethyl-2(3H)-imidazolethione
H_2omt	N-(o-nitropheny)-N'-(methoxycarbonyl)thiourea
tmtu	tetramethylurea
ettu	ethylenethiourea
dmtu	dimethylthiourea
detu	diethylthiourea
etu	ethylthiourea
TOPO	tri-n-octylphosphine oxide
TOP	tri-n-octylphosphine
HDA	hexadecylamine

Instrumentation

IR	infrared
NMR	nuclear magnetic resonance
XRD	X-ray diffraction
TEM	transmission electron microscope
SAED	selected area electron diffraction
TGA	thermo gravimetric analysis
PL	photoluminescence

APPENDIX

OUTCOME OF RESEARCH ACTIVITIES

A. PEER REVIEWED PUBLICATIONS

1. Title: Synthesis and characterization of some N-alkyl/aryl and N, N`- dialkyl/aryl thiourea cadmium(II) complexes: the single crystal X-Ray structures of $[CdCl_3(CS(NH_2)(NHCH_3)_3]_n$ and $CdCl_2(CS(NH_2)NHCH_2CH_3)_2$ M. J. Moloto, M. A. Malik, P. O'Brien, M. Motevalli, G. A. Kolawole, *Polyhedron* Volume 22, Issue 4 , 15 February 2003, Pages 595-603

2. Title: Title: N-alkylthiourea cadmium (II) complexes as novel precursors for the synthesis of CdS nanoparticles. *Journal of Materials Science: Materials in Electronics* 15 (5): 313-316, May 2004, M. J. Moloto, N. Revaprasadu, P. O'Brien, M. A. Malik

3. Title: The synthesis and characterization of Cu_xS_y and PbS nanoparticles from their alkylthiourea lead and copper complexes, *South African Journal of Science*, **In Press**, M. J. Moloto, N. Revaprasadu, G. A. Kolawole, P. O'Brien, M. A. Malik.

4. Title: X-ray structures of dichlorobis(N,N'-dimethylthiourea-S) cadmium, *Acta Crystallographica*, **In Press**, M. J. Moloto, N. Revaprasadu, G. A. Kolawole, P. O'Brien, M. A. Malik and M. Motevalli.

B. CONFERENCE PROCEEDINGS

1. SACI2002 presentation (Poster):

   Title: Synthesis and characterization of some N-alkyl/aryl and N, N`- dialkyl/aryl thiourea cadmium(II) complexes: their potential use as novel molecular precursors for the synthesis of CdS nanoparticles. SACI International convention July 2002 at the University of Port Elizabeth

2. ICCC35 presentation (Poster):

   Title: Coordination of N-alkyl/aryl and N, N`- dialkyl/aryl substituted thiourea derivatives (R`HNCSNHR) (R = R` = CH_3, CH_2CH_3, C_6H_5) on cadmium(II): single-source precursors for CdS nanoparticles. Held in Germany, Heidelberg.

3. IOM^3: meeting in London organized by the Royal Society of Chemistry in the UK. Attended as an observer. Held on 15 - 16 December 2003.

4. SANI (Nano Africa I) held at the University of Stellenbosch with the UNESCO meeting on the 8 April 2004. The presentation earned a trophy for being the best of all presented by students.

   Title of the talk: Di/alkyl/aryl thiourea cadmium(II) complexes: their potential use as novel molecular precursors for the synthesis of CdS nanoparticles.

ABSTRACT

A number of complexes of various thiourea derivatives with different metals have been synthesized and characterized by a combination of spectroscopic studies, elemental analysis, melting points and X-ray crystallography. Infrared and NMR spectroscopy studies reveal the interaction between a metal and the ligands, thioureas, is mainly through bonding to sulfur. A series of cadmium(II) complexes with N-alkyl/aryl and N, N'-dialkyl/aryl thioureas (RNHCSNHR'; where R = R' = CH_3, CH_2CH_3, C_6H_5 and /or R' = H) have been synthesized and characterized. The structures of $[CdCl_3(CS(NH_2)(NHCH_3)_3]_n$ (I) and $CdCl_2(CS(NH_2)NHCH_2CH_3)_2$ (II), $CdCl_2(CS(NH_2)$-$NHC_6H_5)_2$ (III) and $CdCl_2(CS(NH\text{-}CH_3)_2)_2$ (IV) were determined by single crystal X-ray methods. Complex I have a six coordinate polymeric chain with a $CdCl_3S_3$ core, which together with complex III (a monomer) gave a distorted octahedral geometry. Complexes II and IV are monomers with a distorted tetrahedral geometry around the cadmium(II) ion. The ^1H (nuclear magnetic resonance) NMR spectra in deuterated dimethyl sulfoxide (CD_3SOCD_3) at room temperature reveal the broadened NH peaks in the lower field region (6.0 – 10.0 ppm) and the presence of both *syn* and *anti*-isomers for the N-alkylthioureas. All the spectral data obtained is consistent with the coordination of ligands by sulphur atom to the metal ion. Lead complexes were prepared in aqueous media to give white powder in a four coordinate form. Unlike cadmium and lead, copper gave multinuclear complexes resulting from the reduction of copper (II) to copper (I) by the thiourea ligands to form specifically tetranuclear copper complexes with thiourea behaving as the bridging ligands. Thermal behavior of these complexes both in air and under inert atmosphere gave residues after decomposition, which was predominantly metal sulfides, with little impurities. The presence of the metal sulfide was established by the XRD analysis of the residue from the thermo gravimetric analysis.

These alkyl substituted thiourea complexes of Cd, Pb and Cu were easy to prepare, stable in air, inexpensive, obtained in good yields and decompose at temperatures about 200 – 220 °C, which is convenient to thermal decomposition of precursors in the high boiling

solvents or the suitable capping agents to prepare surface capped metal sulfide nanoparticles. Some of the complexes have been used as single-source molecular precursors in the preparation of copper sulfide, cadmium sulfide and lead sulfide nanoparticles by a process driven by thermal decomposition. Good crystalline particles were obtained from thermolysis of the precursors in tri-n-octylphosphine oxide (TOPO) as a solvent and capping agent, at different temperatures. All nanoparticles, CdS, PbS and Cu_xS_y, were prepared from alkylthiourea complexes, cleanly decomposing to give average size ranges 4 – 26 nm at reasonably lower temperatures. The small size of these particles is a consistent property with the observed blue shift in the band edge of their optical spectra. Photoluminescence spectra of most samples were broadened with a red shift in relation to the band edge indicating the broad size distribution. Some relative quantity of bulk particles of copper sulfide and lead sulfide were obtained from the large yield of the products as insoluble particles in hexadecylamine (HDA) and tri-n-octylphosphine oxide (TOPO). X-ray powder diffraction (powder XRD) patterns are consistent with predominantly hexagonal phase although copper sulfide showed evidence of various stoichiometric ratios. These phases were also confirmed by the images from the transmission electron microscope (TEM), although the CdS nanoparticles showed instability due to quick agglomeration in TOPO. Their patterns were confirmed by the XRD to be predominantly hexagonal. The morphology for most of the particles were close to those of thin needle-like plates, although the collapse is more of spheres which is a preferred mode of arrangement of the CdS particles when they settle on the carbon coated copper grids. High resolution transmission electron microscope (HRTEM) revealed the lattice fringes of all different types of nanoparticles including CdS, which tend to give agglomerates, hence it was difficult to determine particle sizes from the TEM images. All solution studies *viz.* ultraviolet-visible spectroscopy, photoluminescence and copper-coated grid-TEM were all consistent with particles in the nano-size regime. The copper and lead complexes of these thiourea derivatives have been used to prepare PbS and Cu_xS_y, and gave crystalline, cubic or rod-shaped nanoparticles. CdS, PbS and Cu_xS_y nanoparticles showed quantum confinement effects with a blue shift in their absorption spectra. The materials were further characterized by HRTEM images, XRD and selected area electron diffraction (SAED) patterns.

CHAPTER 1

SYNTHESIS AND CHARACTERIZATION OF METAL COMPLEXES

1.1. INTRODUCTION

1.1.1. General background

Coordination of metal ions to ligands with sulfur as the donor atom has been extensively studied following their analogues with oxygen or nitrogen as donor atoms. Among the ligands with sulfur as the donor atom, thiourea has been investigated in fair detail. Thiourea, $(H_2N)_2CS$ (tu), acts as unidentate ligand forming strong complexes with group IB and IIB metal ions, in particular Cu(I), Ag(I), Au(I) and Hg(II). It reduces Cu(II) to Cu(I), Au(III) to Au(I), Pt(IV) to Pt(II) and Te(IV) to Te(II) and forms complexes with the metals in their lower oxidation state.[1] The only metal reported to be N-bonded with thiourea is Ti(IV), all others are S-bonded. The metal sulfide bond stretching frequency υ(M—S) occurs at 300 - 200 cm^{-1}.[2] Infrared absorption measurements have indicated that urea[3] forms nitrogen-to-metal bonds with Pt(II) chlorides and oxygen-to-metal bonds with Cr(III), Fe(III), Zn(II), and Cu(II) chlorides, whereas in thiourea complexes[4] all the metals are sulfur-bonded. Sulfur-to-metal bonds have also been revealed by the X-ray diffraction measurements of Nardelli and co-workers on solid complexes of metal halides with thiourea,[5] ethylenethiourea[6] and tetramethylthiourea.[7] A series of compounds with amide groups have been studied by nuclear magnetic resonance spectroscopy and this includes some thiourea derivatives.

1.1. INTRODUCTION

1.1.1. General background

Coordination of metal ions to ligands with sulfur as the donor atom has been extensively studied following their analogues with oxygen or nitrogen as donor atoms. Among the ligands with sulfur as the donor atom, thiourea has been investigated in fair detail. Thiourea, $(H_2N)_2CS$ (tu), acts as unidentate ligand forming strong complexes with group IB and IIB metal ions, in particular Cu(I), Ag(I), Au(I) and Hg(II). It reduces Cu(II) to Cu(I), Au(III) to Au(I), Pt(IV) to Pt(II) and Te(IV) to Te(II) and forms complexes with the metals in their lower oxidation state.[1] The only metal reported to be N-bonded with thiourea is Ti(IV), all others are S-bonded. The metal sulfide bond stretching frequency υ(M—S) occurs at 300 - 200 cm^{-1}.[2] Infrared absorption measurements have indicated that urea[3] forms nitrogen-to-metal bonds with Pt(II) chlorides and oxygen-to-metal bonds with Cr(III), Fe(III), Zn(II), and Cu(II) chlorides, whereas in thiourea complexes[4] all the metals are sulfur-bonded. Sulfur-to-metal bonds have also been revealed by the X-ray diffraction measurements of Nardelli and co-workers on solid complexes of metal halides with thiourea,[5] ethylenethiourea[6] and tetramethylthiourea.[7] A series of compounds with amide groups have been studied by nuclear magnetic resonance spectroscopy and this includes some thiourea derivatives.

1.1.2. Infrared spectra

The infrared spectra of metal complexes of thiourea were investigated by Yamaguchi and co-workers,[8] who found that coordination takes place through sulfur as well. Flint and Goodgame[9] made a study of metal ligand stretching frequencies by infrared spectroscopy in the region 400-135 cm^{-1} of some thiourea complexes. The metal-sulfur stretching frequency of the complexes reported, $[M(tu)_4Cl_2]$ (tu = thioureas, M = Mn, Ni, Pd), $[M(tu)_2X_2]$ (X = Cl, Br, I; M = Cd, Co, Zn) and $[Ni(tu)_6X_2]$ = Br, NO_3) were observed mainly in the range 300-200 cm^{-1}. Thiourea, like other S-bonded ligands, has a high *trans* effect,[10, 11] which is the basis of the Kurnakov test for distinguishing *cis* and *trans* isomers of dihalogenodiammineplatinum(II).[12]

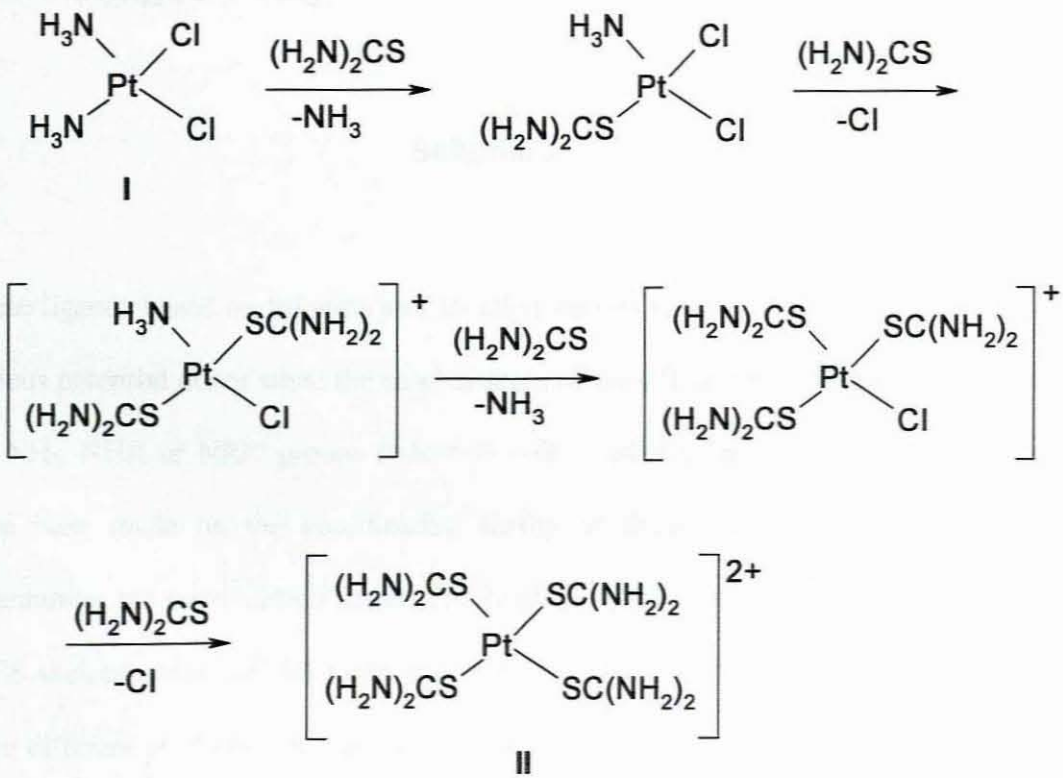

I

II

Scheme 1

The reaction of thiourea with the *cis*-$[PtCl_2(NH_3)_2]$ **(I)** yields $[Pt(tu)_4]^{2+}$ **(II)** (Scheme 1), while with *trans*-$[Pt(NH_3)_2Cl_2]$ **(III)**, thiourea reacts to give $[Pt(NH_3)_2(tu)_2]^{2+}$ **(IV,** Scheme 2).The above and below shown schemes (Scheme 1 and 2) are based on the *trans* effect of the ligands decreasing in the order: tu > Cl > NH_3.

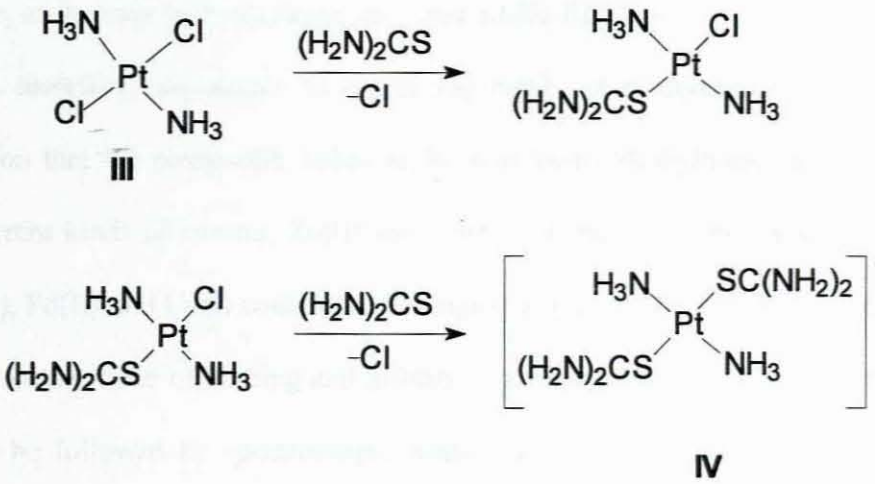

Scheme 2

These ligands based on thiourea and its alkyl derivatives are of interest as they possess various potential donor sites: the sulphur atom of the CS group and the nitrogen atom of the NH_2, NHR or NRR' groups (where R = R' = alkyl or aryl groups). Several studies have been made on the coordinating ability of these ligands mainly with aim of determining the coordination mode. The N-alkyl substituted thiourea, with the coplanar N_2CS skeletal atoms can take two possible conformational forms, *syn* and *anti* whereas three different conformations are possible for N,N'-dialkyl substituted thioureas the *syn-syn*, *anti-anti* and *syn-anti* isomers (Figure 1). NMR studies have been in efforts to determine the extent of the rotation about the S=CN bond in thioureas.[13 - 16]

The normal vibration calculations and assignment of the bands observed in the infrared spectra of thiourea have been previously reported.[17] When an alkyl group as in methyl- or ethylthiourea replaces one of the hydrogen atoms on thiourea, two structures (*syn* and *anti* forms) are conceivable. The spectra of these structural forms can be explained by comparison with both a *syn*-thioamide and thiourea or a *anti*-thioamide and thiourea. However, in the case of methylurea only *anti* amide frequencies appeared in the spectra. It seems therefore, reasonable to assign the bands of methylthiourea spectra on the assumption that the compound exists in the *anti* form. Methylthiourea complexes give two different kinds of spectra, Zn(II) and Cd(II) complexes belonging to the first group and Pt(II), Pd(II) and Cu(I) complexes belonging to the second group. This classification is based on the mode of binding and affinity of metals to either sulfur or nitrogen atom. This can be followed by spectroscopic studies of thiourea metal complexes similar to urea complexes.

The fact that the molecules of the first group coordinate through sulfur and those of the second group coordinate through nitrogen might have been expected from previous studies of metal-urea complexes[3] whose spectra showed that urea form nitrogen-to-metal bonds with Pt(II) and Pd(II) whereas oxygen-to-metal bonds are formed with Cr(III), Fe(II), Zn(II) and Cu(II). The bands due to the N–H stretching frequencies are observed in the region higher than 3000 cm^{-1}. In Zn(II) and Cd(II) complexes the frequencies are almost the same as those of the free ligand. However, there is considerable decrease of the frequencies of N–H upon thiourea ligand coordination in Pt(II) and Pd(II) complexes.

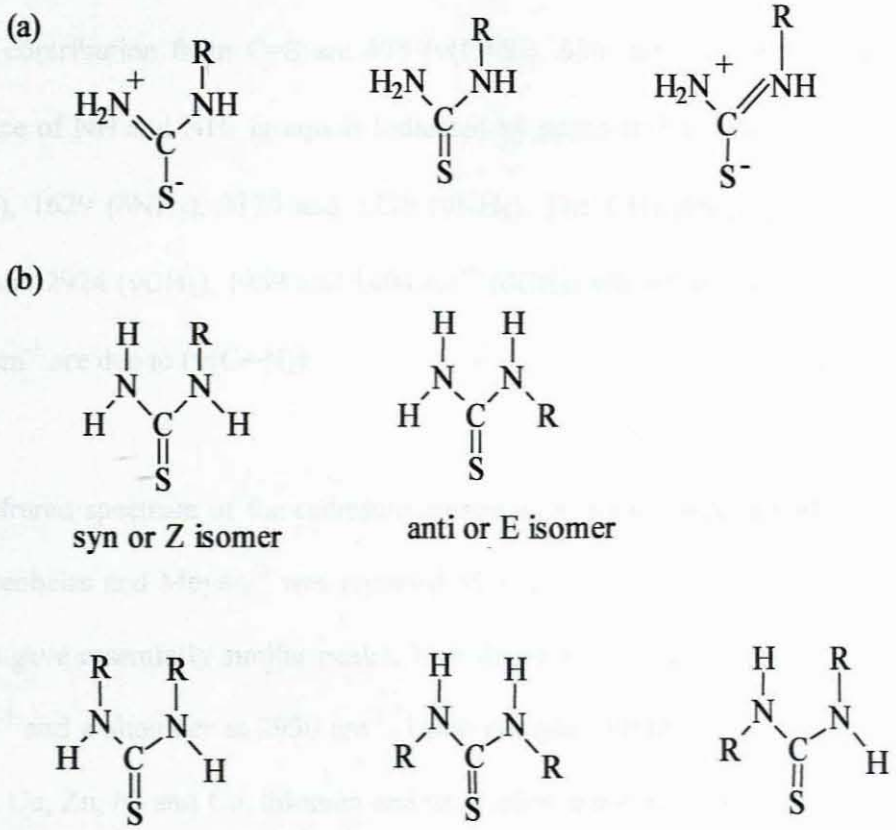

Figure 1: (a) Resonance structure of substituted thiourea showing delocalization of the π-bond and (b) conformational isomers for both mono and di-substituted alkyl/aryl thioureas.

N-methylthiourea (mtu) is the simplest of the N-alkyl substituted derivatives of thiourea, with the coplanar N_2CS skeletal atoms, which can take two possible conformational forms, (Figure 1(b)). A number of studies on the structural conformation of methylthiourea have been done, both in solid and solution.[18 - 29, 30, 31] It was confirmed by Mido *et al.*[32] through Raman and IR spectral, and X-ray structural analyses of methylthiourea that the compound assumes the *syn* configuration in its solid state but not

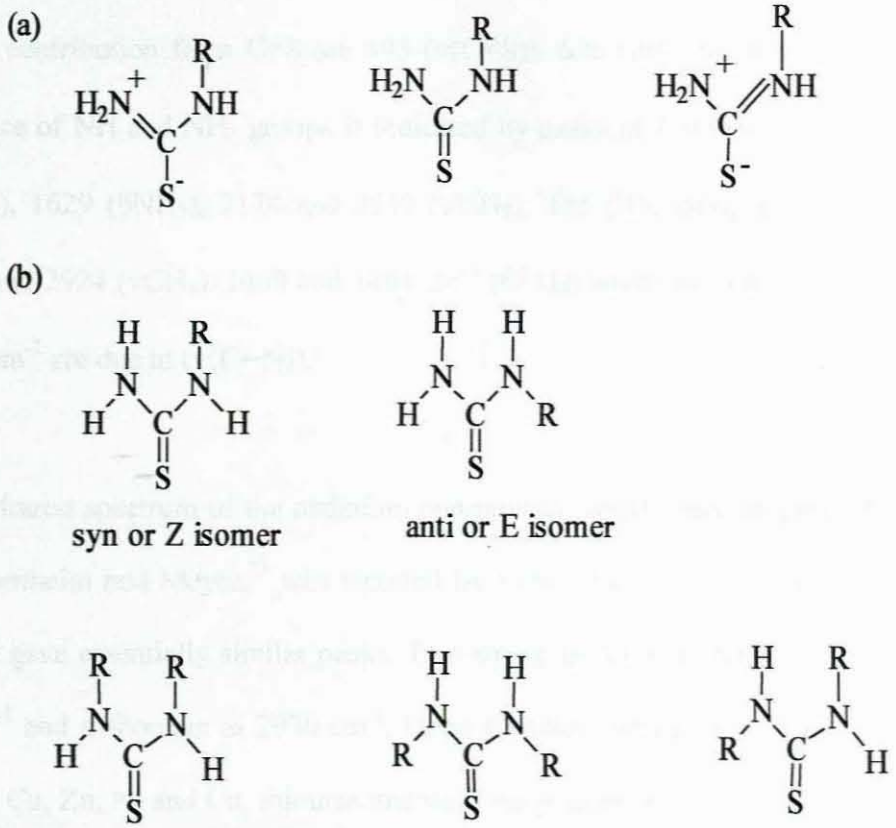

Figure 1: (a) Resonance structure of substituted thiourea showing delocalization of the π-bond and (b) conformational isomers for both mono and di-substituted alkyl/aryl thioureas.

N-methylthiourea (mtu) is the simplest of the N-alkyl substituted derivatives of thiourea, with the coplanar N_2CS skeletal atoms, which can take two possible conformational forms, (Figure 1(b)). A number of studies on the structural conformation of methylthiourea have been done, both in solid and solution.[18 - 29, 30, 31] It was confirmed by Mido *et al.*[32] through Raman and IR spectral, and X-ray structural analyses of methylthiourea that the compound assumes the *syn* configuration in its solid state but not

the *anti* as has been thought for a long time. The three main IR active spectral peaks due to the contribution from C=S are 495 (ν(C=S)), 636 (π(C=S)) and 776 (ν(C=S)). The presence of NH and NH_2 groups is indicated by peaks at 720 (τNH_2), 560 (πNH_2), 1298 (δNH_2), 1629 (δNH_2), 3170 and 3250 (νNH_2). The CH_3 group gives intense peaks at 2854 and 2924 (νCH_3), 1459 and 1404 cm^{-1} (δCH_3) while the intense peaks at 1557 and 1149 cm^{-1} are due to (ν(C–N)).

The infrared spectrum of the cadmium compounds, which were prepared by the method of Rosenheim and Meyer,[33] was reported by Lane, *et al.*[18] The spectra reported by both groups gave essentially similar peaks. Two strong peaks were reported at 3250 (s), 3100 (s) cm^{-1} and a shoulder at 2930 cm^{-1}. Upon complex formation with metals such as Cd, Pt, Pd, Cu, Zn, Ni and Co, thiourea and its N-alkyl substituted derivatives have a number of observable features. In most complexes they bind through the sulphur atom although there are examples of complexes with N-bonded alkylthiourea derivatives. The cadmium (0), cadmium (II) and copper (I) complexes show marked similarity in their structures in that they form clusters,[34] dinuclear[35, 36] or polynuclear complexes.[37, 38] The rest of the other complexes are monomeric.[39 - 41] There is a substantial down shift in the vibrational frequencies of C=S bond when coordinated to a metal, suggesting considerable interactions between the thiourea molecules and the metals.[42] The bands assignable to the N–H stretching vibrations are sharper in the spectra of metal complexes than in the thioureas due to the absence of hydrogen bonding. The NH_2 bending vibrations almost remain at the same frequencies. There is considerable change in the infrared spectra which conforms to the changes in nature of C–N and C=S bonds. The CN bond of the

nitrogen atom non-bonded to the alkyl group in the ligand changes into a double bond while the C=S bond looses its double bond character as per structure in Figure 2.

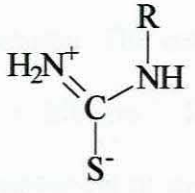

Figure 2: Delocalization of electrons in the NCS unit in the alkyl substituted thiourea.

The strong band observed at 1634 cm^{-1} in the methylthiourea spectrum that corresponds to the bands at 1610 and 1625 cm^{-1} for thiourea are assigned to the NH_2 bending frequencies. This band remains constant in frequency on coordination. The strong band at 1550 cm^{-1} of methylthiourea can be explained as the amide band or N–H deformation plus C–N antisymmetric stretching frequency.[43] On coordination the frequency of the band at 1550 cm^{-1} is increased by 25 - 28 cm^{-1} in the first group and only about 10 cm^{-1} for the second group. The C–N antisymmetric stretching frequency will probably be raised by the increment of the double bond nature of the C–N bond on coordination in the first group.

The most important change of the spectrum on coordination is observed in the complexes of the second group for the band at 1490 cm^{-1} of the ligand, which arises from a vibration consisting of NH_2 rocking, C–N symmetric stretching and C–N stretching motions. The intensity of the band becomes much stronger and the frequency is decreased by 10 - 16

cm^{-1}. In contrast to this there is no appreciable change of frequency and intensity in the first group as in the case of the thiourea complexes. The band at 972 cm^{-1} for methylthiourea can be considered to correspond to the band at 1083 cm^{-1} in the spectra of thiourea, which has been assigned to vibrations consisting of symmetric C–N stretching, NH_2 rocking and C=S stretching vibration. The corresponding bands of the complexes have been found in the region 965 - 990 cm^{-1}. These are considerably decreased in intensity due to the fact that the contribution of the C=S stretching motion in the first group of complexes becomes very small on complexing and consequently, the C–N symmetric stretching becomes the main contributor to the 972 cm^{-1} band. The band at 774 cm^{-1} of methylthiourea is considered to correspond to the band at 731 cm^{-1} of thiourea, which arises from the motion consisting of C=S stretching and symmetric C–N stretching. This frequency corresponds to those of the bands observed in the spectra of the complexes in this region. There is no doubt that the coordination of the first group takes place through sulfur. However, for the second group of complexes the spectral evidence for the coordination through nitrogen is not so conclusive as in the case of urea complexes. This is due to the fact that the C=O stretching frequency in urea or methylthiourea lies well above the C–N stretching frequency, whereas the C=S frequency is not much different from the C–N stretching frequency.

Several new complexes of lead(II) halides and pseudohalides have appeared in the literature in the past ten to fifteen years of which prior to these very little work had been done with regard to synthesis and structural characterization. Williams, *et al.*[44] reported the synthesis and characterization of lead (II) halide complexes with sterically hindered

thioureas, 1,3-dimethyl-2(3H)-imidazolethione (dmit). Wharf, *et al.*[45] reported several new lead(II) halide complexes with O-, N- and S-donor ligands and prior to this, Nardelli and Fava,[46] reported the crystal structure of $[PbCl_2(tu)_2]$. Wharf, *et al.*[45] reported the vibrational spectra of $[PbCl_2(tu)_2]$ and noted the split in the C=S stretch as well as in the NCN asymmetric stretch of thiourea, which are due to the presence of both bridging and terminal thioureas in the solid state structure. They also noted the high melting points due to the polymeric nature of the complex. Herbstein and Reisner[47] substantiated the structure of $[PbBr_2(tu)_2]$ which consisted of six to seven coordinated polyhedra linked by bridging thiourea and halide atoms, and the vibrational spectral data reported by Wharf, *et al.*[45] again showing split in the C=S and NCN vibrational modes.

For dmit complexes of Pb(II), the peak at 1570 cm^{-1} was assigned to the NCN asymmetric stretch while the peak at 1170 cm^{-1} was the C=S stretch. The dmit complexes showed a single peak as opposed to split peaks at frequencies very near the above modes (1565 and 1170 cm^{-1} for the thiocyanato complex and 1570 and 1180 cm^{-1} for the chloro complex) thus suggesting terminal bonding only. However, it was also observed that these modes do not shift greatly upon complexation. Complexes with other metal ions show similar results,[48] and can be explained in part on the basis of little structural difference in the aromatic ring structure of this ligand in the non-complexed versus the complexed states.[49] Thus the IR data is not totally conclusive with regard to the mode of polymerization. But one would expect either splitting or at least line broadening of the observed modes if both bridging and terminal ligands were present, and these modes tended to give relatively sharp peaks in the IR spectra. Another structural conclusions that

may be derived from the solid state IR spectra is the fact that the thiocyanato ligand is N-bonded to the metal, and polymerization is accomplished through a bridging Pb–S bond. The CN stretching frequency of thiocyanate is a diagnostic feature for the bonding mode of where the frequencies near to or below 2050 cm^{-1} are observed for N-bonded species.[50]

For $[Pb(NCS)_2(dmit)_2]$, the peak at 2050 cm^{1} was observed and thus confirming the mode of bonding as described above. The 1:1 complexes of thiourea with lead acetate has been reported to have three sulfur-to-lead bonds[51] and the 2:1 complex of thiourea with lead(II) chloride contains four sulfur-to-lead bonds.[46] The absorption maxima of chief interest in the spectra of tetramethylthiourea and its complexes are those associated with the N–C–N and C=S stretching vibrations. These are expected to shift to high and low frequencies, respectively, on the formation of sulfur to metal bonds. The frequency calculated by Yamaguchi, *et al.*[8] for the N–C–N antisymmetric stretching vibration in thiourea is 1451 cm^{-1} and the observed band ascribed to this vibration is at 1500 cm^{-1}. The absorption at 1504 cm^{-1} in the spectrum of tetramethylthiourea is considered to be associated with this vibration. The absorption maximum at 1100 cm^{-1} in the spectrum of tetramethylthiourea complexes is assigned to the C=S stretching frequency. No significant differences were observed from a series of metal complexes of tetramethylthiourea[52] with the exception of the high frequency (1600 cm^{-1}) of N–C–N stretching vibration for $[PtCl_2(tmtu)_2]$ (tmtu = tetramethylthiourea). This compares with an average of around 1660 cm^{-1} for the C=N stretching frequency in the Schiff bases and is indicative of a large double bond character for one or both nitrogen bonded to C=S bond in the complex.

Lane, *et al.*[18] studied the infrared spectra of several thiourea derivatives in the solid state. They found that N,N'-dimethylthiourea and N,N'-diethylthiourea were *anti–anti* isomers. Subsequent studies on the coordination of these molecules were made using infrared spectra to determine their binding sites.[18, 53, 54] In most complexes they bind through the sulphur atom, although there are examples of complexes with N-bonded alkylthiourea derivatives.[55] The cadmium(II) and copper(I) complexes show marked similarity in their structures in that they form clusters,[56] dinuclear[35, 36] or polynuclear complexes[37, 38] whereas other complexes are monomeric.[39 - 41] There is a substantial downshift in the vibrational frequencies of C=S bond when coordinated to a metal, suggesting considerable interactions between the thiourea molecules and the metals.[53] One of the thiourea substituted ligand, N-(o-nitropheny)-N'-(methoxycarbonyl)thiourea (H_2omt) was found to co-ordinate in cadmium in the complex through both sulfur and nitrogen atoms in a bidentate form and to zinc complex only through the nitrogen atoms.[39] The infrared spectra of both complexes show bands at about 3140 cm^{-1} usually attributed to the NH stretching frequency. The intense band arising from the amide stretching vibration at 1732 cm^{-1} for H_2omt is red-shifted when ligation occurs in the Cd(II) (1648 cm^{-1}) and Zn(II) (1661cm^{-1}) complexes. The C=S band at 867 cm^{-1} for the free ligand has shifted to 855 cm^{-1} in the cadmium complex indicating a binding through the sulfur atom to Cd(II) ion, which is also indicated by the presence of a band at 310 cm^{-1} assignable to the Cd—S bond. The band at 868 cm^{-1} remains unchanged in the zinc complex indicating non co-ordination of the thiolato sulfur atom. It was also suggested by Baranyi, *et al.*[57] that bis-thiourea complexes of zinc(II) and cadmium(II) were N-bonded to the metals with similar CN stretching frequencies. The synthesis of tetramethylurea complexes of $ZnCl_2$, ZnI_2,

$CoBr_2$ and $PbBr_2$ and tetramethylthiourea complexes of $ZnCl_2$, ZnI_2, $CoBr_2$, $CdBr_2$, CdI_2, $PdCl_2$, $PtCl_2$ and $PbBr_2$ have been reported.[52] All the complexes formed in a 2:1 ratio of ligand to metal halide except those of $PbBr_2$ and $PtCl_2$ which were 1:1. The large shifts to high frequencies of the absorption maxima associated with the NCN anti-symmetric stretching vibration in the spectra of all the complexes, and the low frequencies of the C=O stretching vibration in the tetramethylurea complexes, indicate appreciable $^{+}N{=}C{-}S^{-}$ and $^{+}N{=}C{-}O^{-}$ bond character.

The complex, $[Pt(tmtu)Cl_2]$, is expected to give either a dimer of type **A** or **B** (Figure 3). Nardelli and co-workers[58] have reported X-ray diffraction data supporting sulfur bridges of type B in octahedral complexes of thiourea with cadmium and nickel isothiocyanates. The complex of thiourea with lead acetate was reported to contain three sulfur to lead bonds[59] and the lead(II) chloride contained four sulfur to lead(II) bonds.[46] The absorption maxima of the N–C–N and C=S stretching vibrations for the tetramethylthiourea complexes are expected to shift to high and low frequencies, respectively on the formation of sulfur to metal bonds.

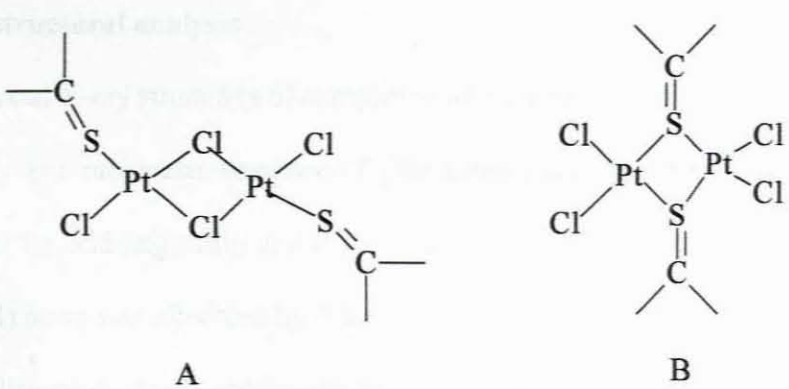

Figure 3: Mode of binding of thiourea ligands to platinum

A number of ethylthiourea complexes of palladium(II) and platinum(II) of the formulae, $[M_2(Etu)_2X_4]$ (where M = Pd, Pt, X = Cl, Br, I, Etu = ethylthiourea) and $[M(Etu)_4A_2]$ (where A = Cl, Br, I, ClO_4, BF_4, CF_3CO_2) have been reported with the halides bridging the two metals in the complexes, $[M_2(Etu)_2X_4]$ and the ethylthiourea ligand coordinated through the sulfur atom. The far infrared spectra showed ν(MS) at 270 – 300 cm^{-1} and for the $[M_2(Etu)_2X_4]$ complexes ν(MX) bands corresponding to the terminal and bridging MX bonds.[59] N,N'-dimethylthiourea complexes of different metals such as Cu(I), Pd(II), Cd(II) and Zn(II) have been classified according to their types of coordination.[22] The first group, which included Cu(I) and Pd(II), showed a smaller increase (10–15 cm^{-1}) of the 1506 cm^{-1} band (band due to the contribution of δ(NH), ν(CS) and ν(NCN)) compared to the second group (Cd(II) and Zn(II)) with an increase in the range 25 – 37 cm^{-1}. The band at ~ 760 cm^{-1} (ν(CS), ν(CN), ν(CN')) is shifted to higher frequencies in the first group and to lower frequencies in the second group. These results showed that the metal complexes of N,N′- dimethylthiourea fall into two group as is the case for methylthiourea complexes reported.[18]

1.1.3. X-ray structural analysis

The single crystal X-ray structures of complexes of thiourea and its alkyl derivatives have been reported. The molecular structure of $[PbCl_2(tu)_2]$ consists of polymeric polyhedra linked together by bridging sulfur and chloride atoms and a coordination number of seven around lead(II) atom was observed by Wharf, *et al.*[45] The monomeric unit of $[Pd(tu)_2Cl_2]$ shows slight distortion from a square-planar to a tetrahedral arrangement with mean Pd–S bond lengths of 2.33 Å.[60] The complex, $[Ni(tu)_4Cl_2]$ is *trans* octahedral with the four M–

S bonds at 2.54 Å, while $[Ni(tu)_2(NCS)_2]$ is octahedral and polymeric: each Ni atom is bound to four thiourea S atoms at 2.54 Å and to two thiocyanate N atoms at 1.99 Å, the S–C bond distance (1.77 Å) is much longer than in thiourea itself (1.64 Å). The compounds $[M(tu)_2(NCS)_2]$ (M = Mn, Co, Cd) are isostructural with $[Ni(tu)_2(NCS)_2]$ but $[Zn(tu)_2(NCS)_2]$ is not. The complex $[Cd(tu)_2Cl_2]$ is tetrahedral, $[Pb(tu)_2Cl_2]$ is polymeric with Pb ion seven coordinate and surrounded by bridging S atoms at 2.9 – 3.1 Å and two bridging Cl atoms at 3.2 Å while the terminal Cl atom is at a distance of 2.75 Å. In $[Te(tu)_4Cl_2]$ each Te atom has a square-planar arrangement of four S atoms.[1] Complexes of the form $[Ln_4(tu)_5Br_{12}].20H_2O$ are also known for all the lanthanides.[61] In $[Ln(tu)_2(ClO_4)_3].10H_2O$, the thiourea ligand is S-bonded.[62]

The addition of thiourea to Cu^{2+} results in its reduction to Cu^{+} leading to copper(I) complexes. Thirteen different structures thiourea-copper(I) complexes of the type $Cu_x(tu)_y$ are reported with the atomic co-ordinates in the Cambridge Structural Database (CSD).[63] All of them contain Cu^{+} single charged cation. They belong to five different classes depending on the Cu–S arrangements viz. monomeric, dimeric, polymeric or ring structures. The copper complex, $Cu(tu)_2Cl$[64] has a polymeric structure with the backbone Cu–S–Cu–S–, whereas in the monomeric complex $[Cu(tu)_4]_2[SiF_6]$[65] the tetrahedral arrangement of Cu^{+} is completed by the four thiourea S atoms. The reaction between copper (I) halides and thiourea (tu) or substituted thioureas frequently generate a variety of complexes, which have unpredictable stoichiometry and stereochemistry. The substituted thiourea ligands generally coordinate to the Cu(I) atom through the S atom as terminal ligands or bridging ligands or both. Terminal coordination is reported in the

complexes $[Cu(dmtu)_3Cl]$ (dmtu = N,N'- dimethylthiourea)[66] and $[Cu(detu)_3Cl]$ (detu = N,N'- diethylthiourea),[67] whereas in the complexes $[Cu(tu)_2Cl]$,[68] $[Cu(tu)_3Cl]$,[69] and $[Cu_2(ettu)_4Cl_2]$, (ettu = ethylenethiourea)[70, 71] the ligands show both terminal and bridging coordination.

A major impetus for research into copper(I) thiourea complexes has been primarily structural and/or has risen from investigations into the chemistry of a soft donor ligand with a soft metal acceptor (copper(I)) or a hard metal acceptor copper(II)). Thiourea[71 - 74] and a series of copper(I) thiourea complexes with various counter anions have been crystallographically characterized.[71 - 75] The complex, $[Cu_2(tu)_5](SO_4).3H_2O$ displays an alternating chain of trigonal planar and tetrahedral copper(I) centers linked through bridging thiourea molecules. The coordination about each copper (I) center is completed by the remaining monodentate thiourea ligands. The compound $[Cu_2(tu)_6](SO_4).H_2O$ contains the binuclear $[Cu_2(tu)_6]^{2+}$ complex in which two tetrahedrally coordinated copper(I) atoms are linked by two bridging thiourea molecules. The other four thiourea molecules are terminally bound, two on each copper atom. $[Cu_4(tu)_6](SO_4)_2.2H_2O$ contains tetranuclear $[Cu_4(tu)_6]^{4+}$ cations in which four trigonally coordinated copper(I) atoms are linked together by the six thiourea molecules, each of which connects a pair of copper atoms.[75] $[Cu_8(tu)_{15}](SO_4)_4.xH_2O$ contains the adamantine-like $[Cu_4(tu)_6]^{4+}$ cations that are linked together by additional doubly bridging thiourea molecules which bind to three of the four copper atoms in each cluster.[76] For the complexes $[Cu_2(tu)_5](SO_4).3H_2O$ and $[Cu_2(tu)_6](SO_4).H_2O$ the CS bands occur at about 710 cm^{-1} slightly lower than for the uncomplexed ligand and with evidence of splitting of this band in the Raman spectra,

probably as a consequence of the different coordination environments of the ligands i.e. bridging or terminal. Splitting of this kind is also observed in the δ(NCN) and δ(SCN) bands, which occur in the 400 – 500 cm^{-1} region. The Cu-S linkages were observed below 300 cm^{-1} which are helpful to establish the vibrational spectra and the structure of the complexes. These X-ray structural analysis of complexes as well as spectroscopic analysis helps to confirm the structures and formulation of compounds.

The ethylenethiourea complex, $[Cu(ettu)_3]_2(SO_4)$ contains two crystallographic inequivalent $[Cu(ettu)_3]^+$ units with trigonal planar CuS_3 coordination at copper. The Cu—S distance in one unit ion (2.269 Å) is appreciably longer than in the other (2.246 Å). Two ν(CuS) bands were observed in the far-infrared at 227 cm^{-1} and 214 cm^{-1}, and these were assigned to the $[Cu(etu)_3]^+$ ions with the shorter and longer Cu—S bond lengths respectively. The complex, $[Cu(etu)_4](NO_3)$[77] contains $[Cu(etu)_4]^+$ ions with tetrahedral CuS_4 coordination with a mean Cu—S distance of 2.344 Å and gives a ν(CuS) band at 184 cm^{-1}. Substituted thioureas are of particular interest due to their steric effect.

1.1.4. NMR spectral analysis

Amides of thiourea compounds have been studied by nuclear magnetic resonance (NMR) spectroscopy more extensively than any other class of organic compounds.[78] Structural features such as relative orientations of the groups within the amides have been revealed. Despite extensive reports on NMR analysis of organic amides, very little has been reported about their corresponding metal complexes. NMR spectroscopy was found useful in determining conformations and isomers in solution. If an amide in solution

occurs as a mixture of *syn* and *anti* isomers, separate signals will be observed if rotation around the C-N bond is slow. Therefore, the *syn/anti* isomer ratio can be determined from NMR analysis. Thioamides are similar to the amides hence they give similar spectral trends. Tompa *et al.* [79] performed a study of the barrier to rotation about the carbon-nitrogen bond in N-methylthiourea in different solvents by the NMR technique. The ratio of *syn* to *anti* isomers were found to depend on temperature as well as the solvent, in which the activation energy of the methyl doublets was found to increase with slightly as the polarity of the solvent, was increased. NMR spectral analysis of thiourea derivatives of platinum complexes was reported by Rochon *et al.*[80] in which the ligand was confirmed to bind to the metal through sulfur atoms. The methyl proton of N-methylthiourea as well as one methyl group protons of N,N′-dimethylthiourea showed resonance at higher field after coordination to the metal. The signals due to NH protons and those of alkyl groups can be clearly distinguished even after the formation of complex.

1.1.5. Applications

Thiourea has a wide variety of applications ranging from thin films deposition used in photovoltaic solar cells, in agriculture as a weedkiller, in the combat of malaria by killing the mosquito larvae in water as it is harmless to aquatic life like fish, plastic manufacturing and to many others. Several thiourea derivatives have been found to have strong anti-thyroid activity. This has been interpreted as due to the formation of disulfide by the reaction of iodine and –SH group (formed by enolization).[81]

Thiourea complexes are starting materials in chemical spray pyrolysis (CSP) processes which are used to produce thin films of binary and ternary sulfides.[82, 83] Metal sulfides have photovoltaic, solar cell semiconductor applications and they are also used to produce thin films gas sensors[84, 85] and conductive electrodes.[86] Thiourea has also been used in the deposition of CdS thin films from aqueous solutions.[87] The chemistry of substituted thiourea derivatives has attracted attention because of their potential use as reagents for the separation of metal ions[88] and in biological applications such as their use: as antibacterial[89, 90] antiviral[91] or antifungal agents.[92] A series of thiourea derivatives containing the ferrocenyl moiety were prepared by treating the products of the reaction of ferrocenyl-carbonyl chloride and potassium thiocyanate with various amines in a search for potentially biologically active materials.[93] The derivative N-(o-nitropheny)-N-(ethoxycarbonyl)thiourea, which was reported to be isolated from the leaves of the resistant *pyricuiria oryzae cav. rice* variety[94] and the preliminary pharmacological tests showed its high antibacterial activity. Whilst the derivative N-(o-nitrophenyl)-N′-(methoxycarbonyl)thiourea was inactive against a number of selected bacteria and fungus such as *B. subtilis* 6633, *S. lutea* 209p , *P diploccus* and *aeruginosa* x313 but slightly active against *E. coli* and *S. yake sake*. The Cd(II) and Zn(II) complexes of this ligand exhibited inhibition activities against a number of bacteria and fungi indicating the enhancement of biological activity on complexation of thiourea.[95]

The biological activity of the complexes with thiourea derivatives has been well documented and thiourea derivatives have been successfully screened for various biological actions[96 - 99] and some N-substituted N′-alkoxycarbonyl thioureas have been

used in commercial fungicides. Metal ions are thought to enhance the biological activity of a wide variety of organic compounds. For example, the Cu(II) complex of 2-acetyloxybenzoic acid (aspirin), a ligand used as an analgesic since the 19th century was reported to be significantly more active as an anti-inflammatory agent than the free ligand.[100, 101] The study of compounds N-benzoyl-N′-alkylthioureas and N-benzoyl-N′,N′-dialkylthioureas has also attracted interest in the view of the potential use of these compounds as highly selective reagents for the concentration and separation of metal cations.[102] One specific use for the substances is the coordination of harmful compounds, which can be achieved in the organism by one or more ligands of appropriate structure. More attention has been devoted to the design and synthesis of new agents able to coordinate these toxic metal ions with a view to obtaining complexes that can be readily eliminated.[103, 104] The two thiourea derivatives of methylanthranilate and the Ni(II) and Pt(II) complexes as well as complexes of Ni(II) with two benzoylthiourea derivatives have been reported.[105] Compounds with methyl anthranilate showed antifungal activity, which is practically the same for morpholine and ethyl-derivative against the major pathogens responsible for important plant disease.

Owing to extensive use of the ϒ-emitter, ^{99m}Tc, in diagnostic nuclear medicine and the potential usefulness of ^{186}Re and ^{188}Re for radio therapeutic purposes, the chemistry of Tc and Re compounds has become an active field of research.[106 - 108] Ligand substitution in suitable precursors is an important route to synthesis of Tc complexes. Thiourea is poor a ligand for Tc(III) which can easily be substituted under mild conditions to turn $[Tc^{III}(tu\text{-}S)_6]Cl_3$ into a useful precursor to other Tc(III) compounds in aqueous and methanolic

media.[109-111] N-methylthiourea and N,N′-dimethylthiourea are also able to stabilize Tc(III) in their complexes, which has been tested as precursors for other Tc(III) compounds.[112, 113] As an example of thiourea derivatives used in catalysis, chiral dithioureas were reported for the hydride transfer reduction of prochiral ketones with isopropanol, giving rise to optically active secondary alcohols. Improvements on these results were reported with metals such as rhodium, iridium and ruthenium.[114] Rhodium(I) complexes with non-chiral thioureas have already been used in the hydroformylation of styrene,[115, 116] which prompted Breuzard, *et al.*[117] to synthesize and investigate the use of other similar complexes. The best results were obtained with N-phenyl-N-(S)-(1-phenylethyl)-thiourea associated to a cationic rhodium(I) precursor and asymmetric induction of 40% was also achieved.

The current investigation of the crystal structures of the alkylthiourea complexes was carried out as part of coordination chemistry of these ligands when complexed to cadmium, lead, copper and other metal ions of similar interest in both the deposition of thin films and preparation of metal sulphide nanoparticles. In this work our interest lies in studying the binding of the substituted thiourea molecules to metal atoms such as cadmium(II), lead(II) and copper(II) through the sulfur atom of the CS group suggest these compounds could be used as precursors in the preparation of metal sulfide nanoparticles. This provides a chemical environment in the compounds where both metal and sulfide ions are present on thermal decomposition and therefore expected to result in the efficient formation of a metal sulfide. This is not only a route to prepare metal sulfide nanoparticles but also useful for preparing thin films for materials applications.

1.2. EXPERIMENTAL

1.2.1. Materials

Cadmium chloride, copper chloride dihydrate, lead chloride, N-methylthiourea, N-ethylthiourea, N-phenylthiourea, N,N′-dimethylthiourea, N,N′-diethylthiourea and N,N′-diphenylthiourea obtained from Aldrich, were used as purchased. Ethanol and methanol (analytical grade) were used without further purification.

1.2.2. Instrumentation

(a) Microanalysis

Microanalysis was performed on a CARLO ERBA elemental analyzer for C, H, N, S while for Cd, Horizon ICP fisons elemental analyzer was used.

(b) NMR and FT-IR spectroscopy

Infrared spectra (400 – 4000 cm^{-1}) were recorded on FT-IR Perkin Elmer paragon 1000 spectrophotometer using nujol mull. NMR spectra were recorded on a Varian Associates Inova spectrometer (400 and 300 MHz).

(c) Thermogravimetry

Thermogravimetric analysis (TGA) was performed initially from 50 °C up to 800 °C on Perkin Elmer Pyris 6 TGA with nitrogen flow and heating rate of 10 - 20 °C. min^{-1}.

(d) X-Ray diffraction

X-Ray diffraction patterns on powdered samples were measured on Phillips X'Pert materials research diffractometer using secondary graphite monochromated CuK_α radiation (λ = 1.54060 Å) at 40 kV/50 mA. Samples were supported on glass slides. Measurements were taken using a glancing angle of incidence detector at an angle of 2°, for 2θ values over 20° – 60° in steps of 0.05° with a scan speed of 0.01 2°θ s^{-1}.

(e) X-ray crystallography

X-ray data were collected on an Enraf Nonius CAD-4 diffractometer. The intensity data were collected on a CAD-4 diffractometer and MoK_α radiation (λ 0.71069 Å) using ω-2θ scan at 180.0(1) K. The unit cell parameters were determined by least-squares refinement on diffractometer angles $11.05 \leq \theta \leq 14.09°$ for 25 automatically centred reflections.[118] All data were corrected for Lorentz-polarization effects by XCAD4[119] and for absorption by semi-empirical methods (ψ scan).[120] The structure was solved by Patterson method using DIRDIF96,[121] and refined anisotropically (non-hydrogen atoms) by full-matrix least-squares on F^2 using SHELXL-97[122] program. The H atoms were calculated geometrically and refined with a riding model. The program ORTEP-3[123] was used for drawing the molecules. WINGX was used to prepare material for publication. Experimental data is given in Table 2a.

1.2.3. Preparation of the complexes

All the cadmium complexes were prepared using a similar method as outlined below (Complex I). The copper complexes were prepared by reflux in methanol or ethanol to give white powder whereas lead complexes were prepared in water by heating a mixture of thiourea compounds and lead chloride. The single crystals for those cadmium complexes that crystallized were grown in warm methanol or ethanol solution, which was allowed to concentrate upon cooling at room temperature overnight. Attempts to grow crystals for the lead and copper complexes yielded no crystals, hence the products obtained were mostly in powder form.

(a) $[CdCl_2(CS(NH_2)NHCH_3)_2]_n$ (I)

In a typical experiment a hot solution of N-methylthiourea (0.150 g, 1.66 mmol) in ethanol (10 mL) was added into a heated solution of cadmium chloride (0.153 g, 0.83 mmol) in ethanol (15 mL). The mixture was stirred and refluxed for 2 h. The colorless solution was filtered hot to remove any traces of unreacted materials and was left in an open beaker at room temperature to crystallize by slow evaporation. Transparent cubic crystals were obtained after 24 hrs. The product was filtered, washed twice with ethanol and dried under vacuum. Yield 55.6%; m.p. 233.2-233.7 °C. Anal. Calcd. C, 13.2; H, 3.3; N, 15.4; S, 17.6; Cd, 30.9. Found: C, 13.3; H 3.3; N 15.0; S 17.0; Cd 31.3. IR (nujol mull)/cm^{-1}: 3342(m), 3293(m), 3195(m), 3140(m), 2925(vs), 2854(s), 1676(sh), 1625(vs), 1573(vs), 1488(w), 1462(s), 1417(m), 1303(m), 1172(m), 1144(m), 991(vw), 779(m), 720(m), 618(w), 579(w), 532(m), 489(m), 361(s). ^1H NMR (δ, DMSO-d_6) ppm: 7.78,

7.48 and 6.95(br, NH, NH_2); 2.80 and 2.64 (br, CH_3). $^{13}C\{^1H\}$ NMR (δ, DMSO-d_6) ppm: 183.73 and 179.90 (s, CS); 30.85 and 29.73(s, CH_3)

(b) $[CdCl_2(CS(NH_2)NHCH_2CH_3)_2]$ (II)

Yield 67%; m. p. 201-201.8 °C. Anal. Calcd. C, 18.8; H, 4.3; N, 14.2; S, 15.8; Cd, 29.8. Found: C, 18.4; H 4.1; N 14.3; S 16.4; Cd 28.9. IR (nujol mull)/cm^{-1}: 3348(m), 3302(w), 3241(m), 3164(s), 1643(s), 1573(vs), 1569(s), 1497(sh), 1317(s), 1109(s), 1011(m), 815(w), 779(w), 718(m), 689(m), 625(m), 567(w), 485(s). ^1H NMR (δ, DMSO-d_6) ppm: 8.09, 7.61 and 6.96(br, NH, NH_2); 3.06 (br, 4H, CH_2); 1.03 (t, 6H, CH_3). ^{13}C $\{^1H\}$ NMR (δ, DMSO-d_6) ppm: 182.32 and 176.64 (s, CS); 38.86(s, CH_2) 14.89 and 13.97(s, CH_3).

(c) $[CdCl_2(CS(NH_2)NHC_6H_5)_4]$ (III)

Yield 94%; m.p. 210.7-211.2 °C. Anal. Calcd. C, 35.4; H, 3.1; N, 11.3; S, 12.4; Cd, 22.8. Found: C, 35.1; H 3.4; N 11.7; S 13.4; Cd 23.5. IR (nujol mull)/cm^{-1}: 3418(m), 3388(m), 3295(s), 3201(s), 1621(vs), 1596(m), 1544(s), 1490(s), 1456(s), 1320(m), 1272(m), 1191(m), 1062(w), 912(w), 857(vw), 792(m), 756(s), 721(s), 692(s), 633(m), 597(s), 562(s), 492(s), 447(w). ^1H NMR (δ, DMSO-d_6) ppm: 9.78(s, 6H, NH, NH_2); 7.47 (d, 4H, C_6H_5); 7.31 (t, 4H, C_6H_5); 7.11(t, 2H, C_6H_5). ^{13}C $\{^1H\}$ NMR (δ, DMSO-d_6) ppm: 179.38 (s, CS); 139.29, 128.30, 124.29 and 123.38 (s, C_6H_5).

(d) $[CdCl_2(CS(NHCH_3)_2)_2]$ (IV)

Yield 98%; m.p. 203.1-203.6 °C. Anal. Calcd. C, 18.5; H, 4.1; N, 14.0; S, 15.5; Cd, 29.8. Found: C, 18.4; H 4.1; N 14.3; S 16.4; Cd 28.9. IR (nujol mull)/cm^{-1}: 3286(vs), 3045(w),

1592(vs), 1536(vs), 1308(s), 1190(m), 1150(m), 1040(s), 1023(m), 721(s), 673(m), 569(s), 546(s), 445(w). ^{1}H NMR (δ, DMSO-d_6) ppm: 7.53 (br, 4H, NH), 2.78(br, s, 12H, CH_3). ^{13}C {^{1}H} NMR (δ, DMSO-d_6) ppm: 181.75 (s, CS); 31.07 (s, CH_3).

(e) $[CdCl_2(CS(NHC_6H_5)_2)_2]$ (V)

Yield 91%; m.p. 198.2-199.0 °C. Anal. Calcd. C, 48.5; H, 3.5; N, 8.6; S, 9.9; Cd, 17.8. Found: C, 48.8; H 3.8; N 8.8; S 10.0; Cd 17.6. IR (nujol mull)/cm^{-1}: 3333(m), 3162(m), 1614(sh), 1593(s), 1543(vs), 1508(s), 1313(w), 1295(m), 1249(m), 1129(vs), 1073(w), 1024(w), 1003(w), 941(s), 899(w), 761(s), 725(m), 690(vs), 633(m), 601(s), 508(m), 473(w). ^{1}H NMR (δ, DMSO-d_6) ppm: 9.79(s, 4H, NH); 7.48 (d, 4H, C_6H_5); 7.32 (t, 4H, C_6H_5); 7.11(t, 2H, C_6H_5). ^{13}C {^{1}H} NMR (δ, DMSO-d_6) ppm: 179.38 (s, CS); 139.29, 128.30, 124.29 and 123.38 (s, C_6H_5).

(f) $[CdCl_2(CS(NHCH_2CH_3)_2)_2]$ (VI)

Yield 76%; m.p. 204.5-204.9 °C Anal. Calcd. C, 26.8; H, 5.4; N, 12.5; S, 14.4; Cd, 25.1. Found: C, 27.0; H 5.6; N 12.5; S 15.4; Cd 26.7. IR (nujol mull) cm^{-1}: 3342(m), 3312(w), 3198(m), 3159(s), 1650(vs), 1583(s), 1529(s), 1477(m), 1308(m), 1092(s), 808(s), 785(m), 758(m), 692(w), 627(m), 562(w), 485(m). ^{1}H NMR (δ, DMSO-d_6) ppm: 7.36 (br, NH); 3.32 (br, 8H, CH_2); 1.04 (t, 12H, CH_3). ^{13}C {^{1}H} NMR (δ, DMSO-d_6) ppm: 182.76 (s, CS); 43.83(s, CH_2) and 19.59(s, CH_3).

(g) $[Cu_4Cl_4(CS(NH_2)\ NHCH_3)_4]$ (VII)

In a typical experiment a hot solution of N-methylthiourea (0.220 g, 2.44 mmol) in methanol (15 mL) was added into a heated solution of copper chloride dihydrate (0.208 g, 1.22 mmol) in methanol (15 mL). The mixture was stirred and refluxed for 2 h to give a white solid suspension in a green solution. The solution was filtered to remove any traces of unreacted materials while hot and was allowed to cool to room temperature. The product was filtered, washed twice with methanol and dried under vacuum. Yield 56.6%; m.p. 189.8-199.1 °C (decomposes). Anal. Calcd. C, 12.7; H, 3.2; N, 14.8; S, 16.9; Cl, 18.7. Found: C, 12.1; H 3.0; N 13.5; S 15.5; Cl 18.1. IR (nujol mull)/cm^{-1}: 3316(vs), 3193(m), 1650(s), 1537(m), 1454(m), 1415(w), 1320(s), 1211(m), 1062(s), 1062(s), 1005(m), 894(vw), 759(s), 613(w), 575(w), 432(w), 364(w).

(h) $[Cu_4Br_4(CS(NH_2)\ NHCH_3)_4]$ (VIII)

The complex was prepared in a similar manner to complex **VII** above. Yield 60.6%; m.p. 202.9-203.6 °C (decomposes). Anal. Calcd. C, 10.3; H, 2.6; N, 11.9; S, 13.7. Found: C, 10.1; H 2.3; N 11.4; S 12.8. IR (nujol mull)/cm^{-1}: 3367(sh), 3289(vs), 3157(s), 2923(vs), 2852(vs), 1651(sh), 1634(vs), 1620(m), 1585(vs), 1493(w), 1456(s), 1417(m), 1305(m), 1162(m), 977(w), 763(m), 721(w), 677(m), 604(m), 501(m), 480(w).

(i) $[Cu_4Cl_4\{(CS(NHCH_3)_2\}_4]$ (IX)

The complex was prepared in a similar manner to complex **VII**. Yield 64.7%; m.p. 212.9-213.7 °C. Anal. Calcd. C, 17.7; H, 3.9; N, 13.8; S, 15.8; Cl 17.5. Found: C, 17.7; H 4.0; N 13.5; S 15.7; Cl 17.6. IR (nujol mull)/cm^{-1}: 3255(m), 3187(s), 3034(vs), 2853(vs),

1615(vs), 1532(vs), 1458(s), 1464(s), 1309(w), 1197(w), 1150(w), 1112(sh), 1048(s), 1021(m), 752(sh), 718(m), 632(m), 593(m), 535(w), 447(w).

(j) $[Cu_4Cl_4\{(CS(NHCH_2CH_3)_2\}_4]$ (X)

The complex was prepared in a similar manner to complex **VII**. Yield 74.7%; m.p. 218.7-219.3 °C. Anal. Calcd. C, 25.9; H, 5.2; N, 12.1; S, 13.9; Cl 15.4. Found: C, 25.9; H 5.4; N 11.9; S 14.1; Cl 15.2. IR (nujol mull)/cm^{-1}: 3346(m), 3242(w), 3161(s), 2853(vs), 1625(sh), 1590(s), 1590(vs), 1515(w), 1455(s), 1301(w), 1156(w), 813(vw), 774(w), 720(w), 681(s), 618(s), 483(s).

(k) $[ZnCl_2(CS(NH_2)NHCH_3)_2]$ (XI)

The preparation was similar to cadmium complexes, where the zinc chloride and methylthiourea were refluxed in ethanol in a 1 : 2 mole ratio. Yield 68.5%; m.p. 217.6-218.3 °C. Anal. Calcd. C, 15.2; H, 3.8; N, 17.7; S, 20.3; Cl 22.4. Found: C, 15.1; H 3.8; N 17.1; S 20.2; Cl 22.5. IR (nujol mull)/cm^{-1}: 3322(m), 3181(m), 3156(m), 2936(vs), 2814(s), 1683(sh), 1631(vs), 1563(vs), 1483(w), 1467(s), 1216(m), 1170(m), 1152(m), 977(vw), 787(m), 715(m), 589(w), 484(m), 358(s). ^1H NMR (δ, DMSO-d_6) ppm: 2.48 (br, NH_2); 2.79 and 2.62 (br, CH_3). ^{13}C $\{^1H\}$ NMR (δ, DMSO-d_6) ppm: 184.00 and 179.27 (s, CS); 31.27 and 30.29 (s, CH_3).

(l) $[Cu_4Cl_4(CS(NH_2)_2)_4]$ (XII)

In this synthesis, a hot solution of thiourea (0.89 g, 11.69 mmol) in ethanol (15 mL) was added into a hot solution of copper chloride dihydrate (1.008 g, 5.91 mmol) in ethanol

(15 mL). The mixture was stirred and refluxed for 1 h to give white solid suspension. The solution was filtered while hot and was allowed to cool to room temperature. The product was filtered, washed twice with ethanol and dried under vacuum. Yield 82.4%; m.p. 208.3-209.5 °C. Anal. Calcd. C, 6.9; H, 2.3; N, 15.9; S, 17.3; Cl 20.3. Found: C, 6.7; H 2.4; N 14.7; S 16.6; Cl 19.4. IR (nujol mull)/cm^{-1}: 3374(m), 3281(s), 3174(vs), 2952(vs), 2853(sh), 1517(m), 1461 (m), 1110(w), 721(m), 473(m), 358(s). ^1H NMR (δ, DMSO-d_6) ppm: 2.49 (br, NH_2).

(m) $[PbCl_2(CS(NHCH_3)_2)_2]$ (XIII)

Lead chloride (3.03 g, 10.89 mmol) was added into the boiling solution of N, N′-dimethylthiourea (3.21 g, 30.81 mmol) in water (100 mL) to give a colorless solution. The solution was heated for about 10 min and filtered while hot. The filtrate was allowed to cool, concentrated and white precipitate formed. The precipitate was filtered and dried under vacuum. Yield 74.3%; m.p. 206.7-207.2 °C. Anal. Calcd. C, 14.8; H, 3.3; N, 11.5; Cl 14.6 Found: C, 13.2; H 2.9; N 10.0; Cl 14.2. IR (nujol mull)/cm^{-1}: 3263(m), 2923(m), 2852(s), 2936(vs), 1576(s), 1526(vs), 1456(s), 1417(w), 1296(m), 1190(m), 1144(m), 1037(w), 1012(m), 718(m), 574(w), 541(m), 442(s).

(n) $[PbCl_2(CS(NHCH_2CH_3)_2)_2]$ (XIV)

The synthesis was performed similarly to the above complex **XIV**. Yield 67.3%; m.p. 211.7-212.3 °C. Anal. Calcd. C, 22.1; H, 4.5; N, 10.3; Cl 13.1. Found: C, 22.2; H 4.0; N 10.6; Cl 13.8. IR (nujol mull)/cm^{-1}: 3313(vw), 3278(w), 2922(vs), 2853(vs), 1569(s),

1508(s), 1458(vs), 1324(sh), 1253(m), 1167(w), 1131(w), 1053(m), 945(w), 918(w), 797(m), 757(sh), 617(s), 563(w), 503(m), 447(w).

1.3. RESULTS AND DISCUSSION

All complexes were obtained in a reasonably good yield. A combination of analytical tools including elemental analysis, infrared and NMR spectroscopy, melting points, X-ray crystallography and thermogravimetry were used. A series of substituted thiourea metal complexes were prepared by first dissolving alkylthioureas and appropriate metal salts, in hot ethanol, methanol or in aqueous media, followed by refluxing. The products obtained for cadmium were air stable and colorless to white crystals, formed upon concentrating the solution at room temperature.

Eq. 1

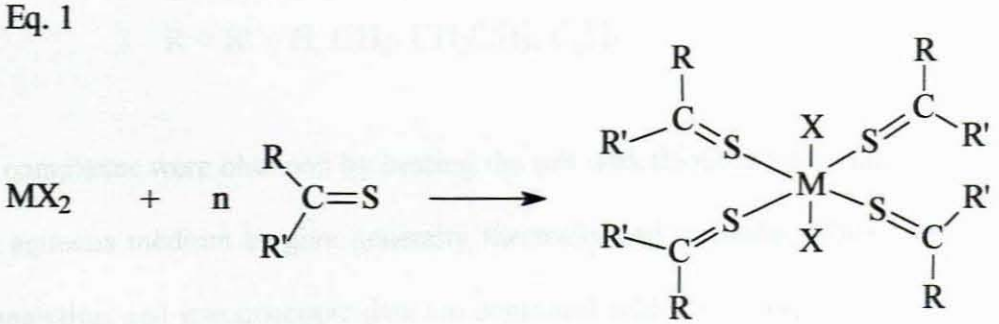

M = Cd, Pb; X = Cl
R = R' = H, CH_3, CH_2CH_3, C_6H_5
n = 2 - 3

The copper complexes were obtained as *multinuclear* species bridged by the thiourea ligands with copper reduced to a copper(I) state irrespective of the mole ratio of the starting reagents (Equation 2). Although they were stable over a period of time they eventually became oxidized to copper(II) and this can be observed by the colour change from white to green. Some of the copper complexes gave low analysis of S and N otherwise they were analyzed pure except complexes VII and XIV, which appeared apparently impure. This could be attributed to their instability due to their oxidation resulting in the formation of mixed copper (I) and (II) complexes.

Eq. 2

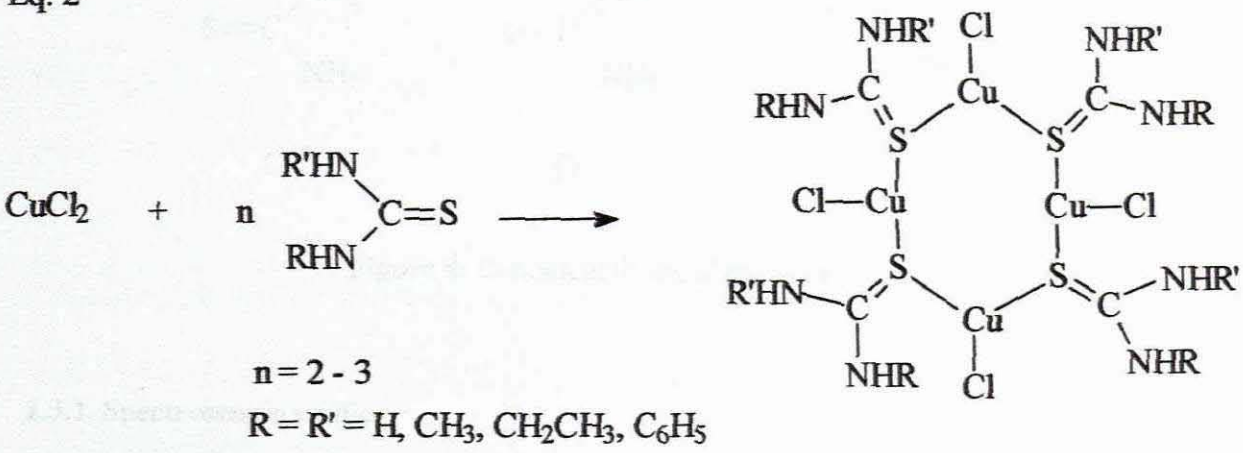

Lead complexes were obtained by heating the salt with thiourea compounds (Equation 1) in an aqueous medium to give generally thermally and air-stable white solid products. The analytical and spectroscopic data are consistent with the proposed formulation of the complexes except that traces of impurity are evident in some of the microanalysis. All cadmium complexes were pure in all the analytical data. Some of the cadmium complexes were further characterized by X-ray crystallography to confirm the

formulation of the structure. Their melting points indicates the formation of monomers, which range from 198 °C to 210 °C, compared to the polymeric compound, $[CdCl_3(CS(NH_2)NHCH_3)_3]_n$, with the highest melting point of 233 °C. The melting points correspond to the patterns of the thermogravimetric curves obtained for these complexes, which confirmed the initial decomposition around 200 °C. Infra-red and Raman spectra, and crystallographic studies have shown that in thiourea and its derivatives there are almost equal contributions from the canonical forms **C**, **D** and **E** shown in figure 4.

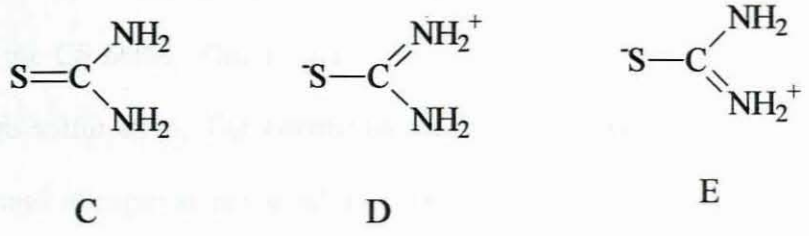

Figure 4: Canonical forms of thiourea

1.3.1. Spectroscopic studies

1.3.1.1. Infrared spectra

Thiourea and its derivatives are potentially capable of forming co-ordinate bonds through both sulfur and nitrogen atoms although the extremely low basicity of the ligand militates against the formation of metal-nitrogen bonds. [32, 124] Mido, *et al.*[32] and Matsuura *et al.*[53] were able to confirm from their spectral observations and the single crystal X-ray structure analysis that the N-methylthiourea molecule is in a *syn* form as opposed to the *anti* form. One of the previous results, showed from the infrared spectra that the ν(NH)

bands (3345, 3250 and 3165 cm^{-1}) of ethylthiourea are not significantly influenced upon coordination to metals and this served as indication that the ligand might be binding through sulfur rather than the nitrogen atom.[18, 30] The ligand band at 1542 cm^{-1} together with a shoulder at 1560 cm^{-1} assigned mainly to ν(NCN) asymmetric stretching with some contributions from ν(CS) and NH_2 deformation, increases in energy on coordination (1570 – 1598 cm^{-1}) indicating an increased double bond character of the CN bond. The band associated with the ν(CS) stretching was assigned to 738 cm^{-1}, which upon coordination is split and one or both the new bands are shifted to lower frequencies (720 – 750 cm^{-1} and 660 – 730 cm^{-1}). This is in agreement with the decreased double bond character of the CS bond. This is consistent with the coordination of the ligand to the metal through sulfur atom. The coordination of the thiourea ligands to the metals can either be through nitrogen atoms or sulfur atom, which is indicated by the IR bands.

There are a number of observable features that relate to the binding of ligand molecules to the metal. Table 1 shows infrared spectral values of selected bands of interest for all complexes. First, for the complex, $[CdCl_3(CS(NH_2)NHCH_3)_3]_n$, the C=S out-of-plane bending mode (πC=S) and its stretching vibrational mode (νC=S) show a remarkable downshift from 636 and 495 cm^{-1} to 618 and 489 cm^{-1}, respectively. The vibrational mode (both stretching and bending) due to the contribution of C–N bond appears at 1557, 1298 and 1149 cm^{-1} and is shifted to 1573, 1303 and 1172 cm^{-1} respectively in the complex. The changes, which range from 5 to 20 cm^{-1} are attributed to the change in bonding character of both C–N and C=S bonds on coordination. The C=S bond tends to change into a partial double bond character whereas the C–N bond gains electron density

raising its bond order. A similar observation was made for all other complexes in their wavenumbers associated with CS and CN modes of vibrations (Table 1). This was consistent with the previously reported data.[8, 9, 18, 30, 95, 125]

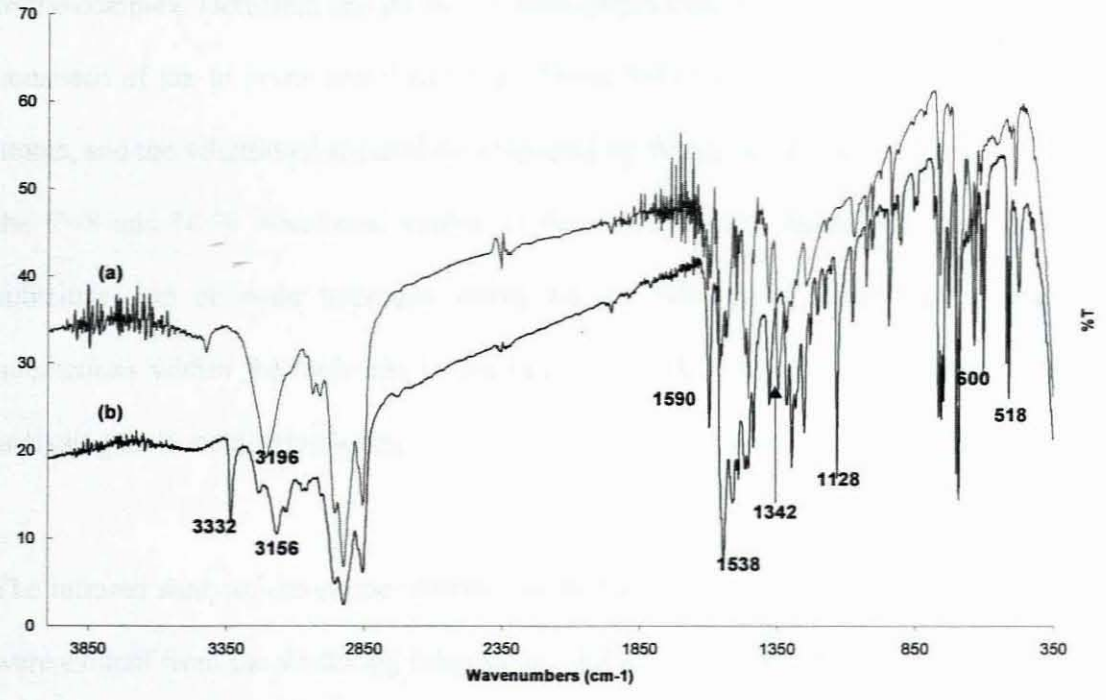

Figure 5: Infrared spectra of free phenylthiourea (a) and its cadmium complex **V** (b).

An exception has been observed in particular to the bands associated with NH bond in the cadmium complexes of phenyl and diphenylthioureas. The band around 3196 cm^{-1} is split with an additional intense peak at about 3332 cm^{-1} for complex **V** (Figure 5). In this complex the band associated with CN bond at 1590 cm^{-1} only increase in intensity from the free ligand to coordinated complex. The change in the frequency of this band is small and influenced by the delocalisation of electrons on the phenyl rings.

Wharf, *et al.*[45] reported the vibrational spectra for the polymeric complex, $[PbCl_2(tu)_2]_n$ and noted the split in the C=S stretch as well as in the NCN asymmetric stretch of thiourea which are due to the presence of both bridging and terminal thioureas in the solid state structure. They also noted the high melting points due to the polymeric nature of the complex. Herbstein and Reisner[126] substantiated the structure of $[PbBr_2(tu)_2]$ which consisted of six to seven coordinated polyhedra linked by bridging thiourea and halide atoms, and the vibrational spectral data reported by Wharf, *et al.*[45] again showed a split in the C=S and NCN vibrational modes. In the current study the alkyl group is used to substitute one or more hydrogen atoms on the NH_2 group. This makes electronic interactions within the molecule to become very important, as is the type of metal, in analysing their metal complexes.

The infrared study of the copper complexes showed similar results as in cadmium. These were evident from the stretching frequencies of the C–N, C=S and N–H from the thiourea ligands upon co-ordination to the copper metal. Some of the notable features include the splitting of the NH_2 peaks in the region 3150 – 3360 cm^{-1} upon the alkylthiourea coordinating to copper (Figure 6). In all copper complexes the alkyl substituted thiourea ligands are bridging through the sulfur atom changing the double bond character of the C=S. The C–N bond character changed from a single bond to what is evidently close to a partial double bond with the peaks changing from 1548 to 1570 cm^{-1}. Some of the frequencies associated with the ν(CS) stretching are shifted from 776 to 762 cm^{-1} and 612 to 606 cm^{-1}, which is a change towards lower frequency due to a change of the double bond to a single bond character. This, as expected, shows changes associated with double

bond character of C–N and a single bond character of CS bond, whereas no significant shifts were observed for the NH_2 group except for the fine splitting of the peak. Similar to cadmium complexes the coordination of the alkylthiourea ligands in the copper complexes is mainly through sulfur atoms and not nitrogen.

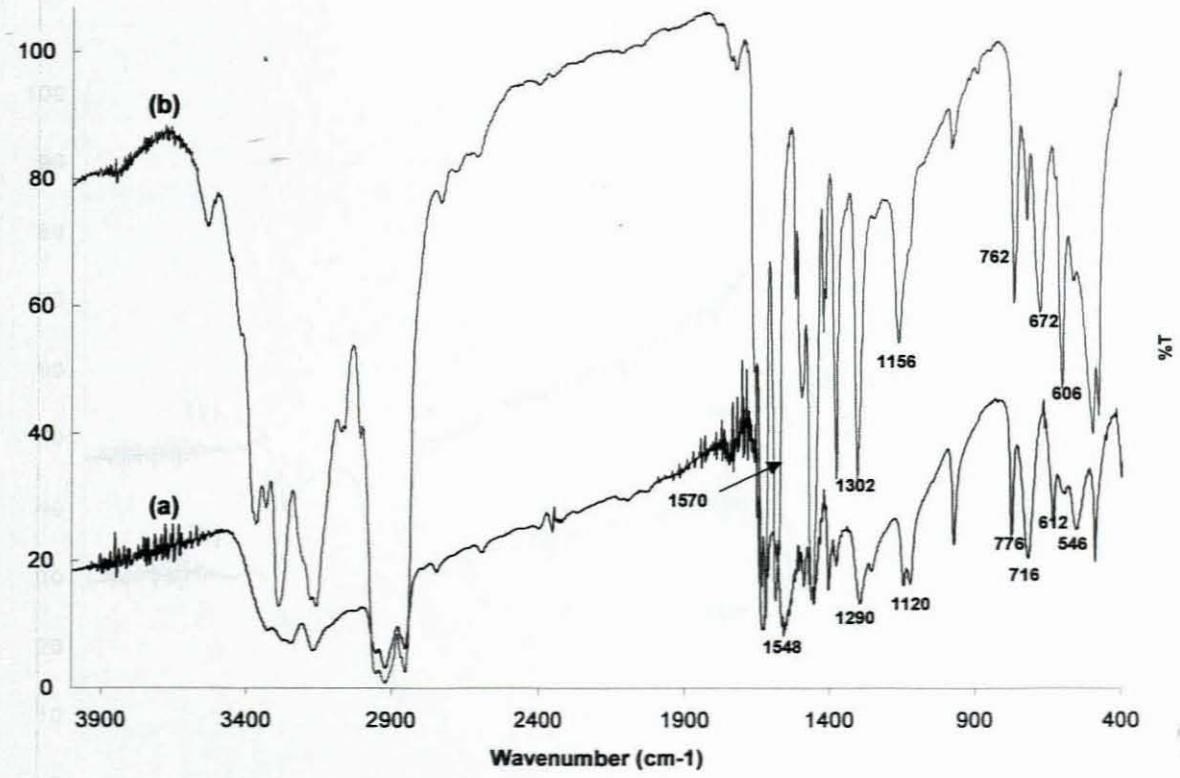

Figure 6: Infrared spectra of free methylthiourea (a) and its copper bromide complex (b).

In the lead complex of the diethylthiourea (Figure 7), there is an observable additional band in the lower frequency (446 cm^{-1}), which could be attributed to the Pb–S bond. Similarly to copper and cadmium complexes, the infrared spectral differences between the ligand and its lead complex lies in the bands associated with the CS and CN bonds. The bands due to ν(CS) observed at about 926, 636 and 544 cm^{-1} for the ligand

corresponds to bands at 918, 620 and 496 cm^{-1} for its complex, respectively. Those due to ν(CN) stretching frequency for the ligand at about 1526, 1232, 1366 and 790 cm^{-1} are shifted to higher frequencies such as 1560, 1244, 1374 and 794 cm^{-1}, respectively upon co-ordinating to the metal. This is also in agreement with the coordination through the sulfur atom although the NH groups are little perturbed electronically due to change in bond characters of most specifically CN bond.

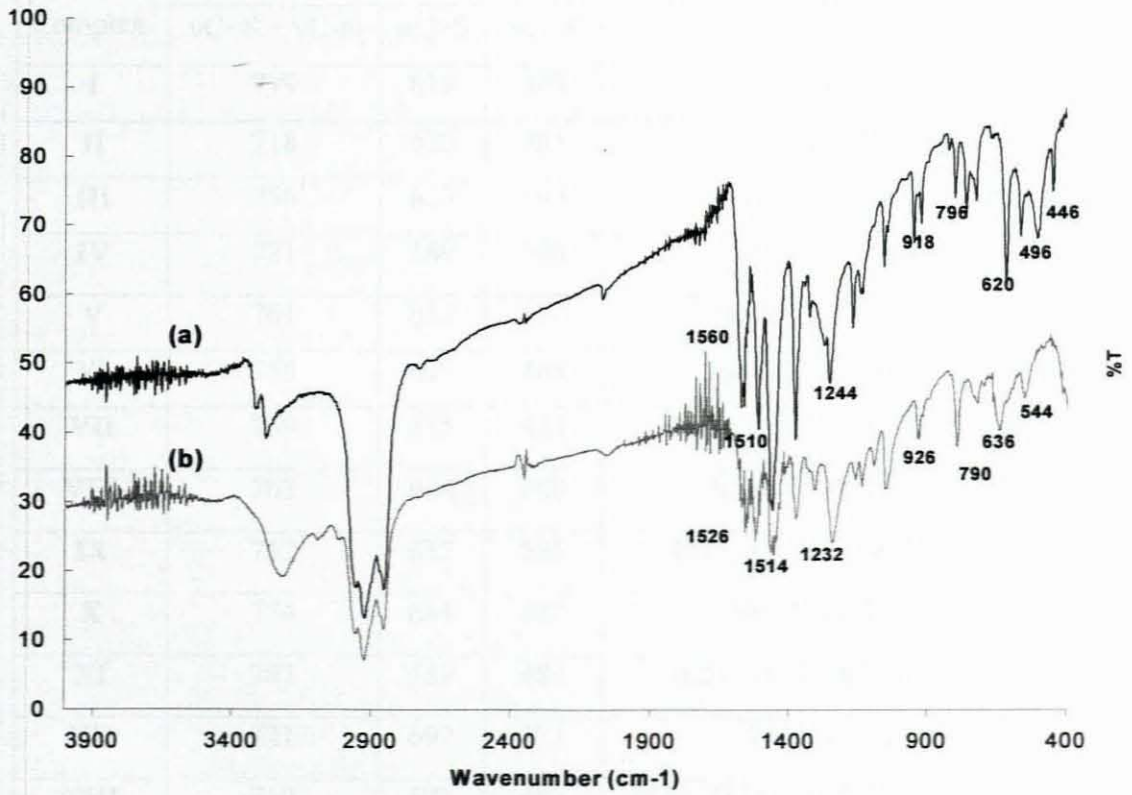

Figure 7: Infrared spectra of the free diethylthiourea ligand (b) and its lead chloride complex (a).

Previous results based on the infrared spectrum of ethylthiourea[30] showed that the ν(NH) bands (3340 - 3150 cm^{-1}) are not significantly influenced upon coordination to metals and this served as indication that the ligand might be binding through sulfur and not the

nitrogen atom. This has been one of the general observations for all type alkylthiourea complexes irrespective of the type of metal. This indicates that indeed there is a strong affinity of the metals to sulfur atoms other than nitrogen and all results in metal-sulfur bond in the formation of a complex.

Table 1: Selected IR data for all complexes.

Complex	Vibrational modes (cm^{-1})			
	νC=S + νC-N	πC=S	νC=S	νC-N
I	779	618	489	1557, 1298, 1149
II	718	625	485	1573, 1569, 1317, 1011
III	756	633	492	1621, 1596, 1544, 1320, 1062
IV	721	569	546	1592, 1536, 1308, 1190
V	761	633	473	1614, 1593, 1543, 1249, 1073
VI	758	627	485	1583, 1529, 1477, 1308, 1092,
VII	759	575	432	1650, 1537, 1454, 1320, 1062
VIII	763	604	480	1634, 1573, 1493, 1305, 1162
IX	752	632	535	1615, 1532, 1458, 1309, 1150, 1112
X	774	681	483	1590, 1515, 1455, 1301, 1156
XI	787	589	484	1631, 1563, 1483, 1467, 1170, 1152
XII	721	697	473	1517, 1461, 1437, 1110
XIII	719	574	442	1576, 1526, 1417, 1296, 1190, 1037, 1012
XIV	795	555	421	1570, 1522, 1304, 1243, 1158, 1136, 1052

In addition the nature of bonding is such that the CN and CS alternate between double and single bond orders from the free ligands to a coordinated ligand. Hence, infrared spectroscopy helps to elucidate not only mode of binding of the thiourea ligands but also

the effect of bonding of sulfur atoms on the nature of bonds that exist in the organic molecules. Although different infrared spectra were observed from the variation of the alkyl groups, there has not been a clear trend as to the effect of the alkyl groups on the coordination of the alkylthiourea ligands. Other spectroscopic analysis could help to determine the ratios of the *syn-anti* isomers possible of these alkyl-substituted thioureas.

1.3.1.2. NMR spectra

Nuclear magnetic resonance studies of the rotational barrier about the central C–N bond in amides and thioamides have indicated that the energy barrier is greater than for a normal C–N bond because of electron delocalisation.[127-131] The behaviour of N-methylthiourea is an example of the simple alkylthiourea system well studied by NMR techniques. There are two possible configurations of N-methylthiourea due to the restricted rotation about the C–N bond.[79] The two isomers of N-methylthiourea, *syn* and *anti*, show a chemical shift difference between the methyl protons due to differences in shielding by the sulfur atom.

The NMR spectral results of these complexes were recorded at room temperature using deuterated dimethyl sulfoxide (CD_3SOCD_3) in a standard 5 mm tube at 300 and 400 MHz. There is a collapse in the multiplicity of the signals of protons associated with the nitrogen atoms, either neighbouring or directly bonded to them. This observation is consistent with studies of these compounds by variable temperature NMR by Brown and Katekar.[15] At higher temperatures the peaks for the substituted thioureas become well resolved, whereas at lower temperatures there is broadening and coalescence of the peaks

associated with NH groups. This effect is attributed to the slow rotation around the S=CN bond at low temperature and it appears that only two of the three possible rotational isomers of N, N'-diethylthiourea are present, namely the *syn-syn* and the *syn-anti*.[13] The *anti-anti* isomer is not detectable, probably due to the steric interaction between the two *anti*-ethyl groups. The low-energy barrier to free rotation around the S=CN bond in thioureas is evidenced by the low temperature at which different isomers have different resonance frequencies due to the competition between the two amide bonds for electron delocalisation (Figure 4). There was a further evidence in NMR studies that the rotation about this amide bond is either rapid or one isomer predominates over the other.[14] However, resonances due to the *syn* and *anti* rotational isomers have been reported for N-methylthiourea molecule,[79] with the methyl group *syn* to the sulfur atom resonating at higher field compared to the *anti* methyl. The NMR spectral study of the thiourea derivatives has been performed to confirm the existence of different rotamers of these ligands due to the partial double bond character of the thioamide bond.

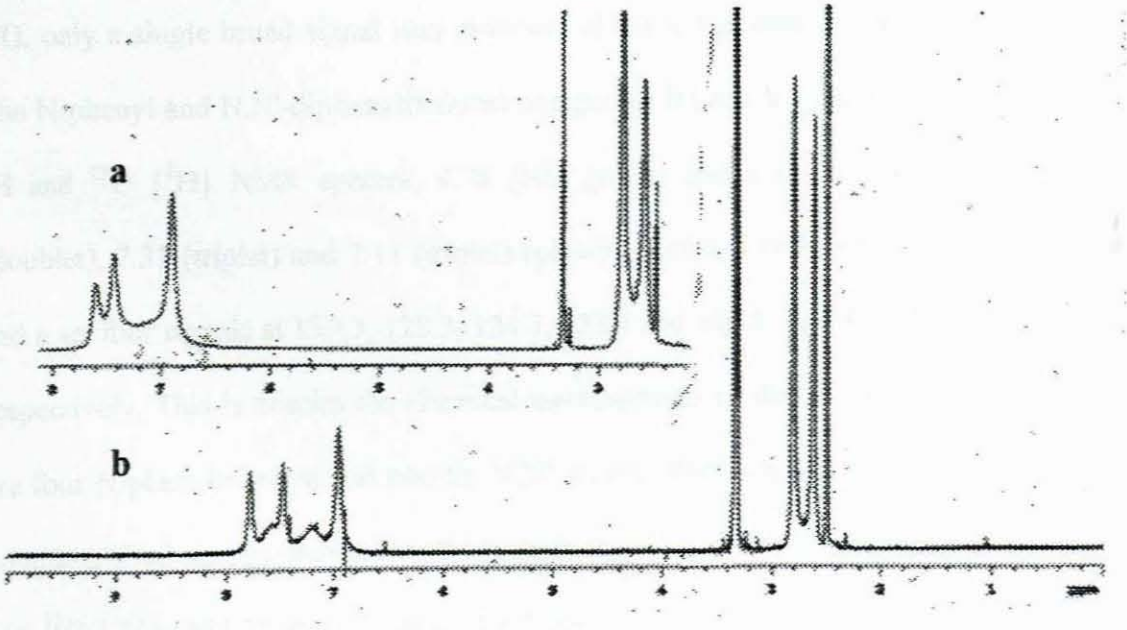

Figure 8: NMR spectra of free methylthiourea (a) and its cadmium complex **I**, $[CdCl_3(CS(NH_2)NHCH_3)_3]_n$ (b).

The ^{1}H NMR spectra of both complexes **I** and **II**, gave three broad peaks in the lower field (6.96 – 8.10 ppm) due to the NH protons. Two broad signals at 2.80 and 2.64 ppm for the methyl groups in complex **I** were observed (Figure 8), which coincide with the ^{13}C $\{^{1}H\}$ NMR signals at 30.85 and 29.73 ppm. The two CH_2 signals on the ^{1}H NMR spectrum of complex **II** appears at 3.31 and 3.06 ppm, whereas the signals due to the carbon on CH_2 group appear to have merged with the solvent peaks on the ^{13}C $\{^{1}H\}$ NMR spectrum while the second peak appears at 38.36 ppm. The carbon atoms of the CS group of complex **II** gave two signals at 183.73 and 179.90 ppm on the ^{13}C $\{^{1}H\}$ NMR spectrum, which were close to those of complex **I** (182.32 and 176.64 ppm), which is consistent with the presence of the two rotational isomers, i.e. the *syn* and *anti* isomers in these N-alkylthiourea complexes **I** and **II**.

Both the ^{1}H and ^{13}C NMR spectra of complex **III** gave resonances, which indicate the dominance of the *syn* isomer. Similarly to the N, N'-dialkylthiourea complexes (**IV** and **VI**), only a single broad signal was observed in the lower field of the ^{1}H NMR spectra. The N-phenyl and N,N'-diphenylthiourea complexes **III** and **V** gave similar peaks in both ^{1}H and ^{13}C $\{^{1}H\}$ NMR spectra; 9.78 (NH group) and a set of three peaks at 7.47 (doublet), 7.31 (triplet) and 7.11 (triplet) (phenyl group); 179.38 and 179.94 (CS group) and a set four signals at 139.3, 128.3, 124.3, 123.4 and 139.8, 128.9, 124.9, 124.1 (C_6H_5), respectively. This is despite the chemical environments of the phenyl groups since there are four N-phenylthiourea and two for N,N'-diphenylthiourea ligands for each metal in a complex. Two signals were observed in both the ^{1}H (7.53 ppm-NH and 2.78 ppm-CH_3) and ^{13}C $\{^{1}H\}$ (181.75 ppm-CS and 31.07 ppm-CH_3) NMR spectra of complex **IV**. The

NMR results showed that there is a detectable amount of *anti*-isomer in the N-alkylthiourea (complexes **I** and **II**) whereas no *anti*-isomer was detected for the arylthiourea complex **III**. NMR spectral results for all complexes and their corresponding free alkylthiourea ligands indicate binding through the sulfur atoms, which is also electron-withdrawing and hence affect the protons and carbon atoms in their respective magnetic resonances. The NH/NH_2 groups are less affected by the alkyl or aryl groups attached to the nitrogen atoms in the ligands.

Table 2: ^{1}H and $^{13}C\{^{1}H\}$ NMR spectral data on selected complexes.

Complex	Proton NMR (ppm)				Carbon-13 NMR (ppm)			
	CH_3	NH_2/NH	CH_2	C_6H_5	C	CH_3	CH_2	C_6H_5
I	2.80, 2.64	2.49	-	-	183.73, 179.89	30.85, 29.73	-	-
II	1.03	2.48/8.09, 7.61, 6.96	3.06	-	182.31, 176.63	14.86, 13.97	38.35	-
III	-	2.49	-	7.11, 7.31, 7.47	179.37	-	-	139.29, 128.30, 124.28, 123.51
IV	2.78	2.48/7.53	-	-	181.75	31.07	-	-
V	-	2.49	-	7.11, 7.32, 7.48	179.94	-	-	139.81, 128.85, 124.86, 124.08
VII	2.63, 2.71, 2.86	2.48	-	-	173.91	30.44	-	-
XI	2.79, 2.62	2.48	-	-	184.00, 179.27	31.27, 30.29	-	-

1.3.1.3. X-ray structural analysis

All complexes subjected to single crystal X-ray structural analysis crystallized in ethanol or methanol by slow evaporation at room temperature to give transparent cube-shaped crystals. All complexes are stable to air and moisture with melting points greater or equal to 200 °C. The formulae of the resulting complexes were consistent with the molecular structures and other forms of analyses such as microanalysis, infrared and NMR spectroscopy. Efforts to grow crystals for the copper and lead complexes were unsuccessful. A combination of analytical techniques was used in the case of copper and lead complexes to establish the resulting formulae, structure and coordination. Details of the crystal data and structure refinements are provided in Tables 3a and b. ORTEP diagrams of complexes **I**, **II**, **III** and **IV** with the non-hydrogen atomic labeling scheme are shown in Figures 9, 10, 11 and 12, respectively. Selected bond lengths and angles are given in Tables 4, 5, 6 and 7.

The structure of complex **I** (Figure 9a) comprise of an unusual polymeric structure with alternating bridging groups through the two chlorides and sulphur atoms. The cadmium ion in each unit, $CdCl_3S_3$, consists of three Cd–Cl bonds and three Cd–S bonds. There are two bridging bonds and one non-bridging bond for each type of ligand. The Cd–S bond distances are slightly longer than for the corresponding dichlorobis(S-thiourea)cadmium(II) (Cd–S; 2.517 Å), which range from 2.632 Å for the terminal N-methylthiourea to 2.743 Å and 2.782 Å for the bridging ligands. A similar observation was made for the Cd–Cl bond distances, which range from 2.577 Å for the terminal chlorides and, 2.644 and 2.700 Å for the bridging chloride ligands. In each monomer

unit, the metal core is constituted by three chloride and three N-methylthiourea ligands. Hence the formulation of the chemical structure, $[CdCl_2(CS(NH_2)NHCH_3)_2]_n$. Zhen-Fan Sun *et al.*[36] made similar observation in the bond distances of Cd–S in a mixed ligands cadmium(II) complex of xanthic acid and N,N′-bis(4-methoxyphenyl)thiourea. The xanthate chelate ligand has longer bond distances (2.831 Å) for the bridging sulfur atoms and shorter distances (2.606 Å) for the non-bridging ones.

The C–S and C–N bond distances for the terminal methylthiourea ligand, 1.726 and 1.319 Å (average of C2–N3 and C2–N4) respectively, agree with those of thiourea molecules reported in the Cambridge Structural database (CSD by Allen, *et al.*[132] in 1991) i.e. 1.726 (C–S) and 1.322 Å (C–N). The additional C–N bond due to the methyl substituent is 1.467 Å. The C–S and C–N bond distances for the bridging methylthiourea ligands, 1.740 and 1.315 Å (average of C1–N1 and C1–N2) respectively, are within the expected range of bond distances of thiourea molecules. The C–N and C–S bonds are intermediate between a single and double bond but closer to a C=N double bond distance (1.27 Å) and a normal C–S single bond distance (1.81 Å). The co-ordination polyhedra around the Cd(II) ion is a distorted octahedron. Three N-methylthioureas are S-bonded. The Cl–Cd–Cl (°) and S–Cd–S (°) angles are lowered and increased from octahedral values. Though *anti* Cl–Cd–Cl, S–Cd–S and Cl–Cd–S bond angles are shortened from 180° (varying from 168.98 (0.05) to 172.77° (0.03)). The *syn* bond angles around the cadmium ions vary from 79.68 (0.04) to 99.40° (0.04). The lowest angles (79.68 and 83.75°) were observed for the bridging sulfur-bonded N-methylthiourea and chloride ligands respectively, the other bond angles especially for the terminal ligands are hence slightly

below or above 90° and 180°. This forces the structure of the compound to assume a zigzag pattern with the rectangular shaped Cd_2Cl_2 bridge lying vertical and almost perpendicular to the Cd_2S_2 bridge. The Cd–S–C bond angles are slightly greater than the tetrahedral value, varying from 116.3° (0.15) to 117.89° (0.15). The S–C–N and N–C–N bond angles are within the expected range of tetrahedral geometry (varying from 117.64° (0.35) to 122.56° (0.34).

The structure of complex **II** and the packing diagram are shown in Figures 10a and b respectively. The structure is based on a discrete monomeric molecule. The coordination polyhedra around the Cd(II) ion is a distorted tetrahedral. The two N-ethylthiourea ligands are sulfur-bonded to the metal atom. In this four-co-ordinate structure, molecular units are arranged so that one of the chloride ions (Cl(1)) and the metal atom lie on a crystallographic three-fold axes which relates to the two thiourea ligands and the second chlorine atom (Cl(2)). The S(1)–Cd(1)–Cl(2), S(2)–Cd(1)–Cl(2) and S(1)–Cd(1)–Cl(2) bond angles are 111.20, 111.81 and 112.89°, respectively. These angles deviate from the regular tetrahedral value of 109.47°, which could be explained by the steric interaction between the two ethyl groups. Intermolecular hydrogen bonding interactions between the NH protons and both sulphide and chloride ions of adjacent molecules stabilize the molecular structure (Figure 9b). The parameters of the hydrogen bonds are as follows: N(5)–H(5) 0.86 Å, H(5)---S(4) 2.58 Å, N(5)–H(5)---S(4) 170.1°; N(6)–H(6a) 0.86 Å, H(6a)---Cl(2a) 2.36 Å, N(6)–H(6a)---Cl(2a) 153.4° and N(7)–H(7) 0.86 Å, H(7)---Cl(2b) 2.51 Å, N(7)–H(7)---Cl(2b) 172.6° (Figure 2b).

The Cd–S bonds (2.49 and 2.52 Å) are shortened upon coordination as a result of the electron-donating effect of methyl group in the N-methylthiourea ligand, which suggest that the σ–bond character of this bond is stronger. The S=C (1.73 Å) and N–C (1.34 Å) bonds are close to those observed in complex **I**. In both cases the C–N and S–C bonds show intermediate bond character to the single and double bond, which is attributed to the delocalization of electron in the amide bond. N-alkylthioureas can exist in two different configurations where the thioamide hydrogen atom and the thiocarbonyl bond are either in *syn* or *anti* form.[75] From the above-described N-alkylthiourea complexes each thiourea ligand in a polymer and a monomer are arranged in a *syn* form. The structural analysis of this complex is in agreement with the spectroscopic data obtained for this compound.

Table 3a. Crystal data and detailed structure refinement for complex **I** and **II.**

	I	**II**
Empirical formula	$C_6 H_{18} Cd Cl_3 N_6 S_3$	$C_6 H_{16} Cd Cl_2 N_4 S_2$
Formula weight	489.14	391.65
Temperature	160(2) K	293(2) K
Wavelength	0.71073 Å	0.71073 Å
Crystal system	Triclinic	Triclinic
Space group	PBAR1	PBAR1
Unit cell dimensions	a = 6.975(8) Å; α = 71.97(6)°. B = 9.162(8) Å; β = 76.27(6)°. c = 9.944(6) Å; γ = 69.75(8)°.	a = 8.547(7) Å; α = 95.50(8)°. b = 9.841(10) Å; β = 114.44(6)°. c = 9.902(10) Å; γ = 101.36(9)°.
Volume	560.8(9) $Å^3$	728.6(12) $Å^3$
Z	2	2
Density (calculated)	2.153 Mg/m^3	1.785 Mg/m^3
Absorption coefficient	2.757 mm^{-1}	2.130 mm^{-1}
F(000)	356	388
Crystal size	0.50 x 0.13 x 0.05 mm^3	0.40 x 0.40 x 0.30 mm^3
θ range for data collection	2.18 to 24.98°.	2.31 to 24.99°
Index ranges	0<=h<=8, -10<=k<=10, -11<=l<=11	-10<=h<=9, 0<=k<=11, -11<=l<=11
Reflections collected	2184	2780
Independent reflections	1964 [R(int) = 0.0063]	2558 [R(int) = 0.0080]
Completeness to θ (24.98°)	99.5 %	99.7 %
Max. and min. transmission	0.8744 and 0.3394	0.5675 and 0.4830
Goodness-of-fit on F^2	1.055	1.092
Final R indices	R1 = 0.0201, wR2 = 0.0537	R1 = 0.0378, wR2 = 0.0968
R indices (all data)	R1 = 0.0236, wR2 = 0.0553	R1 = 0.0542, wR2 = 0.1043
Extinction coefficient	0.0285(13)	
Largest diff. Peak and hole	0.647 and -0.769 $e.Å^{-3}$	1.837 and -0.593 $e.Å^{-3}$

Table 3b. Crystal data and detailed structure refinement for complex **IV** and **III.**

	IV	**III**
Empirical formula	$C_6 H_{16} Cd Cl_2 N_4 S_2$	$C_{28} H_{32} Cd Cl_2 N_8 S_4$
Formula weight	391.65	792.16
Temperature	293(2) K	160(2) K
Wavelength	0.71073 Å	0.71073 Å
Crystal system	Monoclinic	Monoclinic
Space group	Aa	I 2/a
Unit cell dimensions	A = 12.791(3) Å	a = 25.098(6) Å
	B = 8.992(2) Å	b = 8.133(2) Å
	C = 13.271(3) Å	c = 16.768(3) Å
Volume	1446.2(6) $Å^3$	3341.2(13) $Å^3$
Z	4	4
Density (calculated)	1.799 Mg/m^3	1.575 Mg/m^3
Absorption coefficient	2.146 mm^{-1}	1.097 mm^{-1}
F(000)	776	1608
Crystal size	0.40 x 0.20 x 0.20 mm^3	0.40 x 0.30 x 0.20 mm^3
θ range for data collection	2.78 to 24.94°.	2.49 to 24.97°.
Index ranges	-15<=h<=14, -3<=k<=10, -2<=l<=15	0<=h<=29, 0<=k<=9, -19<=l<=19
Reflections collected	1386	3070
Independent reflections	1330 [R(int) = 0.0046]	2934 [R(int) = 0.0135]
Completeness to θ = 24.94°	99.7 %	99.9 % (θ = 24.97°)
Final R indices	R1 = 0.0444, wR2 = 0.1337	R1 = 0.0238, wR2 = 0.0705
R indices (all data)	R1 = 0.0606, wR2 = 1.062	R1 = 0.0290, wR2 = 1.091
Max. and min. transmission	0.6736 and 0.4807	0.8104 and 0.6681
Refinement method	Full-matrix least-squares on F^2	Full-matrix least-squares on F^2
Data / restraints / parameters	1330 / 2 / 140	2934 / 0 / 172
Goodness-of-fit on F^2	1.075	1.127

Table 4: Selected bond distances (Å) and bond angles (°) for complex **I**.

Bond distances (Å)		**Bond angles (°)**	
Cd(1)-Cl(1)	2.577(0.0013)	Cl(1)-Cd(1)-Cl(2)#2	171.86(0.04)
Cd(1)-Cl(2)	2.700(0.0016)	S(1)-Cd(1)-S(2)	168.98(0.05)
Cd(1)-S(1)	2.743(0.0012)	Cl(2)-Cd(1)-S(1)#1	172.77(0.03)
Cd(1)-S(2)	2.633(0.0012)	S(1)-Cd(1)-Cl(2)	93.33(0.04)
Cd(1)-Cl(2)#2	2.644(0.0013)	S(2)-Cd(1)-Cl(2)	97.66(0.05)
Cd(1)-S(1)#1	2.782(0.0017)	Cl(1)-Cd(1)-Cl(2)	88.41(0.05)
S(1)-C(1)	1.740(0.0044)	Cl(2)-Cd(1)-Cl(2)#2	83.75(0.04)
S(2)-C(2)	1.726(0.0045)	Cl(1)-Cd(1)-S(2)	83.79(0.04)
N(1)-C(1)	1.310(0.0059)	Cl(1)-Cd(1)-S(1)	95.69(0.04)
N(3)-C(2)	1.313(0.0061)	S(2)-Cd(1)-Cl(2)#2	99.40(0.04)
N(2)-C(1)	1.320(0.0057)	S(2)-C(2)-N(3)	122.56(0.34)
N(4)-C(2)	1.327(0.0057)	S(2)-C(2)-N(4)	117.64(0.35)
N(4)-C(3)	1.467(0.0058)	S(1)-C(1)-N(1)	121.86(0.34)
		S(1)-C(1)-N(2)	117.85(0.32)

The molecular structure of complex **IV** is based on a monomer where cadmium is bonded to two chloride ions (Cd–Cl 2.4443 and 2.4782 Å) and two sulfur atoms from the thiourea ligands (Cd–S 2.5010 and 2.5212 Å; C–S 1.7963 and 1.6425 Å). The co-ordination geometry around cadmium can be described as a distorted tetrahedron. The bond angles are close to those of a perfect tetrahedron, S(2)–Cd(1)–S(1) 108.43°, S(2)–

Cd(1)–Cl(1) 110.57°, S(1)–Cd(1)–Cl(1) 108.10°, Cl(2)–Cd(1)–Cl(1) 108.83°, Cl(2)–Cd(1)–S(1) 110.12° and Cl(2)–Cd(1)–S(2) 110.75° around cadmium ion. In a unit cell, the methyl groups in each thiourea ligand lie closer to the sulfur atoms of the neighboring compound, due to the existence of hydrogen bond interactions. These hydrogen bond interactions exist also between the chloride ions and the other methyl group.

Table 5: Selected bond distances (Å) and bond angles (°) for complex **II**.

Bond distances (Å)		Bond angles (°)	
Cd(1)-Cl(1)	2.502(0.0016)	S(1)-Cd(1)-S(2)	111.20(0.06)
Cd(1)-Cl(2)	2.456(0.0016)	S(1)-Cd(1)-Cl(2)	112.89(0.06)
Cd(1)-S(1)	2.522(0.0018)	S(2)-Cd(1)-Cl(2)	113.80(0.06)
Cd(1)-S(2)	2.495(0.0018)	Cl(1)-Cd(1)-Cl(2)	106.40(0.06)
S(1)-C(1)	1.736(0.0073)	Cl(1)-Cd(1)-S(2)	107.70(0.06)
S(2)-C(2)	1.714(0.0053)	Cl(1)-Cd(1)-S(1)	104.10(0.06)
N(1)-C(1)	1.333(0.0090)	Cd(1)-S(2)-C(2)	106.60(0.19)
N(3)-C(2)	1.317(0.0077)	Cd(1)-S(1)-C(1)	97.32(0.26)
N(2)-C(2)	1.309(0.0075)	S(2)-C(2)-N(3)	122.15(0.46)
N(4)-C(1)	1.356(0.0092)	S(1)-C(1)-N(1)	119.99(0.52)
		N(1)-C(1)-N(2)	118.67(0.66)
		S(1)-C(1)-N(4)	121.33(0.57)

(a)

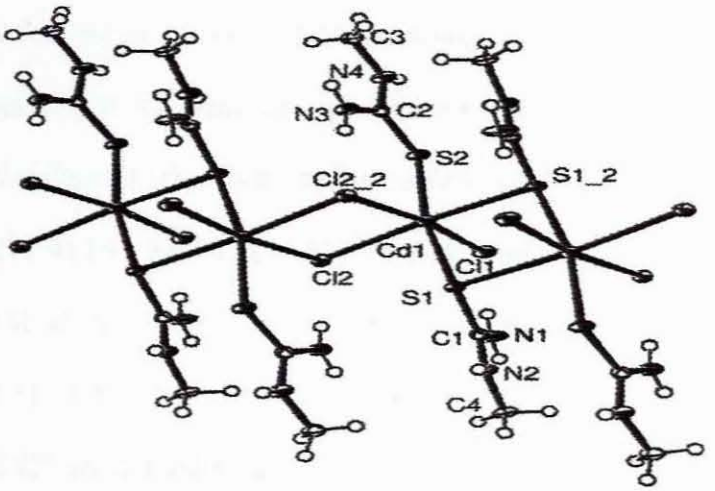

(b)

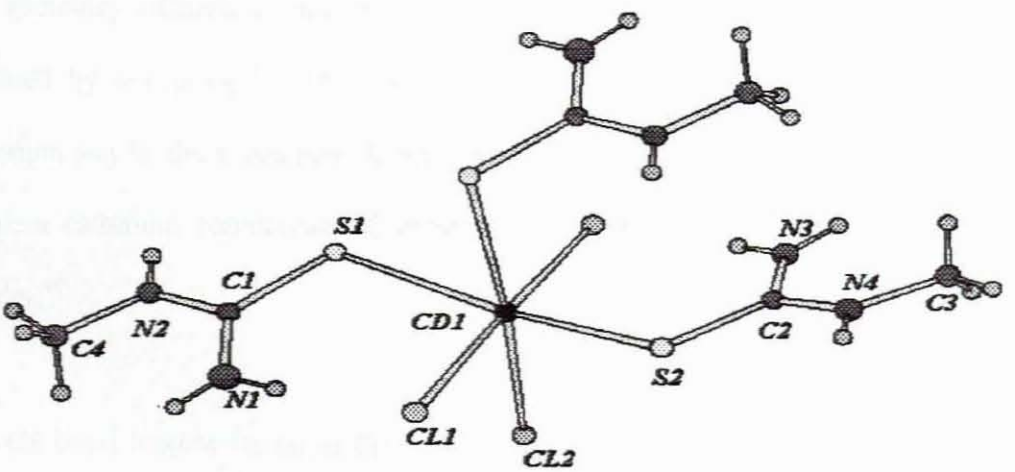

Figure 9: Polymeric structure (a) and molecular unit (b) for complex **I**, $[CdCl_3(CS(NH_2)NHCH_3)_3]_n$.

The cadmium(II) ion in complex **III** is bonded to two chloride ions (Cd–Cl 2.7557 and 2.4782 Å) and four sulfur atoms from the thiourea ligands (Cd–S 2.6282 and 2.7429 Å; C–S 1.7095 and 1.7214 Å), hence the co-ordination geometry around it can be described as a distorted octahedron. The bond angles (Table 6) are those of a distorted octahedron, S(2)–Cd(1)–S(1) 91.19°, S(2)–Cd(1)–Cl(1) 90.28°, S(1)–Cd(1)–Cl(1) 87.49°, Cl(1)#1–Cd(1)–Cl(1) 180.0°, S(1)–Cd(1)–S(1)#1 180.0°, S(2)–Cd(1)–S(2)#1 180.0°, Cl(1)#1–Cd(1)–S(1) 92.51°, Cl(1)#1–Cd(1)–S(2) 89.72°, S(1)–Cd(1)–S(2)#1 88.81° and Cl(1)#1–Cd(1)–S(2) 89.72° around cadmium. The common feature in the two structures is the coordination behavior of the thiourea ligands in that both are mono-coordinated by sulfur atoms to the cadmium atom. The geometry (distorted octahedral) for complex **III** is similar to the polymeric complex, $CdCl_2(CS(NH_2)NHCH_3)_2$, whereas complex **IV** shares the geometry (distorted tetrahedral) with the complex, $CdCl_2(CS(NH_2)NHCH_2CH_3)_2$ reported by our group.[134] The bond length variations and the geometries around the cadmium ion in these compounds are consistent with other similar N-alkyl substituted thiourea cadmium compounds (Complexes **I** and **II**)[135] and the bis(thiourea)cadmium halides.[40]

The CS bond lengths lie on in the range associated with CS single bonds (1.70 – 1.80 Å)[135] for complex **IV**, whereas for complex **III**, they lie at the lower end. The phenyl groups in complex **III** adopt a pseudo-anti-periplanar arrangement in order to minimize their steric crowding. The C–N bond lengths of the amide group of the thiourea ligands are intermediate between a single and a double bond (1.3182 – 1.3403 Å) in complex **III**, whereas they lie on both end of the single and double bond (1.2428 – 1.4185 Å) in

complex **IV**. This is attributed to the delocalization of electrons in the amide bond of the thiourea ligands. The CN and CS bond lengths for complexes **III** and **IV** are similar in character to those in complexes **I** and **II,** which indicates intermediate bonds between a single and a double bond. The average CN and CS bond lengths in complex **III** were observed as 1.329 and 1.715 Å, respectively. In complex IV the average bond lengths for CN and CS were observed as 1.323 and 1.72 Å.

Table 6: Selected bond distances (Å) and bond angles (°) for complex **III**.

Bond distances (Å)		**Bond angles (°)**	
Cd(1)-Cl(1)	2.7556 (9)	S(1)-Cd(1)-S(2)	91.19 (2)
Cd(1)-Cl(1)#1	2.7556 (9)	S(1)-Cd(1)-Cl(1)#1	92.51 (2)
Cd(1)-S(1)	2.6282 (8)	S(2)-Cd(1)-Cl(1)#1	89.72 (2)
Cd(1)-S(1)#1	2.6282 (8)	Cl(1)-Cd(1)-Cl(1)#1	180.00 (15)
Cd(1)-S(2)	2.7429 (7)	Cl(1)-Cd(1)-S(2)	90.28 (2)
Cd(1)-S(2)#1	2.7429 (7)	Cl(1)-Cd(1)-S(1)	87.49 (2)
S(1)-C(1)	1.708 (2)	S(1)-Cd(1)-S(2)#1	88.81 (2)
S(2)-C(8)	1.722 (2)	S(1)-Cd(1)-S(1)#1	180.00 (2)
N(1)-C(1)	1.324 (3)	S(2)-Cd(1)-S(1)#1	88.81 (2)
N(3)-C(8)	1.323 (3)	S(2)#1-Cd(1)-S(1)#1	91.19 (2)
N(2)-C(1)	1.338 (3)	S(2)-Cd(1)-S(2)#1	180.00
N(4)-C(8)	1.333 (3)	S(1)#1-Cd(1)-Cl(1)#1	87.49 (2)
		S(2)#1-Cd(1)-Cl(1)#1	90.28 (2)
		S(2)#1-Cd(1)-Cl(1)	89.72 (2)

Symmetry transformations used to generate equivalent atoms:

$-x + ½, -y + ½, -z + ½$

(a)

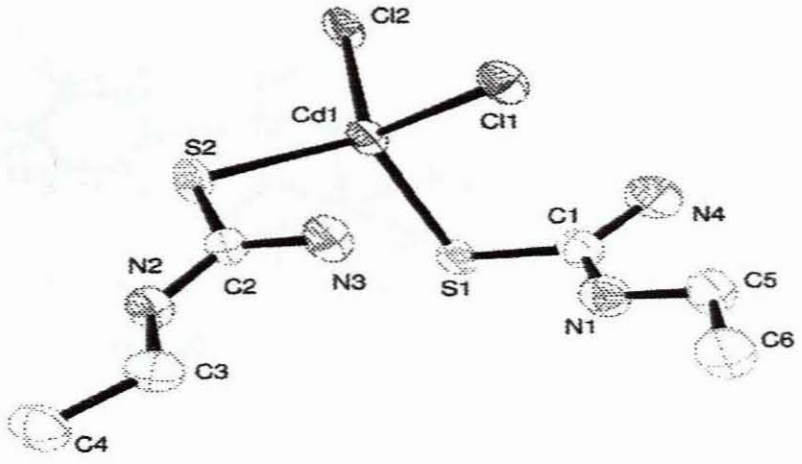

(b)

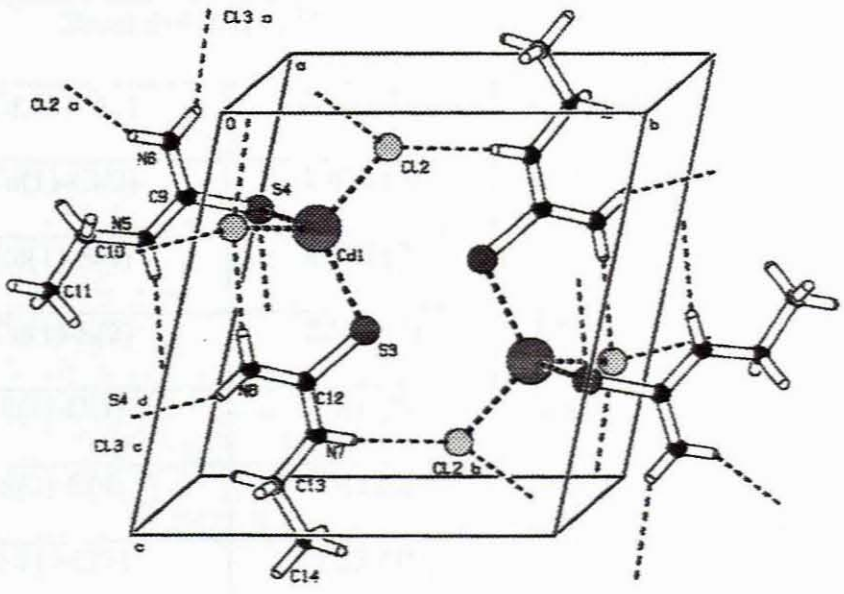

Figure 10: Molecular structure (a) and packing diagram (b) for complex **II**, $CdCl_2(CS(NH_2)NHCH_2CH_3)_2$.

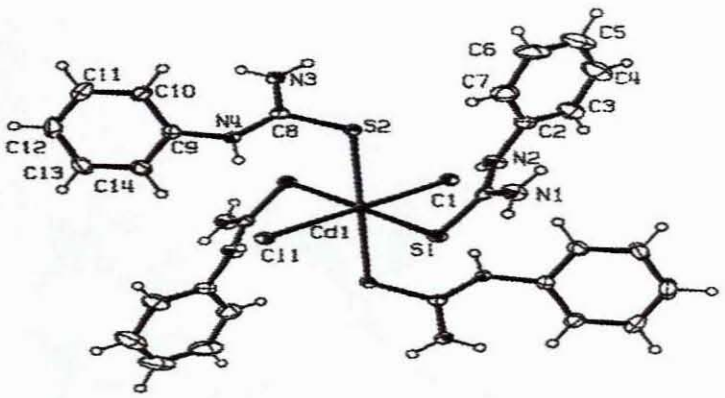

Figure 11: ORTEP drawing for complex **III**, $CdCl_2(CS(NH_2)NHC_6H_5)_4$.

Table 7: Selected bond distances (Å) and bond angles (°) for complex **IV**.

Bond distances (Å)		**Bond angles (°)**	
Cd(1)-Cl(1)	2.472 (8)	S(1)-Cd(1)-S(2)	108.43 (10)
Cd(1)-Cl(2)	2.450 (9)	S(1)-Cd(1)-Cl(2)	110.3 (2)
Cd(1)-S(1)	2.502 (7)	S(2)-Cd(1)-Cl(2)	111.0 (3)
Cd(1)-S(2)	2.521 (7)	Cl(1)-Cd(1)-Cl(2)	108.83 (13)
S(1)-C(1)	1.81 (2)	Cl(1)-Cd(1)-S(2)	110.4 (3)
S(2)-C(4)	1.63 (2)	Cl(1)-Cd(1)-S(1)	107.9 (3)
N(1)-C(1)	1.33 (3)		
N(3)-C(4)	1.30 (3)		
N(2)-C(1)	1.22 (4)		
N(4)-C(4)	1.44 (3)		

(a)

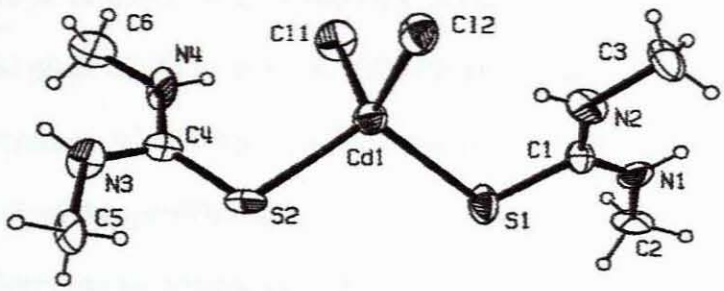

(b)

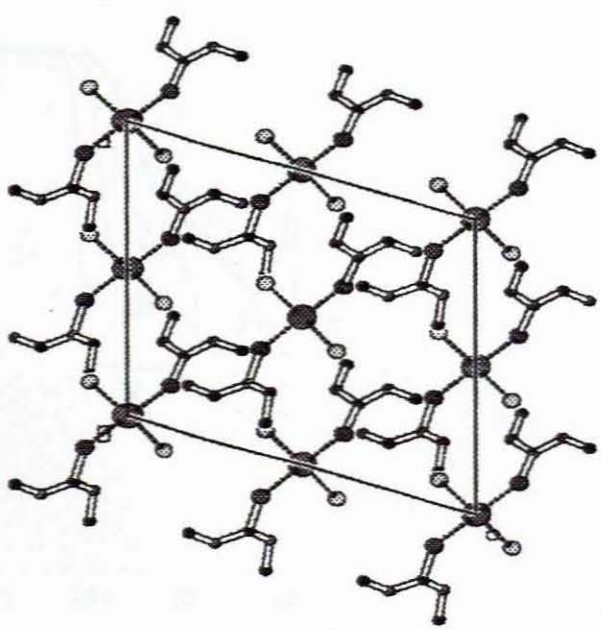

Figure 12: ORTEP drawing for complex **IV**, ($CdCl_2[CS(NHCH_3)_2]_2$) (a) and its packing diagram (b).

1.3.1.4. Thermogravimetric analysis of complexes

Thermal decomposition of thiourea-metal complexes of copper, zinc and tin in static air led to the formation of metal sulphides in a main degradation step between 200 °C and 300 °C.[136] There is evidence of an exothermic process from TGA resulting from the conversion of the metal sulphides to metal oxides at temperatures well above 350 °C. The thermal decompositions of the complexes **I-V** reported in this work (Figure 13) were also studied by using thermogravimetric (TGA) and differential thermal analysis (DTA) methods under inert and air atmosphere. The residues obtained from the decompositions of some selected cadmium complexes were subjected to XRD analysis. X ray diffraction patterns of the residues obtained from complex **II** is shown in Figure 14 and the data listed in Table 8.

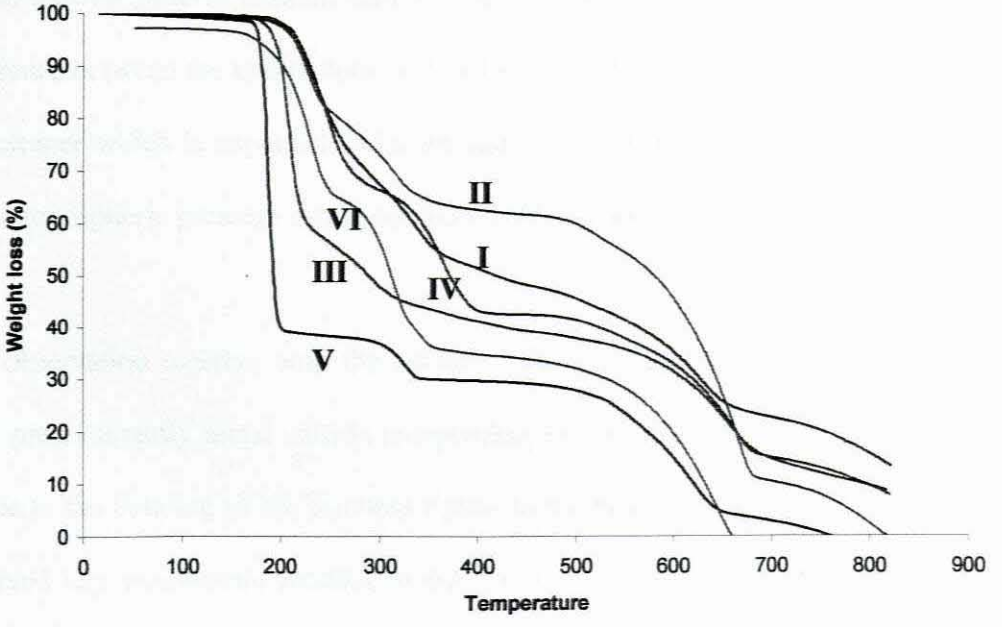

Figure 13: TGA curves for complexes **I – VI** under inert atmosphere.

1.3.1.4. Thermogravimetric analysis of complexes

Thermal decomposition of thiourea-metal complexes of copper, zinc and tin in static air led to the formation of metal sulphides in a main degradation step between 200 °C and 300 °C.[136] There is evidence of an exothermic process from TGA resulting from the conversion of the metal sulphides to metal oxides at temperatures well above 350 °C. The thermal decompositions of the complexes **I-V** reported in this work (Figure 13) were also studied by using thermogravimetric (TGA) and differential thermal analysis (DTA) methods under inert and air atmosphere. The residues obtained from the decompositions of some selected cadmium complexes were subjected to XRD analysis. X ray diffraction patterns of the residues obtained from complex **II** is shown in Figure 14 and the data listed in Table 8.

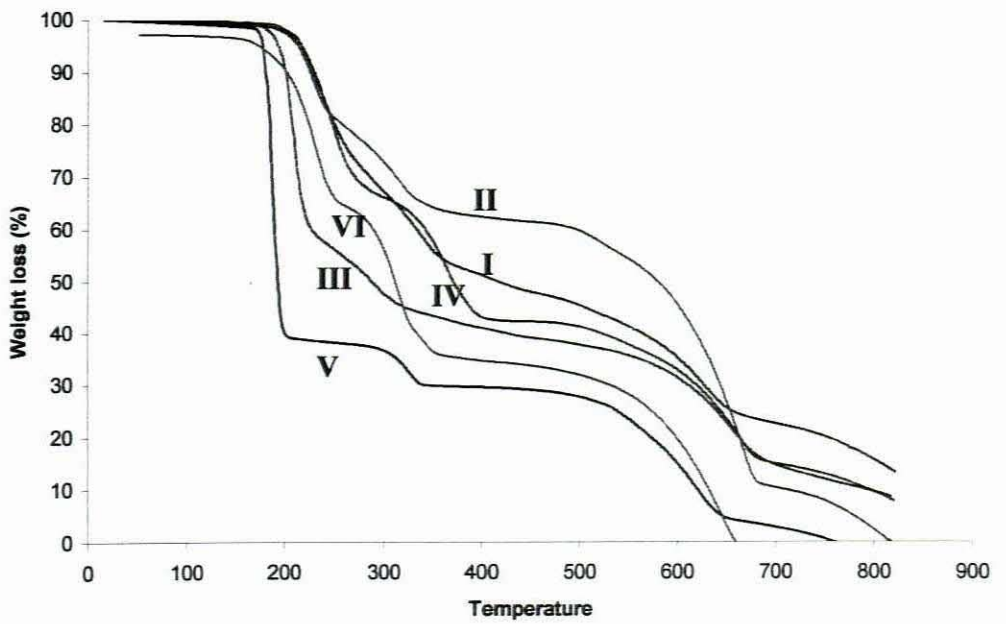

Figure 13: TGA curves for complexes **I – VI** under inert atmosphere.

Under nitrogen cadmium complexes initially appear to melt, the melted products rapidly change to a pale yellow solid. Under air, the compounds undergo similar changes at the start of decomposition, but as the temperature is increased the yellow solid changes further to orange and finally to dirty green. The TGA curves (Figure 13) indicate that the loss of weight started in each compound around 200 °C and continue to about 400 °C where most of the organic part of the molecule and the chlorides has been lost. A period of slow loss of mass led to the formation of the metal sulphide, which was completed at about 500 – 600 °C. This conforms to the theoretical percentages of CdS expected to be formed the complexes as follows: **I** (39.7%), **II** (36.9%), **III** (30.2%), **IV** (36.9%) and **V** (27.6%). A further loss of weight was observed at temperatures well above 600 °C. The residues collected in both cases were analyzed by X-ray diffraction methods (Figure 14a, b) and showed patterns predominantly of the wurtzite phase of CdS (Table 8). The only difference between the two patterns is that the diffraction pattern in Figure 14a is sharper and cleaner which is expected under nitrogen atmosphere whereas the residue obtained under atmospheric pressure shows comparatively broader peaks with some impurities.

This observation together with the colour of the residue indicated that these complexes yield predominantly metal sulfide independent of the atmospheric conditions. This may be due to the bonding of the thiourea ligand to the metal as sulfide source. We have not observed any exothermic process in our TGA curve (Figure 13) in contrast to those observed for copper, zinc and tin thiourea complexes[136] in which cases the metal sulfides were converted to their metal oxides. No such conversion of cadmium sulfide into cadmium oxide was observed during thermal decomposition of complexes reported in

this work under air. This is also evident from the TGA curves obtained of these complexes in which there is no change of residue from the sulfide to oxide, which is usually accompanied by the slight increment of the curve at very high temperatures. Further characterization of the residue of the thermal decomposition of the precursor complexes was done mainly for cadmium complexes as a preliminary study to investigate the possibility of these complexes being used as precursors for the preparation of nanoparticles. This follows the successful use of the single-source molecular precursor to prepare metal sulfide nanoparticles and their volatility as primary requirements for the deposition of thin films.

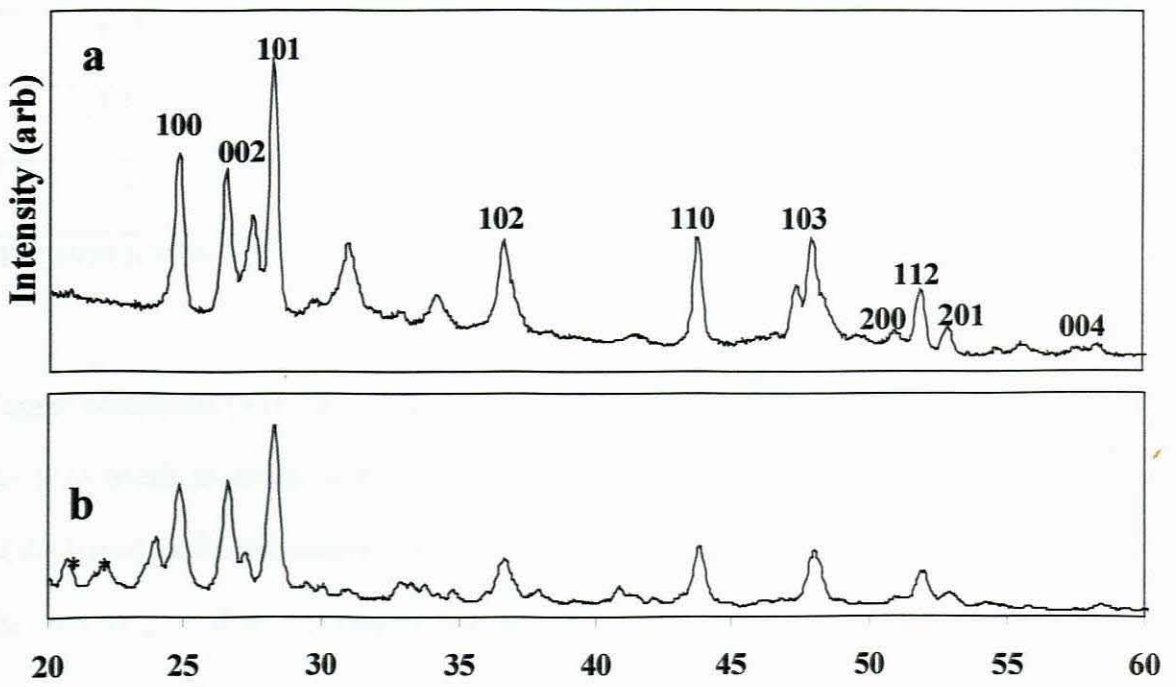

Figure 14: XRD patterns of the residue obtained from thermal decomposition of complex **II**, both in air (b) and under N_2 (a) atmosphere (* - impurities).

Table 8: Experimental XRD data of the residues from TGA analysis of complex **II**

d(lit*)/Å	d(exp)/ Å		hkl
	a (nitrogen)	B (air)	
3.57	3.61	3.59	100
3.34	3.37	3.36	002
3.14	3.17	3.16	101
2.44	2.44	2.45	102
2.09	2.06	2.07	110
1.91	1.89	1.90	103
1.78	1.79	1.79	200
1.75	1.76	1.77	112
1.72	1.73	1.73	201
1.67	1.68	1.69	004

* Ref 1999 JCPDS

Copper complexes (**VII**, **IX** and **X**) thermally decompose to give black residues in which the TGA trends is similar to those of cadmium complexes (Figure 15). The organic part of the ligand easily decomposes initially and followed by the loss of the chlorides, with the resulting residue corresponding to percentage of copper sulfide obtained experimentally. The onset of thermal decomposition for all the copper complex ranges from about 201 to 230 °C and this correspond to their melting points region. This continues to about 400 °C where most of the organic parts of the molecule and the chlorides have been lost. A period of slow loss of mass led to the formation of sulfide,

which was completed by about 500 – 600 °C. This conforms with the theoretical percentages of copper sulfide in the complexes as follows: **VII** (52.3), **IX** (45.6) and **X** (36.7). No further loss of weight was observed at temperatures well above 600 °C.

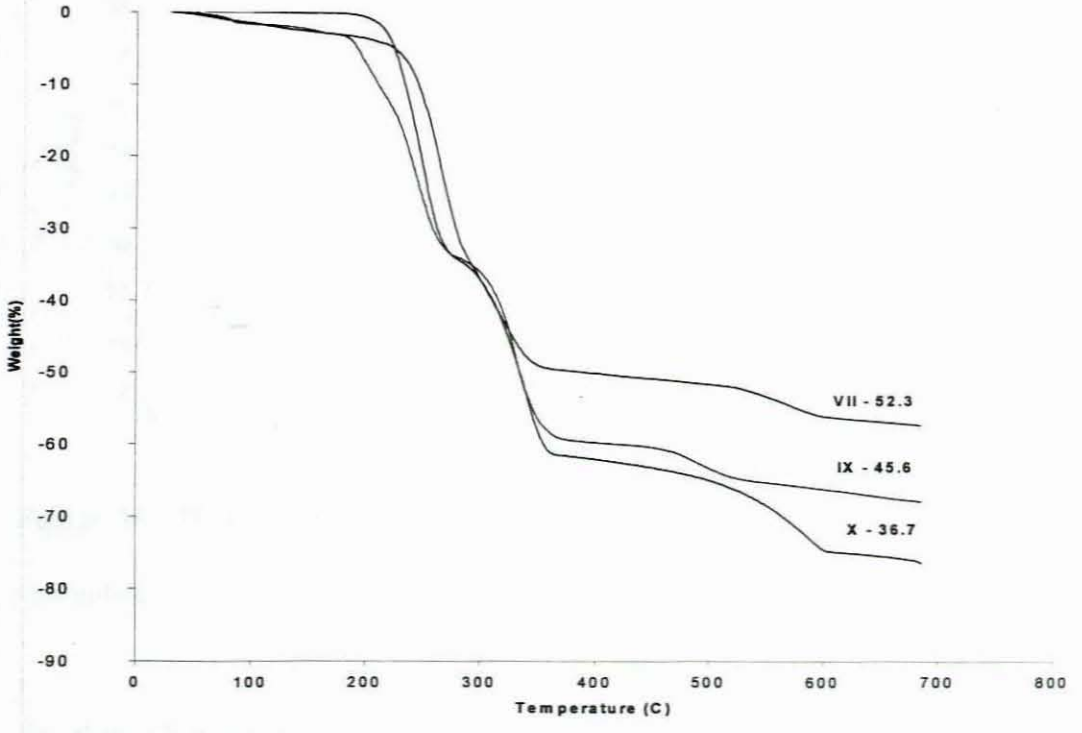

Figure 15: TGA curves for copper complexes **VII, IX** and **X** under inert atmosphere.

The zinc complex (complex **XI**) decomposes in a similar pattern to the corresponding cadmium complex **II** in Figure 13, with the onset at about 216 °C and this continues until the curve flattened when the entire residue left is only zinc sulfide. Mass loss continues to about 350 °C where most of the organic component of the precursor complex and the chlorides has been lost. A period of slow loss of mass led to the formation of the sulfide, which was completed by about 450 – 550 °C.

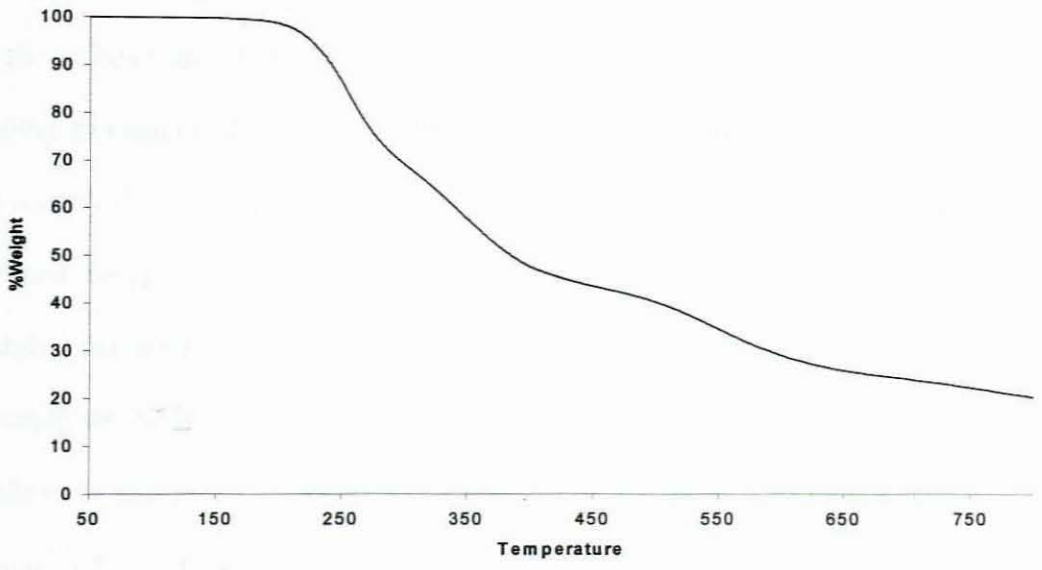

Figure 16: TGA curve for zinc complex, $ZnCl_2(CS(NH_2)NHCH_3)_2$ **(XI)** under inert atmosphere.

The theoretical percentage of zinc sulfide in the complex, 30.78% is relatively in good agreement with the flattening of the curve (Figure 16), which corresponds to about 27.8%. The trends in decomposition of these complexes yielded products, which in colour corresponds to the Cu, Pb and Cd sulfides. It follows from the detailed analysis of CdS from these residues that Cu and Pb would also be useful for preparing nanoparticles and for their potential for deposition of thin films. This sets good precedents for the use of these complexes as single-source precursors to the preparation of nanoparticles and thin films by chemical vapor deposition.

1.3.1.5. Conclusion

The structures of the cadmium complexes **I, II, III** and **IV** indicated that bonding of the N-alkylthiourea ligands is through sulphur atom of the CS group. This is also supported by the infrared and NMR spectroscopic studies of all complexes, which revealed the binding characters of the thiourea ligands. All alkyl groups on the thiourea have no particular influence on the binding of the ligands either through nitrogen or sulfur atom to different metals. Complex **I** is polymeric with alternating chlorine and sulphur atoms bridging the adjacent metal centres. Both ligands are in a *syn* conformational form; however, the NMR spectral results reveal some detectable amounts of the *anti* isomer in solution. In addition to the X-ray diffraction results, the infrared spectral results indicate a change in the bond character of the C—S and C—N bonds in the thioamide core.

Thermogravimetric studies and the XRD data of the decomposed residue revealed the wurtzite CdS particles, which is a clear indication that these complexes can be used as precursors for the deposition of CdS thin films and nanoparticles. Both structures are monomeric with a distorted tetrahedral geometry for complex **IV** and a distorted octahedral geometry for complex **III**. In both cases the thiourea ligands were co-ordinated to the metal atom by sulphur atoms. Copper complexes also gave distinct structures in that they form multi-nuclear systems with sulfur atoms bridging the copper atoms in an oxidation state of +1. As expected the reaction between copper and thiourea causes reduction from Cu(II) to Cu(I). A combination of analytical techniques used also revealed that lead complexes are monomeric, with sulfur atom binding the alkylthiourea ligand to the metal in a similar way to cadmium and copper complexes. The complexes

appear to be suitable for the deposition of thin films as well as preparation of nanoparticles as they have both the metal and sulfide in a single compound, easy to prepare, inexpensive and highly air and moisture stable.

CHAPTER 2

SYNTHESIS OF CADMIUM, COPPER AND LEAD SULFIDE NANOPARTICLES

2.1. INTRODUCTION

2.1.1. General background

Nanotechnology is the development and utilisation of structures and devices with a size range from 1 nm (molecular size) to about 20 nm, where new physical, chemical and biological properties might occur by comparison to bulk materials. This is an emerging technology of the 21st century. The size range and particularly the new phenomena set apart nanotechnology from micro-electrical-mechanical systems and/or micro systems technologies. Current interest in nanotechnology is broad based and includes the following:

- Synthesis, processing, properties, characterisation, modelling, simulation and use of nanostructured materials including high-rate production of nanoparticles for potential industrial use.
- Research and development on thermal spray processing and chemistry based techniques for depositing multi-layered nanostructured coatings, processing of nanoscale powders into bulk structures and coatings.
- Nanofabrication with particular focus on the electronic industry that includes development of technologies seeking improved speed, density power and functionality beyond that achieved by simply scaling transistors, operation at room temperature, use of quantum well electronic devices and computational nanotechnology addressing physics and chemistry related issues.
- Research on nanoscale materials for energy applications with focus on synthesis and processing of materials with controlled structures, surface passivation and

interface properties. The targeted applications are catalysis, opto-electronics and soft magnets.

- ❖ Miniaturisation of spacecraft systems and the theoretical modelling addressing the physical and chemical aspects of nanostructures.
- ❖ Biomimetics, smart structures, micro-devices for tele-medicine, compact power sources, superlattices and buckminsterfullerene are developed in interdisciplinary environment.
- ❖ Nanoparticles are also used in drug delivery. They are used to deliver drugs that have poor water solubility in which they are coated with polymers to provide controlled release systems. Pre-clinical results of delivering insulin in an inhaled form, subcutaneously or orally, using calcium phosphate nanoparticles have been reported.
- ❖ Nanoparticulate silver is commercially produced in antibacterial dressings and nanoparticulate zinc is used as a fungicide.
- ❖ The surface area-to-volume ratio of particles increases as the size is reduced, making the surface effects dominant. Catalysis generally occurs on the surface of materials and nanoparticles offer a greater reaction surface for a given amount of material and hence it can create improved catalysts.

During the past decade "small particles research" has become quite popular in various fields of chemistry and physics. These materials are clusters of atoms or molecules of metals and semiconductors, ranging in size 1 nm to 20 nm. These are particulate semiconducting materials most often referred to as quantum dots, Q particles or

nanoparticles. Nanocrystalline semiconductors are materials with intriguing electronic properties intermediate between those macro crystalline solids and molecular entities. One interesting possibility is the use of particle size as a control parameter in order to tailor band gap, which provides a novel approach to the development of materials for device applications; several uses are anticipated, including photocatalysis,[136] light emitting diodes,[137, 138] and in electrochemical cells.[139] Nanocrystallites have been prepared by a wide range of synthetic methods.[136, 140 - 145] One of the approaches which has received much attention involves the classical techniques of colloidal chemistry, which for some semiconductors such as metal chalcogenide have disadvantages, including the use of noxious compounds such as H_2Se or H_2S and a potential for the adventitious incorporation of oxide.

The use of single source molecular precursors, as initially reported by Trindade and O'Brien[146, 147] has proven to be an efficient route to high quality crystalline monodispersed nanoparticles of semi conducting material. Air-sensitive alkyl cadmium dithio- and diselenocarbamates were also used as precursors for the preparation of CdS and CdSe nanoparticles, with later work extending to the preparation of ZnS[148] and ZnSe[149] by using the zinc analogues. Recently air-stable (methylhexyl)dithio/diseleno- carbamatocadmium/zinc complexes have been used as precursors for the deposition of thin films of group II/VI materials by metal organic vapour deposition (MOCVD)[150, 151] and also for the growth of nanoparticles.[152, 153]

Nanoparticles are highly dispersed having a large ratio of surface atoms to those located in the crystal lattice.[154] There has been considerable interest in the electronic and optical properties of semiconductor nanocrystallites, or quantum dots. Samples with absorption and emission properties confined in the near infrared region are increasingly receiving attention because of their applications in devices. Large absorptive and dispersive nonlinearities are predictive for such systems if the quantum-dots transitions are not broadened excessively.[155,156] The dominant intrinsic source of line broadening is expected to be exciton-phonon coupling and motivated studies for the strength and time scale of carrier-phonon interactions in the quantum dots. Strong confinement is most readily achieved in narrow band-gap semiconductors, in which the excitons have a large Bohr radii.[155]

2.1.2. Electronic properties of bulk semiconductors

The study of nanometre-sized crystallites provides an opportunity to observe the evolution of semiconducting material properties with size. This intermediate size regime is where the collective behaviour of bulk materials emerges from the discrete nature of the molecular properties. The differing rate with which each of the bulk properties develops provides the possibility of observing and perhaps controlling novel behaviour. Non-linear optical effects from highly polarizable excited states and novel photochemical behaviour are two such examples.[145,157-159] The physical properties of semiconductor nanocrystallites are dominated by the spatial confinement of excitations (electronic and vibrational). Quantum confinement generally refers to the widening of the HOMO-LUMO gap with decreasing crystallite size. Their

applications for the electronic structure and photophysics of the crystallites have generated considerable interest.[160-164] Although considerable progress has been made in the controlled synthesis of metal chalcogenide semiconductor crystallites, interpretation of sophisticated optical experiments often remains difficult due to polydispersity in size and shape, surface electronic defects due to uneven surface derivatization and poor crystallinity.

The study of an appropriate high quality model system is essential in distinguishing properties truly inherent to the nanometer size regime from those associated with variations in sample quality. Each sample must display a high degree of monodispersity (size and shape), regularity in crystallite core structure and a consistent surface derivatization (capping agent). Macrocrystalline semiconductors, free of defects, consist of three-dimensional networks of ordered atoms. The translational periodicity of the crystal imposes a special form on the electronic wave functions. An electron in the periodic potential field of a crystal can be described using the Bloch type wave function (equation 3) where u(r) represents a Bloch function modulating the plane wave $\phi(\kappa r)$ of wave vector κ.

$$\psi(r) = \phi(\kappa r)u(r) \qquad (3)$$

$$u(r + n) = u(r) \qquad (4)$$

In a bulk semiconductor the large number of atoms leads to the generation of sets of molecular orbitals with very similar energies which effectively form a continuum. At

0 K the lower energy levels or valence band, are filled with electrons while the conduction band consisting of higher energy levels is unoccupied. These two bands are separated by an energy gap (E_g), the magnitude of which is a characteristic property of the bulk macrocrystalline material (at a specific temperature). Materials normally considered to be semiconductors typically exhibit band gaps in the range 0.3 – 3.8 eV. At temperatures above 0 K, electrons in the valence band may receive enough thermal energy to be excited across the band gap into the conduction band. An excited electron in the conduction band together with the resulting hole in the valence band forms an "electron-hole pair". The conductivity (σ) of the semiconductor is governed by the number of electron-hole pairs, the charge carrier concentration (n) and their mobility (μ). Thus conductivity can be expressed as the sum of the electrical conductivities of electrons and holes, eq. 5 (q is the charge of the carrier). In conventional semiconductors electrons (e) and holes (h) are the charge carriers. Although they exist in small numbers as compared to conductors, the charge carrier mobilities in semiconductors are substantially larger than in many conductors.

$$\sigma = qn_e\mu_e + qn_h\mu_h \qquad (5)$$

The charge carriers in a semiconductor can form a bound state when they approach each other in space. This bound electron-hole pair, known as a Wannier exciton is delocalized within the crystal lattice and experiences a screened Coulombic interaction. The Bohr radius of the bulk exciton is given by equation 6 (ϵ represents

the bulk optical dielectric coefficient, e the elementary charge and m_e^* and m_h^* the effective mass of the electron and hole respectively.

$$A_B = \hbar^2 \epsilon / e^2[1/ m_e^* + 1/ m_h^*] \qquad (6)$$

2.1.3. Properties of nanocrystalline semiconductors

For nanocrystalline semiconductors there are two fundamental factors both related to the size of the individual nanocrystal that distinguish their behaviour from the corresponding macrocrystalline material. The first is the high dispersity i.e. large surface/volume ratio associated with the particles, with both the physical and chemical properties of the semiconductor being particularly sensitive to the surface structure. The second factor is the actual size of the particle, which can determine the electronic and physical properties of the material. The absorption and scattering of light in larger colloidal particles is different from nanocrystalline particles. However, the optical spectra of nanocrystalline metal sulfide semiconductors, which show blue shifts in the absorption edge as the size of the particle decreases, cannot be explained by classical theory.[165-168]

Such size-dependent properties are examples of the size quantization effects, which occur when the size of the nanoparticle is smaller than the bulk-exciton Bohr radius, a_B of the semiconductor ($l << R < a_B$). Equation 6 defines for a spherical particle of radius R, the region of intermediate character between that of a "molecule" and that of the bulk material (l is the lattice spacings). Charge carriers in semiconductor

nanocrystallites are confined to three dimensions by the crystallite. The wave function of an ideal quantum confinement has to satisfy the boundary conditions, $\psi(r \geq R) = 0$. For nanoparticles the electron and hole are closer together than in the macrocrystalline material, and as such the Coulombic interaction between electron and hole cannot be neglected; they have higher kinetic energy than in the macrocrystalline material. Brus[166-168] showed on the basis of effective mass approximation that for CdE (E = S or Se) nanocrystallites the size dependence on the energy of the first electronic transition of the exciton (or the band gap shift with respect to the typical bulk value) can be approximated using the equation,

$$\Delta E \cong (\hbar^2\pi^2/2R^2)[1/ m_e^* + 1/ m_h^*] - (1.8e^2/\epsilon R) \qquad (7)$$

where R = radius of the particle, ε = bulk optical dielectric coefficient, m_e^* = effective mass of the electron and m_h^* = effective mass of the hole.

This approximation of the first electronic transition of an exciton, can be described by a hydrogenic Hamiltonian,

$$\hat{H} = (-\hbar^2/2m_e^*)\nabla_e^2 - (\hbar^2/2m_h^*)\nabla_h^2 - e^2/\epsilon\, r_e - r_h \qquad (8)$$

From equation 7 the Coulomb term ($1.8e^2/\epsilon R$) shifts the first excited electronic state to lower energy, R^{-1}, while the quantum localisation term ($\hbar^2\pi^2/2R^2$) shift the state to higher energy, R^{-2}. Consequently the first excitonic transition (or band gap) increases in energy with decreasing particle diameter. This prediction has been confirmed

experimentally for a wide range of semiconductor nanocrystallites[140,144,154,159,169,170] with a blue shift in the onset of the absorption of light being observed with decreasing particle diameter. Moreover, the valence and conduction bands in nanocrystalline materials consist of discrete sets of electronic levels. Equation **7** does not account for the coupling of electronic states and effects attributed to surface structure. The constants used in the model (dielectric constants and effective masses) are those for macrocrystalline solids, hence the model is not quantitatively accurate with calculations deviating from experimental values especially for very smaller nanocrystallites. In such small particles the first electronic transition is located in a region of the energy band in which the normal effective mass approximation is not valid. Other theoretical methods have been used to explain the size-dependent electronic properties of nanoparticle semiconductors.[145,171-175] These models provide reasonable estimates for the band gap shifts observed experimentally for nanoparticles (e.g. II/VI semiconductors), provided the particles are not too small (typically > 4 nm). The empirical pseudopotential method described by Krishna and Friesner[175-177] correlate well with experimental values over a wide range of particle sizes.

Typically, bulk samples of CdS, irrespective of their size once greater than about 20 nm, wi ll absorb all electromagnetic radiation with an energy greater than the band gap ($h\upsilon$ = 2.42 eV), which is classified in this case as direct.[178-182] However, as particles become smaller, their electronic structure changes, eventually the description of the material as containing continuous bands breaks down and there are discrete bonding and antibonding levels in the material.[181-183] The electronic properties of such

small particles are hence more like those of a molecule than an extended solid. The electronic, optical and catalytic properties of such small particles will depend on their size and the material they are composed of.[154,184-186] For a semiconductor such as cadmium sulfide, these effects were predicted for some years to become important in the size range of about 1 to 10 nm. The preparation of stable particles in this size range has presented a considerable challenge to the chemist and such materials have been synthesised from aqueous solutions, adapting the approaches of colloid chemistry, or by the controlled decomposition of organometallic compounds. Such small particles have relatively large surface areas and control of their surface chemistry has been important in developing stable forms of these materials and in controlling their properties.

The 'band gap' of a quantum-confined semiconductor is greater than that of the parent bulk material from which it is derived. This is an effect, which is a consequence of the confinement of the electron in a three-dimensional 'box' with discrete energy levels rather than in the quasi-continuous band of a bulk material[187] (Figure 17). The absorption of electromagnetic radiation by quantum dots, of materials such as CdS, is hence relatively easy to appreciate. However, explaining the luminescent behaviour of such materials is more complicated but crucially important in identifying materials of sufficient quality for potential practical applications. The ideas emerging from these phenomena illustrate interesting interplay between experiment and theory. The coordination of surface atoms in nanoparticles is incomplete, making them highly reactive, which can lead to particle agglomeration.

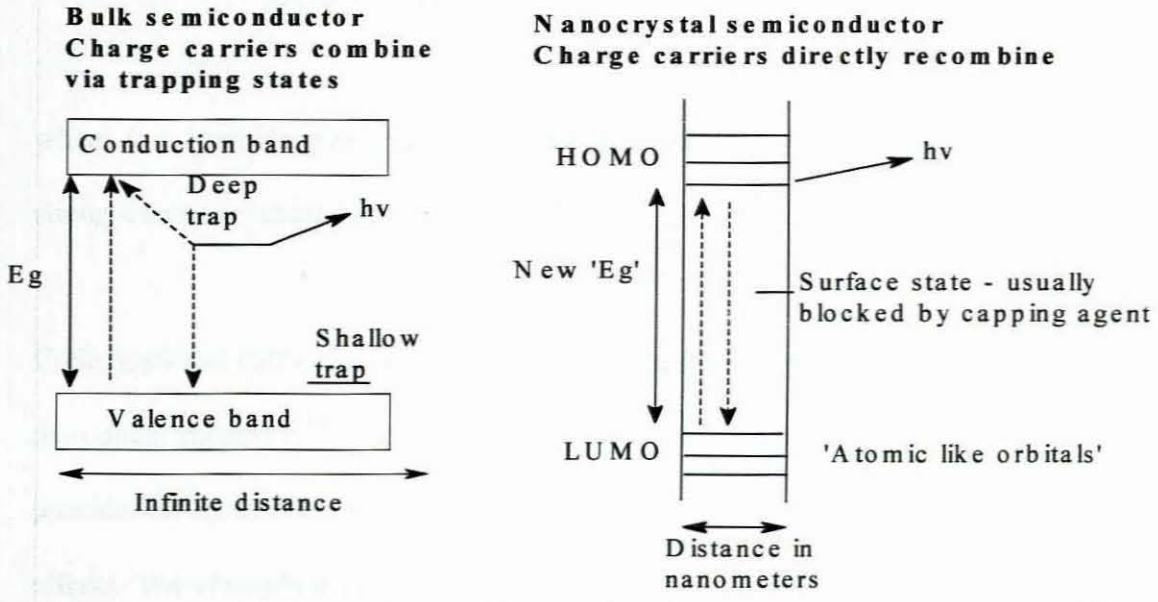

Figure 17: Spatial electronic state diagram for bulk semiconductor and nanoparticles after Brus and co-workers[187]

The problem of agglomeration of particles tends to be overcome by passivating (capping) the surface atoms with protecting groups. The capping or passivating of particles not only prevents agglomeration from occurring, it also protects the particles from its surrounding environment, and provides electronic stabilisation to the surface. The capping agent usually takes the form of a Lewis base compound covalently bound to surface metal atoms. In addition to the blue shift in the absorption edge, the presence of a peak, often described as excitonic, is taken as evidence of quantum confinement, that is, the spectrum starts to resemble a molecule with discrete absorptions rather than a solid absorption with continuous band. Moreover, a decrease in the radius of the particles such that it is much less than the Bohr radius leads to higher oscillator strength:

$$f/f_{ex} = ¾(a_B/R)^3, \quad (9)$$

where R = particle size, f_{ex} = oscillator strength in bulk material, f = oscillator strength and a_B = excitonic Bohr radius.[188]

CdSe, CdS and CdTe are examples of materials that show strong excitonic features in the optical spectrum.[189] The optical absorption spectrum of a nanocrystalline particle provides an accessible and straightforward method for the evaluation of quantum size effects. The absorption of a photon leading to the excitation of an electron from the valence band to the conduction band is associated with the band gap, E_g. The absorption of a photon with energy similar to that of the band gap, $h\upsilon \geq E_g$, leads to an optical transition producing an electron in the conduction band of the semiconductor along with a hole in the valence band. Absorption of a photon with energy much greater than E_g leads to excitations above the conduction band edge; these electrons can loose excess energy by a radiationless process. The absorption (A) of light by a semiconductor material with thickness (l) can be expressed by an expression analogous to the Beer law (eq. 11), where α represents the absorption coefficient of the solid and is a function of the radiation frequency.

$$A = \alpha l \quad (10)$$

All electronic transitions are subject to selection rules; for semiconductors the requirements (besides $h\upsilon \geq E_g$) are that the wave vector, **k**, should be conserved.

$\mathbf{k}_{photon}$ is small when compared with the wave vectors of the electron before ($\mathbf{k}_e$) and after excitation ($\mathbf{k'}_e$).

$$\mathbf{k}_e + \mathbf{k}_{photon} = \mathbf{k'}_e \qquad (\mathbf{k}_e = \mathbf{k'}_e) \qquad (11)$$

The absorption coefficient for a photon of a given energy is proportional to probability (P_{if}), the density of states in the initial state (n_i), and the density of available final states (n_f). Therefore, for all possible transitions between states separated by energy difference equal to the energy of the incident photon;

$$\alpha(h\upsilon) \propto \Sigma(P_{if} n_i n_f) \qquad (12)$$

Semiconductors in which there is conservation of the wave vector for optical transitions are referred to as direct band gap semiconductors and have large absorption coefficients. A relationship between absorption coefficient and the photon energy of a direct transition near the threshold is given by;

$$\alpha(h\upsilon) \propto (E_g - h\upsilon)^{1/2} \qquad (13)$$

Therefore the "band gap" energy of nanocrystalline semiconductors can be estimated experimentally from its optical spectrum using the expression in equation 14. Experimentally quantum size effects are observed as a shift to higher energy values for the band edge (a blue shift), as compared to the value of the corresponding

macrocrystalline material. Nanocrystalline particles often show peak(s) in the optical spectra at room temperature. The oscillator strength, which is directly proportional to the absorption coefficient, increases as the particle size decrease. This is due to the strong overlapping of the wave function of confined charge carriers (Figure 18). These effects were clearly demonstrated in a study of CdS nanocrystallites with different but well-defined size distributions.[189] Decreasing the particle sizes of CdS leads not only to a shift in the excitonic peak to higher energy but also to an increase in the molar absorption coefficient.

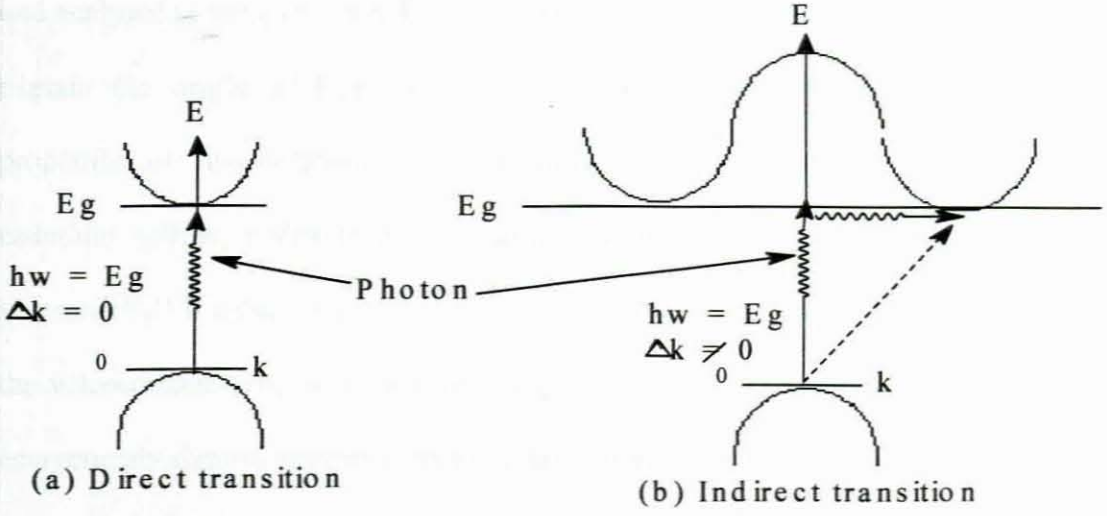

Figure 18: Excitation across the band gap by photon absorption (a) direct process and (b) indirect process

2.1.4. Photoluminescence properties

The absorption of electromagnetic radiation by nanocrystallite materials is relatively straightforward, however, the luminescent behaviour of such particles is more complicated and the ideas that have emerged for explaining these phenomena

illustrate an interesting interplay between experiment and theory. Brus, in his keynote paper,[187] have explained, on the basis of theoretical and experimental studies, the features expected in the luminescence spectra of quantum confined semiconductors and successfully anticipated the results of many subsequent experiments. The luminescence of materials such as CdSe, CdS, CdTe and other nanocrystalline particles show a typical red shift in emission relative to the corresponding absorption spectrum.

The luminescent behaviour of nanocrystalline semiconductors is very complicated and analysed to some extent with controversy. There are two models which attempt to explain the origin of this effect. Brus, *et al.*[187] investigated the luminescence properties of nanocrystalline semiconductors. The investigation was based on cadmium sulfide, which is usually sulfur deficient due to S^{2-} vacancies. The S^{2-} vacancy (V_s^+) is a deep trap for electrons and exothermically extracts an electron from the valence band. The hole localizes away from the defect and the V_s^+ state cannot energetically remove another electron. The V_s^+ vacancy sets a deep (ca. 0.07 eV) trap for a conduction electron, in which they combine forming the V_s^0 state. Luminescence is attributed to the emission from the recombination of the electron in the V_s^0 state and a pre-existing trapped hole. The distribution of the electron-transfer distance R is determined by the density of trapped holes and is independent of the diameter of the cluster. In surface-passivated nanocrystalline materials, the 'plugging' of the surface states by the passivating material minimizes the transfer of electrons to the S^{2-} defects. As a result, electron-hole recombination leads to close to band edge emission. This

has been confirmed experimentally when the surface of nanoparticles are passivated with organic ligands such as tri-n-octylphosphine oxide (TOPO), inorganic phases and/or oxidation of surface molecules, resulting in narrow band edge emission with increased quantum yields.

The second model attributes the red shifted band edge emission observed in luminescence studies on surface passivated CdSe quantum dots to the existence of a "dark exciton".[190-193] The lowest electron-hole pair state or band edge exciton ($1S_{3/2}1Se$) in spherical CdSe quantum dots is eightfold degenerate. However, in non-spherical CdSe quantum dots this degeneracy is split further into five sublevels. This is due to the distortion of the wurtzite lattice of CdSe as a result of crystal field splitting, the non-spherical shape of the particles and the exchange interaction between electron and hole. Of the five sublevels that exist for this system, the levels $|N_m| = 1^U$, 1^L and 0^U are optically active ('bright excitons') and the $|N_m| = 2$ and 0^L states are optically forbidden ('dark excitons'). Transitions from the dark states are forbidden because decay to the ground state requires two units of momentum. This optically forbidden nature of the $|N_m| = 2$ state explains the emission behaviour in CdSe. Excited electrons that occupy the $|N_m| = 1^L$ state relax into the $|N_m| = 2$ state. The energy difference between those two levels accounts for the observed Stokes shift in the luminescence spectrum, which increases as particle size decreases. Emission from the dark state to the ground state occurs when an additional unit of momentum is provided by a phonon. This mechanism also explains the relatively long radiative lifetimes. Photoluminescence studies on a single quantum dot of CdSe with

continuous excitation have recently revealed intermittent light emission,[191] which is attributed to an Auger electron photoionization mechanism. The "on-state" emission occurs from radiative recombination from single electron-hole pairs after photoexcitation. The "off-state" is formed when the particle absorbs two photons, generating two electron-hole pairs and through Auger photoionization there is an ejection of charge (e^- or h^+) outside the dot. Subsequent emission is non-radiative, with the energy being transferred to the carriers, which accounts for the off-state. When the CdSe particles are passivated by another semiconductor, such as ZnS, the average on/off times increases relative to the unpassivated CdSe. This confirms the sensitivity of luminescence to changes at the nanoparticle-matrix interface.

2.1.5. Preparative methods for the synthesis of nanoparticles

Compound semiconductor nanoparticles and nanoparticles of other materials such as metals, metal oxides, carbides, borides, nitrides, silicides, and other elemental semiconductors have been prepared by various methods.[192-200] Ideally, the synthetic method employed should lead to samples of crystalline nanoparticulates of high purity, with a narrow size distribution that are surface derivatized. An example of this is the preparation of nanoparticles of CdS, which involves the reaction between aqueous solutions of $CdSO_4$ and $(NH_4)_2S$ with particle size determined by altering the nucleation kinetics by control of pH.[145] However, although this method works well for the preparation of some semiconductor nanoparticle materials, it is problematic due to air sensitivity and/or poor crystallinity of the material. Other methods involve growth

of nanoparticles in host materials, having defined spaces within their structure that can be viewed as nanosize reaction chambers.[201,202]

2.1.5.1. Colloidal routes

The first reported routes to such small particles involved the controlled precipitation of dilute colloidal solutions and the cessation of growth immediately after nucleation. La Mer, *et al.*[203-205] reported the synthesis of highly monodispersed micrometric colloids in which it was explained if nucleation and growth are properly controlled, particles with dimensions of the order of nanometres can be reproducibly synthesized. Small crystals, which are less stable dissolve and then re-crystallize on larger more stable crystals, a process known as Ostwald ripening. For such methods to be effective the quantum dots must have low solubility, which can be achieved by correct choice of the solvent, pH, temperature and passivating agent. Highly monodispersed samples are obtained if the process of nucleation and growth are distinctly separated that is fast nucleation and slow growth. The colloidal stability of these crystals has been improved by using solvents with low dielectric constants or by using stabilisers such as styrene/maleic acid copolymer.

Henglein,[199] Brus and co-workers[142,200] as well as Weller[140] have made significant contributions to this field especially in the studies of CdS. The control of the size of CdS nanocrystalline was achieved by altering nucleation kinetics using the pH.[142] Some of the most important semiconductors such as CdSe, GaAs, InP and InAs cannot be easily synthesised by this method despite its inefficiency. Annealing of

amorphous particles is also a problem as it involves low temperature, producing poorly crystalline material. Such colloidal particles prepared in aqueous media are not sufficiently stable at higher temperature for annealing without agglomeration. CdS and ZnS have also been produced from methanolic solutions without the use of an organic ligand for stabilisation, using the repulsion of the electrostatic double layer to stop agglomeration.[200]

Zn_3P_2 and Cd_3P_2 have both been produced by aqueous methods, by the injection of phosphine gas into a solution of the relevant metal perchlorate.[206, 207] The control of the particle size was achieved by varying the phosphine concentration and the temperature of the reaction. Samples of both Zn_3P_2 and Cd_3P_2 showed remarkable quantum size effects as observed by changes in the colour of products. They were coloured from white in small Cd_3P_2 particles to brown for the bulk. Surface modifications of semiconductors nanocrystallites can lead to electro- and photoluminescence systems, which may have applications in light emitting devices. One possibility for the preparation of this type of material is the growth of a solid on the surface of another, with the latter acting as a seed for the heterogeneous nucleation of the former. Examples for the use of this method include TiO_2/Cd_3P_2,[208] HgS/CdS,[209] PbS/CdS,[210,211] CdS/HgS,[212] ZnS/CdSe,[213] ZnSe/CdSe[214] and CdSe/ZnS.[215]

Solution methods (Using an aqueous media) provide a cheaper route to synthesis of many nanoparticle materials. However the low temperatures typically used in these

methods mean that any defects formed in the early stages of the preparation are likely to be trapped and the crystallinity of the material will be poor. Also several semiconductors are not easily obtained using these methods, with some being air and/or moisture sensitive e.g. GaAs and InSb.

2.1.5.2. Synthesis in confined matrices

A number of matrices have been used in the preparation of semiconductor nanoparticles and these include, zeolites,[216] layered solids,[217] molecular sieves[218-220] micelles/microemulsions,[221-225] gels,[226-228] polymers[229-233] and glasses.[234] These matrices can be viewed as nanochambers, which limit the size to which crystallites can grow. Their properties are not only determined by the confinements of the host materials but also by the properties of the system, which include the internal/external surface properties of the zeolite and the lability of micelles. Growing particles in the internal cavities of zeolites limits the particle size of materials usually not longer than 20 nm. CdS has been synthesised in two different zeolites by ion exchange from the sodium cationic form to the cadmium cationic form, followed by exposure to H_2S gas. Depending on the amount of cadmium ions utilised, different particle sizes were obtained.[216]

Cadmium telluride nanoparticles have also been prepared in sodium or potassium zeolites. This involved the vapour deposition of tellurium resulting in CdTe clusters. The size of the cluster could be controlled by either a potassium or sodium resin, which altered the pore diameter.[235] PbS nanoparticles were obtained by exchanging

Pb^{2+} into ethylene/methacrylic acid copolymer followed by exposure to H_2S gas. The size of the particles was again controlled by the amount of Pb^{2+} ions resulting with sizes ranging from 13 to 125 nm.[229] A similar technique was used to grow in the interlamellar regions of the layered host, $Zr(O_3PCH_2CH_2COOH)_2$. Conversion of the host to different metals such as Pb, Cd, and Zn followed by treatment with H_2E (E = S, Se) resulted in the growth of metal sulfide and selenide nanoparticles.[236] Cole-Hamilton and co-workers[237-239] have developed an organo- metallic route to polymeric composites of CdSe and ZnSe. This involves the polymer 2-pyridyl-polybutadiene which was reacted with a group IIB metal alkyl, to give an adduct. A toluene solution of polypyridine bound metal alkyl was exposed to H_2Se gas to give particles whose size was mainly controlled by both the solvent and reaction temperature.

GaP nanoparticles have also been prepared in the pores of zeolite Y,[240] in which the vapour transfer of Me_3Ga into a dry Na^+/H^+ exchange zeolite resulted in methane evolution and the formation of $Me_{3-x}Ga$ sites. Exposure of this to excess of PH_3 at various temperatures (200 – 400 °C) resulted in the growth of particles with a size range of 10 – 12 Å. Steigerwald, *et al.*[213,241] prepared capped CdSe, ZnS, ZnS/CdSe, and CdSe/ZnS nanocrystallites from inverse micellar solutions. Silylchalcogenide reagents were added to the microemulsions containing the appropriate metal ions. The particle surfaces were subsequently capped with the phenyl groups or with other semiconductor materials such as ZnS.

$$CdCl_2 + Se(SiMe_3)_2 \xrightarrow{-2Me_3SiCl} CdSe \qquad (14a)$$

$$ZnEt_2 + Se(SiMe_3)_2 \xrightarrow{-2SiEtMe_3} ZnSe \qquad (14b)$$

$$CdMe_2 + Te(Si^iPrMe_2)_2 \xrightarrow{-2Si^iPrMe_3} CdTe \qquad (14c)$$

Silylchalcogenides react readily with metal salts or simple metal alkyls to form metal-chalcogenide bonds as in the equations 14(a), (b) and (c). Another approach to nanocrystallite synthesis in a matrix was developed by Choi and Shea,[226,227] who reported using the porous inorganic-organic xerogel (polysilsesquioxanes) to produce cadmium sulfide and chromium nanoparticles. The chromium precursor used was a zerovalent arene tricarbonyl chromium complex, introduced as a component of the xerogel matrix, which after heating under vacuum produced chromium nanoparticles.

2.1.5.3. Metal-organic routes

A popular method of preparing high quality, crystalline monodispersed nanoparticles was first reported by Murray, *et al.*[189] in 1993. In this method a volatile metal alkyl (dimethylcadmium) and a chalcogen source TOPSe (tri-n-octylphosphine selenide) were mixed in tri-n-octylphosphine (TOP) and injected into hot TOPO (tri-n-octylphosphine oxide), a polar co-ordinating Lewis base solvent. Nucleation of the nanoparticulate CdSe was achieved by the sudden introduction of the concentrated reagents resulting in abrupt supersaturation and the formation of the nuclei, followed by slower growth and annealing, consistent with an Ostwald ripening process. The

nanoparticles were passivated by a monolayer of the solvent ligands and hence could be isolated by solvent/non-solvent interactions.

The size distribution of the nanoparticles is controlled by the temperature at which the synthesis is undertaken, with larger particles being obtained at higher temperatures and lower temperatures yielding smaller particles. The combination of TOP/TOPO allowed for slow steady growth conditions above 280 °C. This method has advantage over other methods including, near monodispersity ($\sigma \cong 5\%$) and high yields. For these methods the surface coverage is such that the percentage of surface sites bound to TOPO molecules, through a metal-oxygen dative bond, increases from 30% to 60% as the particle size decreases from particle diameter of approximately 60 Å to 18 Å, respectively. Variations in surface coverage with particle size can be explained by the steric effects; interactions between surface bound bulky neighbouring capping molecules (TOPO) predominates in larger particles, whereas smaller particles can accommodate higher percentage levels of surface coverage, due to less steric hindrance.

One of the limitations of this method is the use of hazardous compounds such as dimethylcadmium, [$(CH_3)_2Cd$], especially at high temperatures. An approach to overcome this problem involves the use of single molecule precursors, a single compound containing all the elements required for within the nanocrystallite, such as alkyldiseleno or alkyldithiocarbamato complexes.[146,147] The fabrication of semiconductor nanocrystals from single molecule precursors is a one step process,

typically carried out at temperatures in the range 200 – 250 °C. A similar approach was used in which non-air sensitive lead(II) alkyldithio- or alkyldiselenocarbamates, led to the synthesis of cubic phase PbS[242] and PbSe[243] nanocrystallites respectively. Related compounds can be used to prepare compound semiconductor nanoparticles, such as oligomeric $Cd(Se(C_2H_5)_2$[244] or metal dithiocarbamates[245] in 4-ethylpyridine. The conventional TOPO method was reported by Alivisatos, *et al.*[246] in the synthesis of capped InP nanocrystals. The reaction involved dissolving $InCl_3$ in hot TOPO followed by addition of $P(SiMe_3)_3$ (Equation 15) with annealing of the resulting InP nanocrystals.

$$InCl_3 + \text{TOPO} \xrightarrow{100\ ^\circ C,\ 12h} \text{In-TOPO} \xrightarrow{P(SiMe_3)_3,\ 265\ ^\circ C,\ \text{days}}$$

$$\text{InP/TOPO} \xrightarrow{\text{surfactant (S), 100 °C, days}} \text{InP(TOPO + S)} \qquad (15)$$

The band gap for bulk InP is 1.28 eV, whereas InP particles produced exhibit values in the range from 1.7 – 2.4 eV. The percentage surface coverage of InP particles with TOPO was found to range from 30 to 70% depending on the size of the particles. Values of the band edge and deep trap emissions were reported to shift with the mean size of the nanocrystallites, with stronger emission observed for smaller InP particles and when oxidation on the surface has occurred. For InAs, prepared by a similar method using the dehalosilylation reaction between $As[(SiMe_3)_3]$ and $InCl_3$, surface oxidation does not change the properties of the resulting particles.[247] GaAs nanoparticles have been prepared by reacting $GaCl_3$ with $As(SiMe_3)_3$ in boiling

quinoline. However the quantum size effects were not properly determined as unidentified species masked the optical properties.[248,249] Another preparative method for the synthesis of GaAs[250] and InP[251] is by the methanolysis of organometallic compounds such as $[Cp^*(Cl)In(\mu\text{-}P(SiMe_3)_2]_2$. The chemical route involving cadmium[252,253] in equation 16 led to bulk, amorphous, Cd_3P_2 after rapid flocculation of nanoparticles (Equation 17).

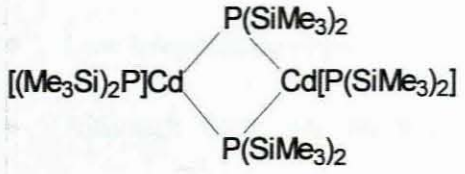

$$+ \quad 8\ MeOH \longrightarrow$$

$$2/3\ Cd_3P_2 + 8\ MeOSiMe_3 + 8/3\ PH_3 \qquad (16)$$

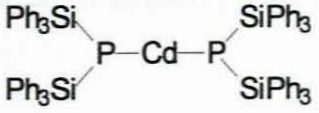

$$+ \quad 4/3\ MeOH \longrightarrow$$

$$\text{nano-}Cd_3P_2 + 4/3\ HP(SiPh_3)_2 + 4/3\ MeOSiPh_3 \qquad (17)$$

To control the kinetics for the decomposition of molecular precursors, a single molecule precursor with bulkier substituents was used, $Cd[P(SiPh_3)_2]_2$.[253,254] The methanolysis gave soluble nanoparticles of Cd_3P_2 with diameters ranging from 30 to 40 Å; however the particles were not crystalline. There are a number of potential advantages of using the single-molecular precursors over the other existing methods:

- Single source route avoids the use of volatile, sometimes toxic and/or pyrophoric precursors.
- Some of the semiconductor nanoparticles are air sensitive. The precursors of such nanoparticles are synthesized under both aerobic and anaerobic conditions, with the resulting precursors being air and moisture stable.
- There is less chance of the incorporation of impurities into the nanoparticles since one involatile precursor is involved
- Low temperature deposition routes are possible.
- Although there are theoretical models predicting the optical properties of semiconductor nanoparticles, the properties of nanoparticles obtained by new synthetic routes are sometimes hard to anticipate and may lead to particles with unique and anticipated, but useful, properties.

Bis(alkyldithio/selenocarbamate)cadmium and zinc compounds have been used as single-molecular precursors in the growth of group II-VI thin films by low pressure and aerosol-assisted chemical vapour deposition (LPCVD and AACVD).[255,256] These compounds have been shown to be good precursors for the preparation of nanoparticles, a process that involves their decomposition in a high boiling point coordinating solvent (Lewis base) such as TOPO or 4-ethylpyridine. The preparation of these compounds follows a simple procedure in which CSe_2 or CS_2 is reacted with an excess of the amine and NaOH or KOH at below 0 °C, to give the dithio/seleno carbamate as the dialkylammonium salt. This compound is reacted with a

stoichiometric quantity of an aqueous solution of $CdCl_2$ or $ZnCl_2$ to give the bis(alkyldithio-/diselenocarbamato)cadmium(II)/zinc(II) compound as a precipitate.

Nanoparticles from single-source precursors employ a "one-pot" synthesis in which there is rapid nucleation and followed by slow particle growth which is essential for narrow size distribution. The synthesis and use of novel single-molecular precursors that produce self-capped nanoparticles have also been explored. Organic group from the precursor should migrate upon thermolysis and act as capping agent on the surface of the nanoparticle. The asymmetric complex dithiocarbamatecadmium, $[Cd\{(S_2CNMe(C_{18}H_{37})\}_2]$, as an example was used to prepare nanoparticles under a dynamic vacuum in the solid state at temperatures ranging between 150 – 300 °C, producing CdS capped nanoparticles.[257]

The spectroscopic analysis, IR and NMR, suggest that the capping group is principally $NHMe(C_{18}H_{37})$. Although the capping agents such as TOPO and 4-ethylpyridine work well to passivate the surface of nanoparticles they are only weakly covalently coordinated to the surface and are relatively labile, which may be advantageous if the capping agent is to be exchanged for a different ligand. However the other method used to passivate the particles with more robust layer, which is not labile, is to grow a second material epitaxially on the surface of the nanoparticle. An example is another metal chalcogenide materials (preferably with a wider band gap) on the surface of another metal chalcogenide nanoparticles, to produce a core-shell nanoparticles such as CdSe-CdS using $[Cd(Se_2CNMe^nHex)_2]$ as a source for CdSe

and [$Cd(S_2CNMe^nHex)_2$] as the CdS source.[258] The high surface to volume ratio of nanocrystalline materials means that the surface plays an important role in the optical and electronic properties. It is for this reason that surface modifications of these particles has been a subject of investigation. Beside surface passivation being achieved by capping nanocrystallites with organic and inorganic groups, colloidal CdS has been passivated for the surface defects by $Cd(OH)_2$ with marked increase in fluorescence reported in surface modified samples.[259]

Organic ligands such as thiopyridines[260,261] and thiolates[262] have been reported to reduce the surface defects and increase the luminescent efficiencies. In the colloidal synthesis of these core-shell structures the core acts as a seed for the heterogeneous nucleation of the shell. Core-shell systems reported include Si/SiO_2,[263] $CdS/Cd(OH)_2$,[259] CdSe/ZnS,[263] CdSe/ZnSe[213,264] and CdSe/CdS[193,258,265,266] which account for improved luminescence quantum yields which is desirable, decreased fluorescence lifetimes and benefits related to tailoring of the band gap positions between the two materials. These properties render these materials potentially useful in optoelectronic devices.

A number of cadmium complexes including dithiobiurea[267] as well as ethylxanthate[268] have been reported for their use as single-source precursors to prepare CdS nanoparticles. This follows the successful use of the cadmium complex of N,N'-bis(thiocarbamoyl)hydrazine as an efficient precursor for CdS nanoparticles.[269] The synthesis was carried out in TOPO as capping agent and solvent medium for the

reaction. Spherical particles with an average size of 4.2 nm were obtained from the ethylxanthate complex. Spherical aggregates of relatively uniform size (50 nm) were obtained at 240 °C while at 150 °C irregular non-spherical particles were observed from the dithiobiurea complex. In nanochemistry alkylxanthate compounds were first introduced as capping agents.[270,271]

2.1.6. Applications of nanosized materials

Nanosized materials have a very wide diversity of applications.[243-248,271-279] Composite materials are used in a variety of applications, from cars to aeroplanes to domestic products but making filling material nanophase (nanoscale particles) changes the material properties. Variety of materials that can be experimented with as fillers are metals, metal oxides, ceramics, silicates or even dendrimers.

2.1.6.1. Energy storage, production and conversion

Nanoparticles are applied as organic light emitting diodes (OLEDs) in digital cameras, whereby they do not only show added brightness than liquid crystals display (LCD), but they also consume less energy since they do not require back-lightning also have the advantage of having a very wide viewing angle. The use of nanostructured materials for new and improved fuel cells, solar cells and novel hydrogen storage systems, will probably have the most impact in the near future. Ideally, these applications will be robust and easily maintained and serviced.

Long term delivery avoids the need for patients to take daily pills at well defined times. Nanotechnology will also reduce transportation costs and even required dosage by improving the shelf-life, thermo-stability and resistance to changes in humidity of existing medications. Nanotechnology-based solutions in developing countries will depend upon cost, supply and ease-to-use, especially where a wide range of screening can occur with relatively inexpensive sensors in a local clinic. e.g. quantum dots for biodetection and bioanalysis, veterinary and agricultural purpose, devices for pathogen detection; medical image enhancers; molecular optical and magnetic labels.

2.1.6.5. Other medical research applications

For genomic and proteomic research, examples are found in DNA based nanosensors, genetic marking devices, DNA sequencing and detection systems, dendrimers for genetic engineering and efficient gene-expression systems. Health monitoring devices involves using nanocomposites and nanodevices that will allow cheaper, robust and potentially non-skilled monitoring of patients outside hospitals.

2.1.6.6. Novel therapeutic agents and organ and tissue transplant and repair

New drugs could have a great impact in diseases for which there are currently no effective or risk-free treatments e.g. HIV, hepatitis, malaria, nanomaterials for drug separation, dendrimers as chelating agents, various microbicidal agents and drug screening devices. The common examples for tissue and organ transplant are found in nanomaterials in scaffolds for bone and other tissue repair, artificial organs, artificial blood and prosthetics including visual and auditory devices.

2.1.6.7. Defence and security/protective applications

Nanoparticles of are already commercially produced in antibacterial dressings. The oxides of titanium and zinc are found to be very good in absorbing ultraviolet radiation. Zinc nanoparticles are also used as fungicide. Nanocrystalline for protection against sunscreen have been produced from zinc and titanium. In deep penetrating skin care, the cream uses a patented 200 nm nanotechnology process to incorporate vitamin A inside a polymer 'capsule'. The capsule acts like a sponge soaking up and holding the cream inside until the outer shell dissolve under your skin. Nanofilm uses nanotechnology to create protective and antireflective ultra-thin polymer for eye-wear to give the glasses anti-reflection and scratch-resistant functionality. Chemical self-assembly is used to form coating, 3 to 10 nm thin on the outer layer of the anti-reflective lenses. This not only seals and repels dirt and skin oils but also makes the lenses more responsive.

2.1.6.8. Increased electrical, chemical and mechanical device efficiency

Industrial mass production by industries in developing countries will benefit from cheaper nanodevices, molecular machines and nanointerfaces with high potential, high performance and efficient usage of natural resources and energy. For example, fullerenes as lubricants, molecular machines and manufacturing of nanomaterials for thermal and electrical insulation and for reduction of friction and wear; molecular engineering of materials.

2.1.6.9. Data transmission, data storage and processing

Examples found are in nanowires, self-assembled monolayers, carbon nanotubes for single electron transistors, DNA and optical memory storage and processing. The devices used to store and retrieve data from hard disks are nanomagnet-base, employing stacks of nanoscale magnetic films. Data storage applications count for more than 90 percent of today's nanomagnet market.

2.1.6.10. Water treatment and remediation

Access to clean water in most areas of the developing world is very limited. Cheap, easily transportable systems that purify, detoxify, and desalinate water (such as nanomembranes and nanoclays) and small and effective nanosensors for the detection of contaminants and pathogens will contribute both to improve health and to maintain a safe supply of water, e.g. nanomagnets for removal of radioactive compounds.

2.1.6.11. Other applications

It is evident from above that nanoparticles have endless applications in technology and in improving the standard of living. This include them being applied in high-performance ski wax, stain repellent and wrinkle-resistant threads, packaging, explosive additives, catalysis, semiconductors, medical and pharmaceutical industries. One of the potential applications of single quantum dots is to use them as luminescent labels in biological systems. Also biological applications are being explored such as water soluble semiconductor nanoparticles fluorophores used to examine mouse fibroblasts. Cheap, resistant textiles with superior functionality will be especially

2.2. EXPERIMENTAL

2.2.1.(a) General

TOPO (tri-n-octylphosphine oxide), TOP (tri^{n}octylphosphine) and hexadecylamine (HDA) were purchased from Aldrich. TOPO was purified by distillation at about 250 °C. Toluene and methanol were obtained from BDH. Toluene was stored over molecular sieves (40 Å, BDH) for overnight before use. Cadmium chloride, lead chloride, copper chloride, N,N'-dimethylthiourea, N,N'-diethylthiourea, N-methylthiourea, N-ethylthiourea, thiourea and ethanol and hexane (analytical grade) obtained from Aldrich, and used as purchased to prepare the precursors.

2.2.1.(b) Optical characterisation

A Perkin Elmer Lambda 20 UV-VIS Spectrophotometer was used to carryout the optical measurements and the solution of the samples were placed in silica cuvettes (1-cm, path length), using toluene as a reference solvent. A Jobin Yvon-spex-Fluorolog-3-Spectrofluorimeter with a xenon lamp (150 W) and a 152 P photomultiplier tube as a detector was used to measure the photoluminescence of the materials. The samples were placed in quartz cuvettes (1-cm path length) with a similar solvent, toluene.

2.2.1.(c) Electron microscopy

The high resolution transmission electron microscope (HRTEM) images and selected area electron diffraction (SAED) patterns were obtained using a Philips CM 200

compustage electron microscope operated at 200 kV with a EDS analyser. The samples were prepared by placing a drop of a dilute solution of sample in toluene on a copper grid (400 mesh, agar). The samples were allowed to dry completely at room temperature.

2.2.1.(d) X-Ray diffraction

X-Ray diffraction patterns on powdered samples were measured on Phillips X'Pert materials research diffractometer using secondary graphite monochromated Cu Kα radiation (λ = 1.54060 Å) at 40 kV/ 50 mA. Samples were supported on glass slides. Measurements were taken using a glancing angle of incidence detector at an angle of °2, for 2θ values over 20° – 60° in steps of 0.05° with a scan speed of 0.01 °2θ.s^{-1}.

2.2.2. The preparation of nanoparticles

The following complexes were used to prepare TOPO and HDA-capped nanoparticles, $CdCl_2(CS(NH_2)NHCH_3)_2$ (**I**), $CdCl_2(CS(NH_2)NHCH_2CH_3)_2$ (**II**), $CdCl_2(CS(NH_2)_2)$ (**III**), $PbCl_2(CS(NHCH_2CH_3)_2)$ (**IV**), $PbCl_2(CS(NHCH_3)_2)$ (**V**), $Cu_4Cl_4(CS(NHCH_3)_2)_4$ (**VI**) and $Cu_4Cl_4(CS(NHCH_2CH_3)_2)_4$ (**VII**). The TOPO capped nanoparticles were synthesised by the injection of the appropriate single molecular precursor dispersed in TOP into hot TOPO under an atmosphere of nitrogen gas.

In a typical experiment, $CdCl_2(CS(NH_2)\ NHCH_2CH_3)_2$ (1.0 – 3.0 g) was dissolved in TOP (10 – 20 ml). This solution was then injected into hot TOPO at different temperatures (200 – 250 °C), a decrease in temperature of 20 – 30 °C observed. The

solution was allowed to stabilise at 250 °C and heated for 30 minutes at this temperature. The solution was allowed to cool to about 70 °C, and an excess of methanol was added to remove excess TOPO. A flocculent precipitate formed. This solid product was separated by centrifugation and redispersed in toluene. Toluene was removed by evaporation under reduced pressure to give pale yellow TOPO capped CdS nanoparticles. The particles were washed three times with methanol and redispersed in toluene.

An alternative route was used for the HDA-capped nanoparticles in which particles were synthesized by direct addition of the solid precursors (0.5 – 2.0 g) into hot HDA at different temperatures (200 – 250 °C) under nitrogen gas atmosphere. A small drop in the temperature was observed and the solution was restored to about 200 °C. The solution was heated further for 15 to 60 minutes at the same temperature. The solution was allowed to cool to about 70 °C, and an excess of methanol was added to remove excess of HDA and a flocculent precipitate formed. To remove excess of HDA hot methanol was added to the product. The separation was obtained by centrifugation and the product redispersed in toluene. Toluene was removed by evaporation under reduced pressure yielding reddish-brown (lead sulfide) to grey-black (copper sulfide) coloured HDA-capped nanoparticles in order to remove further excess of HDA. The step was repeated for third time and finally redispersed in toluene for further analysis.

2.3. RESULTS AND DISCUSSION

Nanoparticles generally exhibit properties distinct from the bulk materials of the semiconductors. These alkylthiourea complexes are also easy to prepare and both air and thermally stable and lastly are inexpensive. The single-source molecular approach provides both elements within a single molecule, which allows the preparation of semiconductor nanocrystals in a one step process by the thermal decomposition of the molecular precursor in a convenient dispersing medium such as tri-n-octylphosphine oxide (TOPO).

The changes in electronic property from the bulk make them useful for the ultraviolet region especially for CdS, visible region for CuS/Cu_2S and near infrared region for PbS. In the synthesis variety of colours characteristic of each type of semiconductor nanoparticles were observed in both TOPO and HDA ranging from yellow (CdS), grey (PbS) and brown to black (CuS). These conditions of preparation are outlined in Table 9 for CdS. Temperatures of 180 °C to 280 °C and times ranging from 5 to 60 minutes were used. A series of nanoparticles were prepared using single source molecular precursor prepared from different alkyl substituted thioureas co-ordinated to the metals. Large amount of the products formed and settled in solution. Both nanoparticles (solid) and the solution were characterized by using ultraviolet-visible spectroscopy and photoluminescence.

The particles obtained from the solution were characterised by a combination of TEM and high resolution TEM together with selected area diffraction patterns. The ideal method for preparing isolated materials must produce monodispersed, pure, crystalline and have suitable surface passivation. Passivation of nanoparticles by organic capping groups or polymers together with controlled synthetic conditions provides environment with controlled particle sizes and shapes.

2.3.1. Synthesis of cadmium sulfide nanoparticles

Following the successful use of the dithiocarbamate[147] and N,N`-bis(thiocarbamoyl) hydrazine[269] cadmium(II) complexes as precursors for the synthesis of CdS nanoparticles, the air-stable, easy to prepare and inexpensive thiourea and N-alkyl substituted thiourea cadmium(II) complexes were explored for the synthesis of TOPO-capped CdS nanoparticles. The complex, $CdCl_2(CS(NH_2)_2$ **(III)**, prepared from unsubstituted thiourea ligand was also used as a single-source precursor for these in order to compare properties and the yields of CdS nanoparticles with those alkyl substituted thiourea complexes. Generally particle growths is dependent on such factors as temperature and time, and the use of single-source precursor method provides an additional factor in the nature of the precursor. This was explored in this work in relation to particle size, shape, structural and optical properties. Detailed studies on CdS nanoparticles indicate the blue shift in the optical properties and red shift of the photoluminescence of various cadmium complexes as single-source precursor. These properties are also observed for xanthates and long chain

alkylthiourea compounds such as dioctyl, dicyclohexyl and diisopropyl thiourea cadmium complexes,[272] are used as single source precursors for CdS nanoparticles.

It is evident that thermolysis of these precursors produced CdS nanoparticles with variety of properties which have little influence from the alkyl groups on the thiourea ligands. Table 9 outlines the detailed experimental conditions for the synthesis of CdS nanoparticles from temperature 200 and 250 °C with time ranging from 30 to 60 minutes. Cadmium complexes of thiosemicarbazide have been reported to produce CdS nanorods, in which their morphology is thought to affect their optical properties.[268,272] This has been an interesting development in the preparation of nanoparticles following the successful preparation of particles of specific morphology under a variety of conditions and precursors.[273-275] It was observed by Li, *et.al.*[276] that temperature in combination of other conditions such as concentration greatly influences the morphology of nanoparticles from rod-shaped to spherical CdS. A minor influence of the alkyl groups on thiourea was observed, which was less than for temperature and time or change of the capping groups on the size and morphology of particles. The longer chain alkyl groups have been observed to influence the morphology of particles. The absorption and photoluminescence properties show dependence on temperature and time of thermolysis of the precursor.

Table 9: Conditions for the synthesis of CdS nanoparticles using cadmium precursors

Complex	Amount (g)	Temperature (°C)	Time (Min)	TOPO (g)
I	2.0	250	60	25
	1.0	200	25	20
II	3.0	250	30	25
	2.0	200	30	20
III	1.0	250	60	25

2.3.1.1. Optical properties

The optical spectra of these particles measured in an organic solvent can be used to calculate the approximate emission band edge using the direct band gap method.[276] Macrocrystalline hexagonal CdS particles have an optical band gap of 2.52 eV (490 nm) at room temperature.[277] The band edges for CdS samples prepared from single-source precursors are blue-shifted in relation to the bulk material. This is associated with the CdS nanoparticles being smaller than the bulk exciton of CdS. During preparation there is generally an increase of particle size of nanoparticles with time, which is consistent with an Ostwald ripening process. After injection of the precursor there is a critical size dependence on the concentration of the precursor. The depletion of the precursor causes the size distribution to broaden because smaller, less stable particles aggregate to form larger particles.

Absorption spectra have also been used to determine the optimum time for growth of particles at specific temperatures from various precursors.[272] A blue shift was observed in the optical spectra as a result of particles nanosize regime exhibiting quantum confinement effects. The optical spectra (Figure 19) for the TOPO-capped CdS are typical of particles smaller than for the bulk material. The absorption edges of CdS particles as calculated by the direct band method from the different precursors are 488 nm (2.54 eV) **I**, 478 nm (2.59 eV) **II** and 490 nm (2.53 eV) **III** (Table 10). These are blue shifts of 25 – 37 nm in relation to the bulk (515 nm, 2.41 eV), corresponding to the particle sizes 5.9 nm, 5.3 nm and 6.0 nm, respectively, as calculated by the Brus equation.[166,167]

Table 10: Details of synthetic conditions, size and band edges for CdS prepared.

Complex	**Duration (Min)**	**Temp (°C)**	**Crystallite size (nm)**	**Band edge (nm)**
			Exp[ϕ]	
I	25	200	4.8	488
II	30	200	4.3	478
III	60	250	32.2	490

[ϕ] determined using the Scherrer method (PC-APD XRD software)

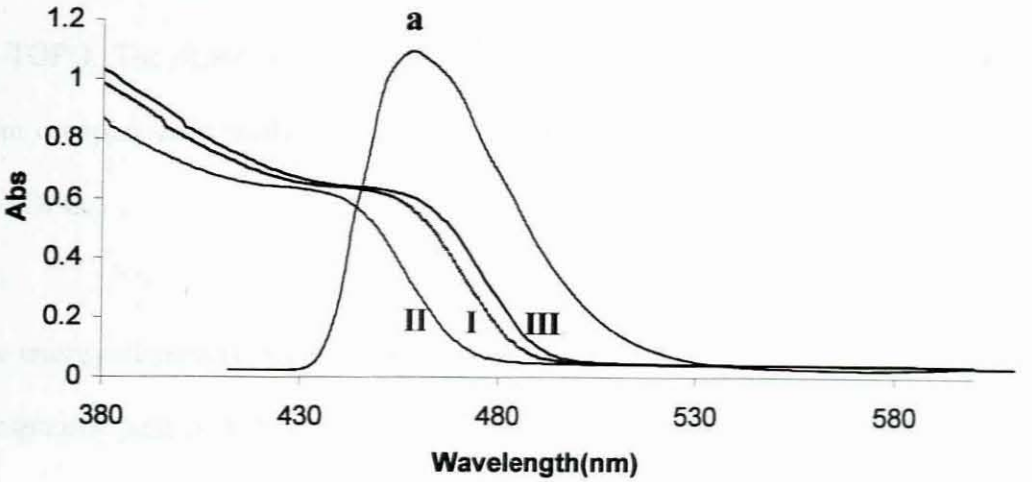

Figure 19: Optical spectra of CdS nanoparticles synthesized from complexes **I** - **III** at 250 °C and typical photoluminescence spectrum (**a**) of CdS nanoparticles obtained from complex **II**.

It has been observed that unsubstituted thiourea complex resulted in large particles even at optimal temperature for TOPO and 25 minutes of particle growth time. This is in contrast to the methyl and ethyl substituted thiourea complexes (**I** and **II**) under the same thermolysis conditions. In contrast to growth at 250 °C in which the band edge (490 nm) is closer to that of the bulk, particles grown at lower temperature 180 °C from the same complex gave extreme blue shift in the band edge. This was observed from the samples collected at 5 minutes intervals to monitor the growth of particles with time. The photoluminescence spectra show broad emission due to the wide distribution of particle sizes, with the emission maxima in the range 425 – 480 nm with an excitation wavelength of 380 nm. The photoluminescence emission maxima are very close to the emission band edges. As the particle size decrease, the surface/volume ratio increases thereby increasing the number of surface traps. These

surface defects normally associated with semiconductor nanoparticles are passivated by TOPO. The observed shift of the photoluminescence spectrum for CdS obtained from complex II is small and could be attributed to the particles not well passivated by TOPO.

The energy-dispersive X-ray fluorescence analysis (EDAX) shows a relatively strong phosphorus peak in addition to cadmium and sulphur, with about 60 and 40 of atomic percentage of cadmium and sulphur, respectively. These results are consistent with the microanalysis of these particles, which indicates higher percentage of cadmium varying from 67 to 74% and 12 to 18% of sulphur. Bulk CdS is reported to have a broad emission maximum in the range 500 – 700 nm region of the luminescence spectrum. The emission is due to recombination from surface defects, predominantly sulphur vacancies,[187] which in this case are passivated by TOPO.

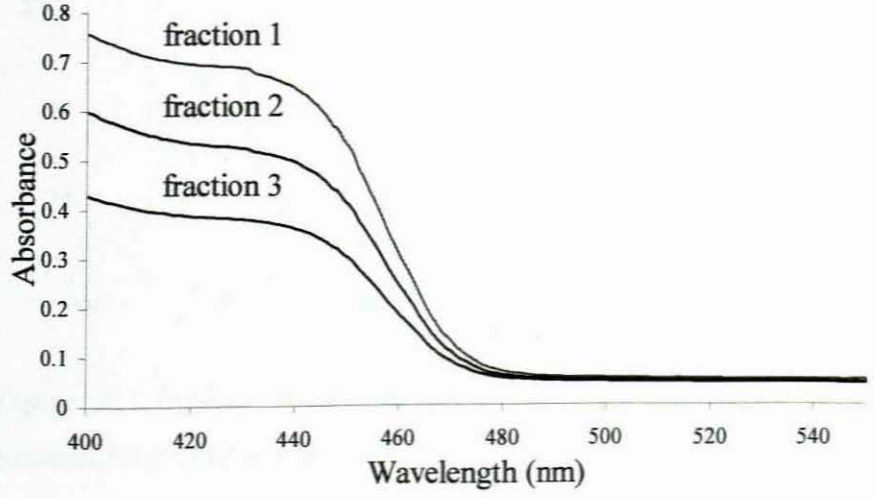

Figure 20: Size fractionation of CdS nanoparticles from complex **II**.

Size fractionation performed from CdS particles obtained from complex **II** indicate a change in the band edge of the optical spectra (Figure 20) in that the sharpness of the band edges increase from fractions 1 to 3 suggesting a change in the uniformity of size distribution. When complex **II** was thermolysed at 200 °C a typical blue shift was observed with corresponding red shift in the photoluminescence emission maximum (Figure 21). The band edge was observed at 463 nm with the emission maximum at about 480 nm with the excitation at the band edge. The band edge is lower than in the particles thermolysed at 250 °C for the same complex.

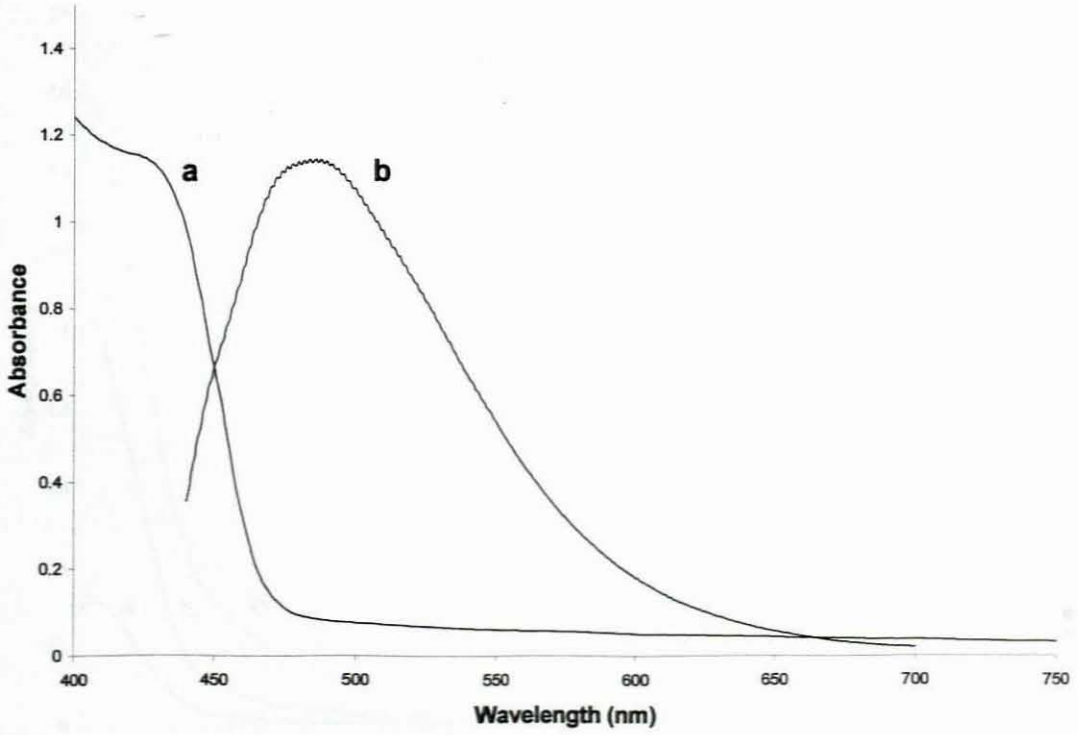

Figure 21: Optical (a) and photoluminescence (b) spectra of CdS nanoparticles prepared from complex **II** at 200 °C.

This is a consistent property of growth of particles with temperature. Further optical studies were performed using complex **III** to prepare CdS at of 180 °C (Figure 22). Fractions were collected after 5, 10 and 15 minutes with the band edges at 326, 340 and 362 nm, respectively. These are extreme blue shift in relation to the bulk, which could be explained by the fact that there is generally an increase of particle size of nanoparticles with time, which is consistent with an Ostwald ripening process. It was again observed that after an injection of the precursor there is a critical size dependent on the concentration of the precursor.

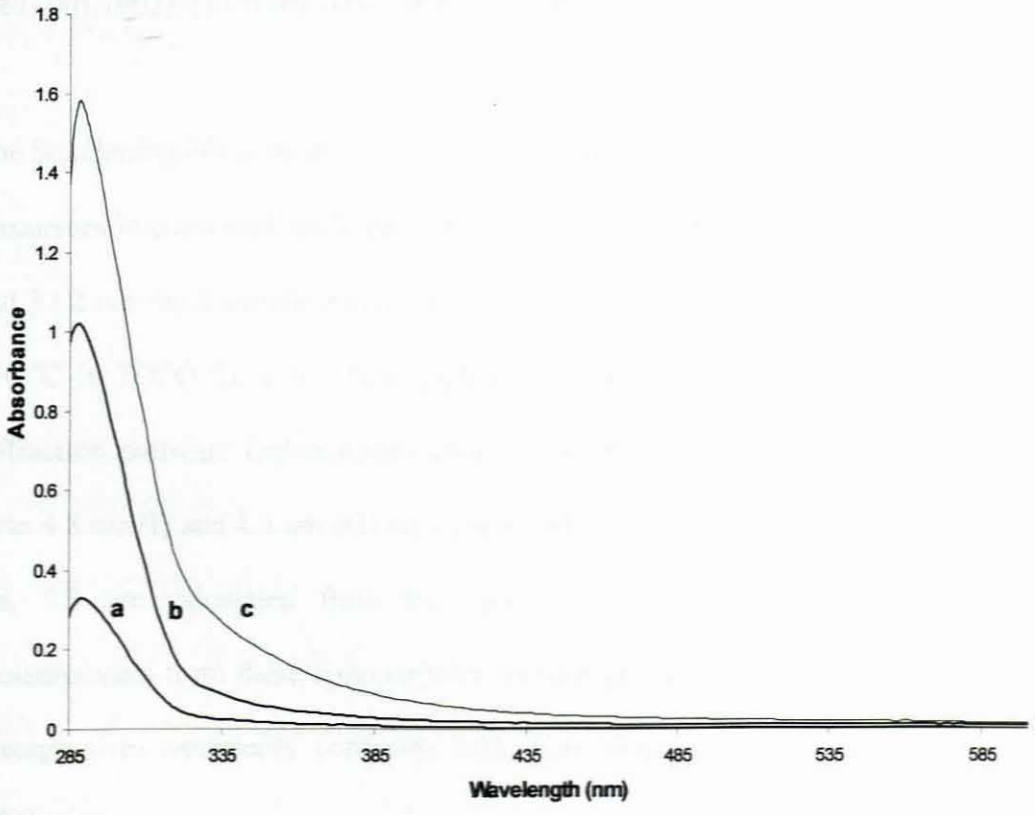

Figure 22: Optical spectra for CdS nanoparticles prepared from complex **III** with fractions collected after 5 min (a), 10 min (b) and 15 min (c).

2.3.1.2. Structural characterisation

CdS nanoparticles can exist either as the cubic or hexagonal phase and the existence of a mixture of cubic and hexagonal phase with the predominance of one over the other was reported by Bawendi *et al.*[278] for CdSe. The XRD patterns of the present CdS particles are entirely consistent with a predominantly hexagonal phase. The (100), (101) and (002) planes are the most intense in all samples and are clearly distinguishable in the patterns as planes of hexagonal CdS phase. The selected area electron diffraction (SAED) patterns (Figure 23) consist of broad diffuse rings, which are indicative of the small size of the particles. The diffraction rings can be indexed to the (100), (002), (110) and (004) planes confirming the wurtzite phase (Table 11).

The broadening of the peaks on the diffractogram (Figure 23) obtained from different precursors is consistent with the particle sizes 4.8 nm (**I**) and 4.3 nm (**II**) at 200 °C and 32.2 nm for a simple thiourea complex, $CdCl_2(CS(NH_2)_2)_2$, (**III**) thermolysed at 250 °C in TOPO for 1 h. These particle sizes were determined using the PC-APD diffraction software (calculation based on the Scherrer method[279,280]). The particle sizes 4.8 nm (**I**) and 4.3 nm (**II**) are in reasonable agreement with the particle sizes 5.9 nm, 5.3 nm calculated from the optical measurements. Although the optical measurements from these nanoparticles showed deviation from monodispersity, their average sizes reasonably conforms with those determined from the broadening of XRD peaks.

Table 11: Experimental XRD and SAED data of CdS particles.

d(lit*)/2θ	D(exp)/ 2θ			hkl	SAED data	
	I	**II**	**III**		d(exp)/ Å(2θ)	hkl
24.90	24.80	24.80	24.87	100	3.29 (27.1)	002
26.69	26.53	26.53	26.53	002	3.61 (24.7)	100
28.42	28.15	28.15	28.24	101	1.99 (45.6)	110
36.84	36.68	36.68	36.68	102	1.67 (54.9)	004
43.29	43.73	43.95	43.73	110		
47.61	48.15	47.88	48.15	103		
51.33	51.02		51.02	200		
52.27	51.96	52.27	51.96	112		
53.26	53.26	53.26	53.26	201		
54.98				004		

* Ref 1999 JCPDS

It was observed that particle sizes increases five- to seven-fold with the increase in temperature and time (Table 10) whereas at lower temperature (200 °C) particles of smaller sizes (4.8 nm-**I** and 4.3 nm-**II**) were obtained. The X-ray powder diffraction of the CdS nanocrystallites obtained in this work has patterns consistent with the hexagonal phase. The broader peaks are indicative of the smaller size of the particles, whereas the larger ones are less broad and sharper (Figure 23), hence electron diffraction in this can be a valuable additional technique for characterisation.

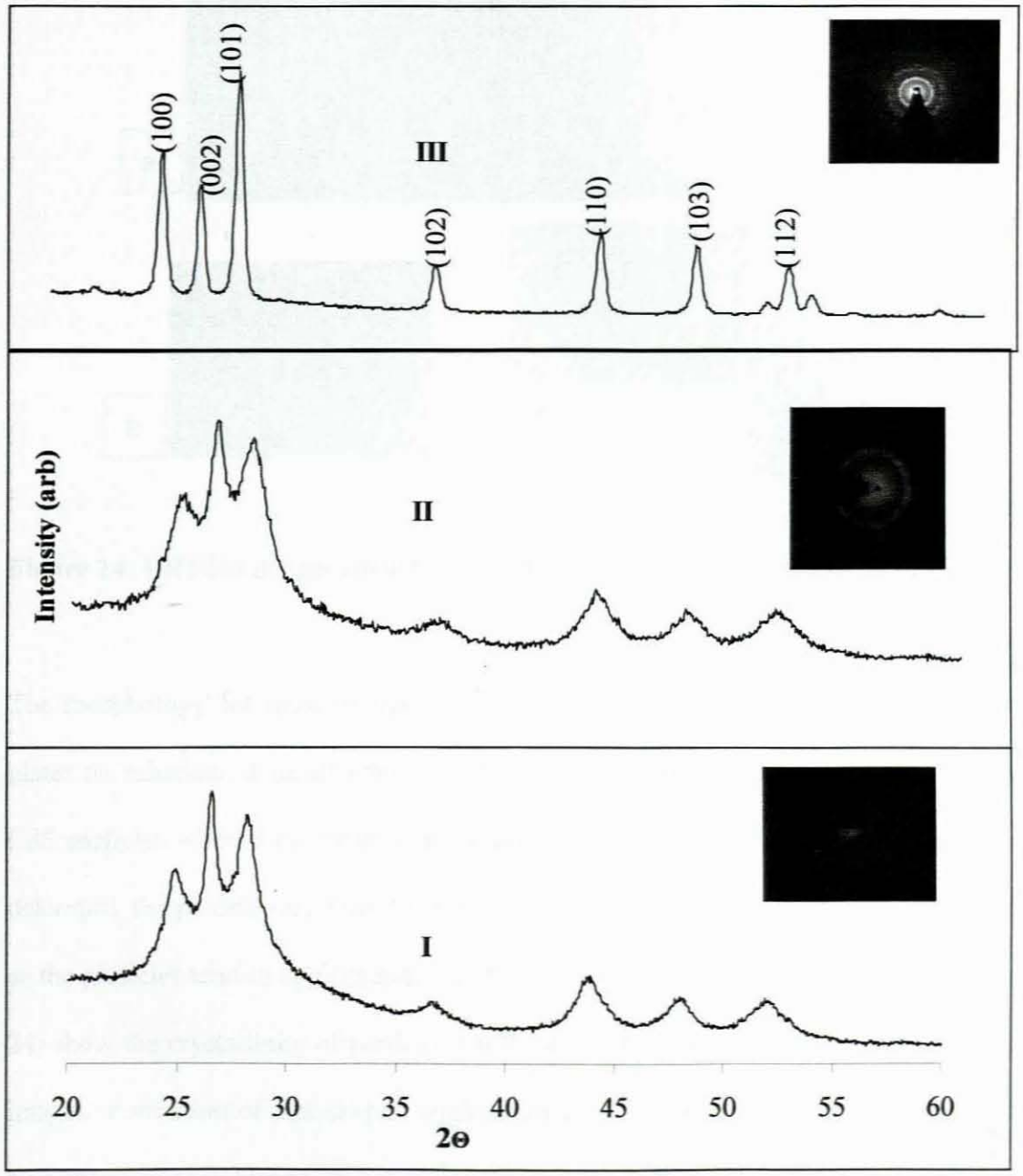

Figure 23: XRD plots of hexagonal CdS phases (**I - III**) and the corresponding selected area diffraction (SAED) pictures.

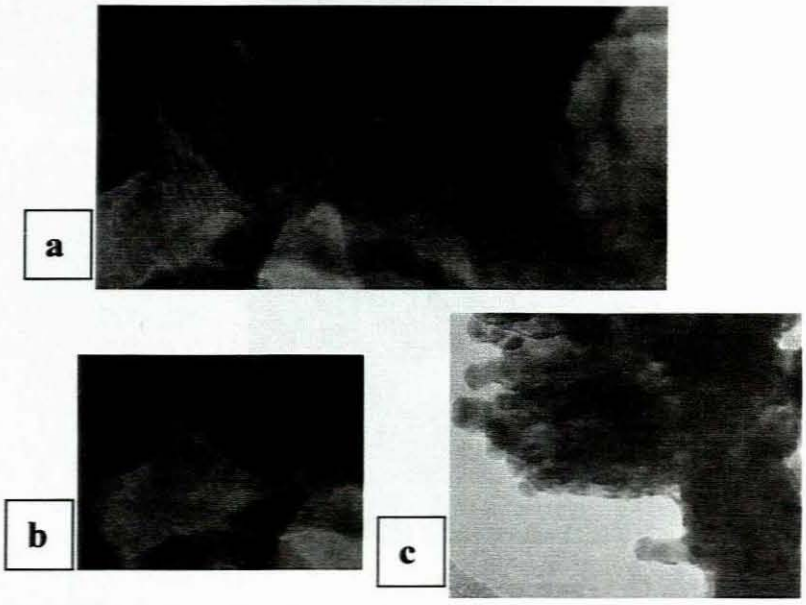

Figure 24: HRTEM images showing lattice planes for complexes **I (a), (b)** and **II (c)**.

The morphology for most of the CdS nanocrystallites is closer to thin needle-like plates to spherical, a result consistent with a preferential mode arrangement of the CdS particles when they settle on the carbon coated copper grid. It was difficult to determine the particle size from the transmission electron microscope (TEM) images, as the particles tend to agglomerate rapidly. The high resolution TEM images (Figure 24) show the crystallinity of particles confirmed by the lattice planes observed on the images. Formation of star-shaped agglomerates of CdS nanoparticles in TOPO was also observed as in Figure 25.

Figure 25: TEM image showing agglomerated particles of TOPO-capped CdS from complex **II**.

2.3.2 Synthesis of lead sulfide nanoparticles

Lead sulfide nanoparticles have been prepared by different types of methods including the reaction of lead salt and sulphur by varying their amounts.[281] The solution reaction of carbon disulfide and lead acetate produced lead sulfide nanoparticles.[282] The use of single source precursor using dithiocarbamate complexes to prepare PbS nanoparticles has also been reported by Trindade, *et. al,.*[242] who prepared these particles with different phases and close to monodispersity. An effort to prepare highly monodispersed PbS nanoparticles has been done using alkylthiourea complexes by a single source precursor method with TOPO and HDA as the capping agents. The nanoparticles were prepared by the routes outlined in the experimental section mainly to improve the yields. Table 12 outlines the detailed experimental conditions for the synthesis of PbS nanoparticles from temperature 200 and 250 °C

for 30 minutes. The use of HDA result from an attempt to investigate if it provides more stable capping around the fast agglomerating PbS nanoparticles.

Table 12: Conditions for the synthesis of PbS nanoparticles using different precursors

COMPLEX	Amount (g)	Temperature (°C)	Time (Min)	HDA (g)	TOPO (g)
IV	0.75	250	30		20
	0.75	200	30		20
V	2.0	200	30	10	

2.3.2.1. Optical properties

PbS is a semiconductor with a band gap of 0.41 eV and could find applications such as near-IR communications.[283] PbS nanocrystals offer unique access to the regime of extreme quantum confinement since the electron, hole and exciton all have large Bohr radii of 20 nm.[282-286] Their band gap is shifted with respect to the spectral regime of 0.7 – 1.5 m (1.77 – 0.82 eV) upon the decrease of the PbS nanocrystal diameter below the size of the excitonic Bohr, due to quantum confinement effect. Quantum confinement of both the electron and hole in all three dimensions leads to increase in the effective band gap of the material with decreasing crystallite size. Consequently, both the optical absorption and emission of quantum dots shift to the blue (higher energies) as the size of the nanoparticles gets smaller. PbS nanoparticles can readily be made in the strong quantum confinement regime with an absorption band edge

near 600 nm, which is a spectral region achievable with CdSe nanoparticles. TOPO-capped PbS nanoparticles show a large blue shift that exhibits exciton absorption peaks at about 332, 390 nm and a broad shoulder at about 650 nm (Figure 26). These are peaks corresponding to the $1S_e - 1P_h$, $1P_e - 1P_h$ and $1S_e - 1S_h$, respectively, for the surface modified PbS nanoparticles as observed from the previously reported PbS-PVA (PVA = polyvinylaniline).[287] A weak, broad shoulder band was observed at the wavelength near 650 nm, which is generally observed for the surface modified particles especially by the organic groups. This observation is related to the inhomogeneity of the radii and the phonon broadening and is attributed to the lower energy side of the transitions $1S_e - 1S_h$. The transition is observed mainly at lower temperature from PbS prepared from the same complex (Figure 27). The use of a single-source molecular precursor method has been reported by Trindade *et. al.*[242] in which the dithiocarbamate complexes of lead were used and TOPO was used as a capping agent to the PbS nanocrystals.

In other reported results, uniform cube shaped PbS nanocrystals with particle sizes of 6 to 13 nm were synthesised in which the particle size was controlled by changing the relative amount of $PbCl_2$ and sulphur.[281] The bands associated with the transitions $1S_e - 1P_h$ and $1P_e - 1P_h$ are prominent at both temperatures are helpful in identifying PbS nanoparticles. At 250 °C the absorption spectrum shows a major band at 390 nm typical of nanoparticles and no broad shoulder was observed at about 600 nm.

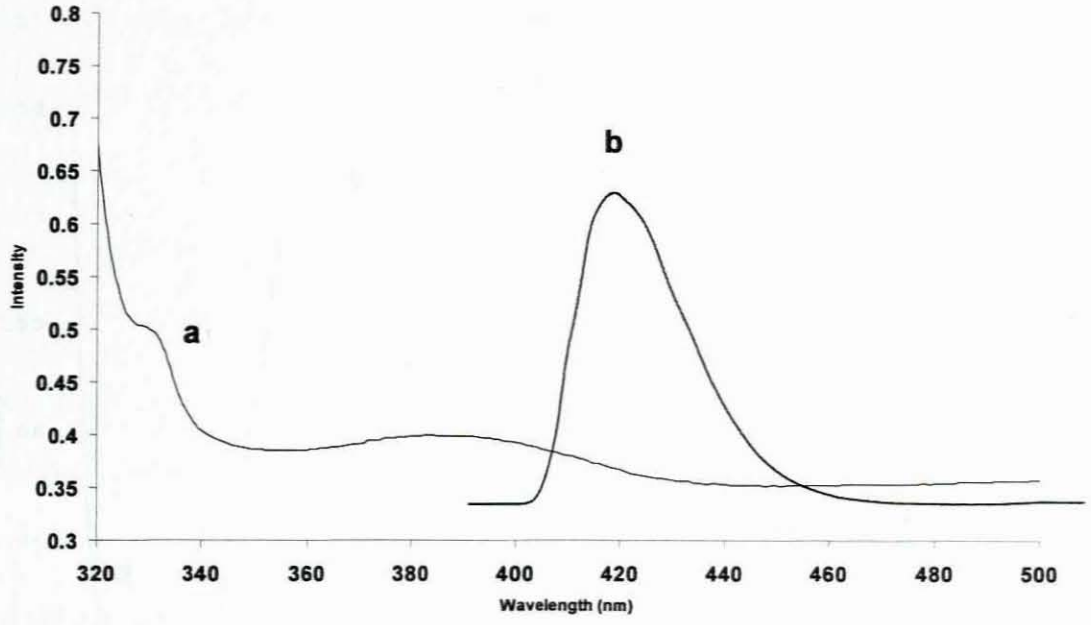

Figure 26: The optical (a) and photoluminescence (b) spectra of TOPO-capped PbS prepared from complex **IV** at 200 °C.

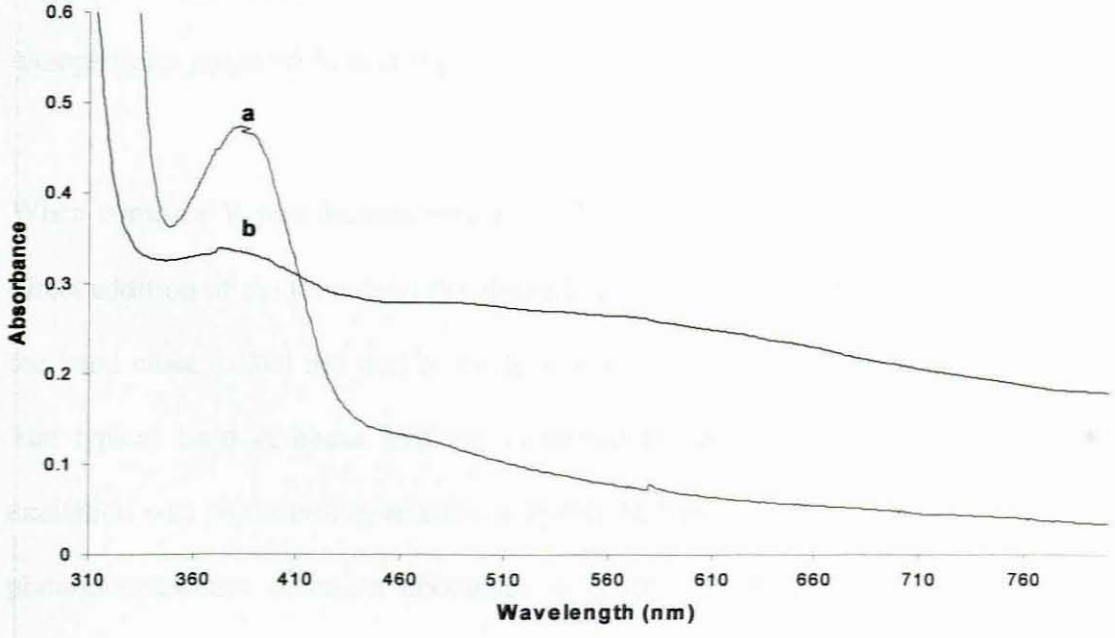

Figure 27: Absorption spectra of TOPO-capped PbS prepared from complex **IV** at temperatures 200 °C (b) and 250 °C (a).

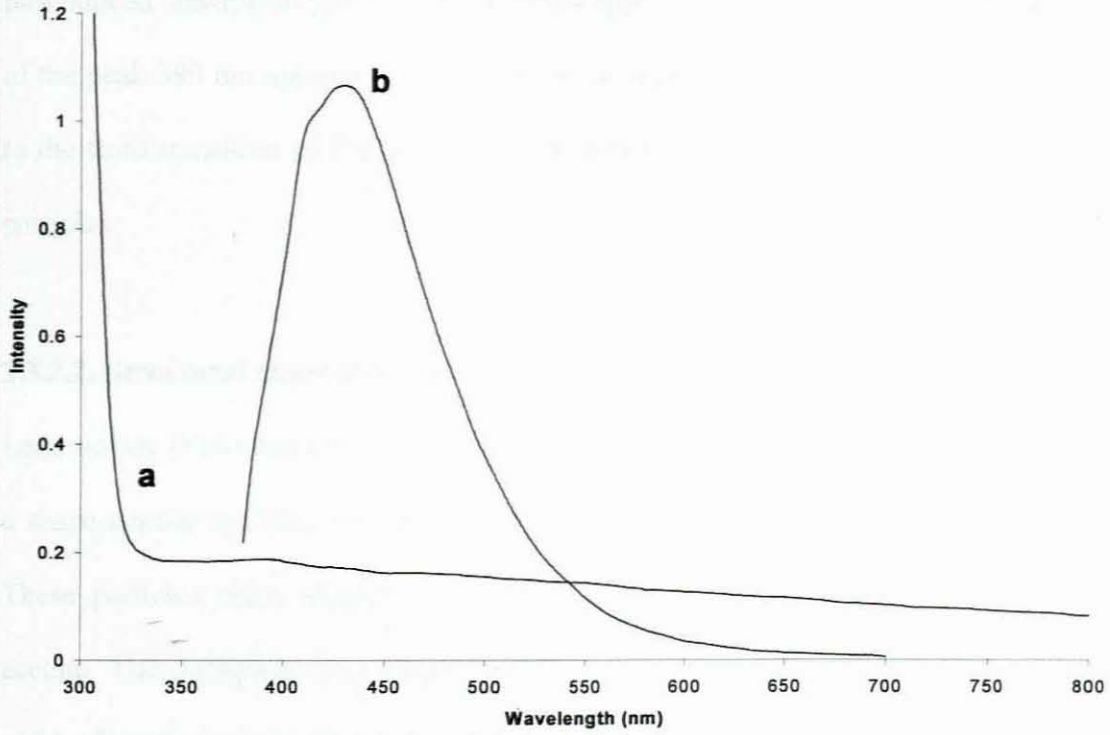

Figure 28: The optical (a) and photoluminescence (b) spectra of HDA-capped PbS nanoparticles prepared from complex **V**.

When complex **V** was thermolysed in HDA at 200 °C using an alternative route of direct addition of the precursor, the absorption spectrum showed the broadening from the band close to 390 nm that is due to the tailing of the shoulder at about 650 nm. The typical band at about 390 nm is shifted to about 383 nm, which when the excitation was performed in relation with this emission band showed red shift in the photoluminescence emission maximum at about 432 nm. The photoluminescence spectrum (Figures 26 & 28) shows well passivated lead sulfide nanoparticles with minimum surface defects. Similar optical features and photoluminescence behaviour were observed irrespective of the type of alkylthiourea precursor. Both HDA and

TOPO provides effective surface capping for PbS nanoparticles with a more pronounced absorption spectrum for TOPO-capped PbS (Figure 26). The broadening of the peak 390 nm appears to be caused by the more pronounced shoulder attributed to the third transition of PbS nanoparticles, which is typical of smaller sizes of PbS particles.

2.3.2.2. Structural characterisation

Lead sulfide (PbS) nanoparticles generally give particles, which are predominantly in a shape similar to cubic rock-salt, although a hexagonal phase was also observed.[282] These particles were prepared by a solution reaction carbon disulfide with lead acetate. The diethylthiourea complex (**IV**) used for this synthesis provided a lower yield of particles in TOPO and also when the precursor was dissolved in TOP but thermolysed in HDA. Greater yields were obtained upon direct addition of the solid precursor into HDA and the solid obtained as product proved to be bulky material upon analysis using the X-ray analysis.

Table 13: Experimental XRD and SAED data of PbS particles from complex **V**.

d(lit*)/2θ	d(exp)/ 2θ	hkl
24.9	25.6	111
28.4	31.2	200
43.3	43.1	220
47.6	51.0	311
53.3	53.5	222
64.9	62.3	400

* Ref 1999 JCPDS

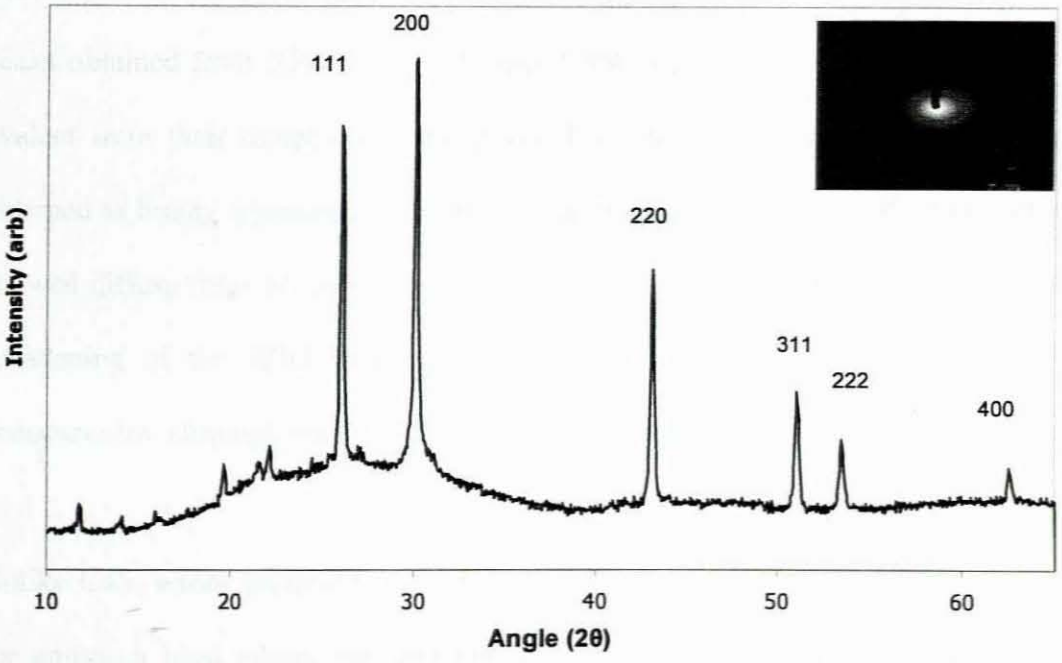

Figure 29: The XRD patterns of TOPO-capped PbS nanoparticles from complex **IV** and its selected area electron diffraction.

The XRD patterns were consistent with those of hexagonal PbS nanoparticles prepared from complex **IV**. The predominance of the hexagonal PbS nanoparticles is indicated by the peaks at 25.6, 31.2, 43.1, 51.0, 53.5 and 62.3 which correspond to the hkl planes indexed in Table 13 to 111, 200, 220, 311, 222 and 400 planes, respectively. This indicates that the complex **IV** was thermolysed cleanly to hexagonal particles similar to CdS. Particles grown in HDA gave broadened peaks, which is an indication of smaller particle sizes. Even though peaks are of those nanosized particles, there are impurities associated with reaction between HDA and the alkylthiourea organic compounds together impurities from the metal and its salt. Some impurities are present also in TOPO-capped particles in minimum amounts.

This could be a measure of the relation of the completeness and cleanliness of the thermolysis of the precursor in HDA with respect to time and concentration. The peaks obtained from XRD of TOPO-capped PbS are indicative of bulk particles as evident from their sharpness of the peaks. For both capping agents particles were obtained as highly crystalline materials. The selected area electron diffraction patterns showed diffuse rings of the crystalline particles typical of the nanosized regime. The broadening of the XRD peaks as in Figure 30 indicates the small size of the nanoparticles, although the PbS particles prepared were impure.

Unlike CdS, where particle sizes were mainly determined from the XRD as well as the emission band edges, particles obtained for PbS showed no tendency to form agglomerates. This can be seen from their TEM images and hence it was possible to determine the particle sizes. For particles prepared at 200 °C an average diameter of 8 nm was obtained from a distribution ranging from 6 to 10 nm (Figure 31). All particles showed similar morphology, hexagonal and consistent with the XRD patterns with the planes 111, 200 and 220 being predominant. A similar morphology was observed at a higher temperature (Figure 32) 250 °C with particles collapsing from hexagonal to close to sphere-like shapes. In addition the size distribution is wider and ranges from 7 to 17 nm with an average diameter of 10.8 nm. This is a notable difference in the average particle sizes for about 2.8 nm from 200 to 250 °C. Temperature is a known factor that influences the growth and size of particles. Higher temperature favour larger particle sizes.

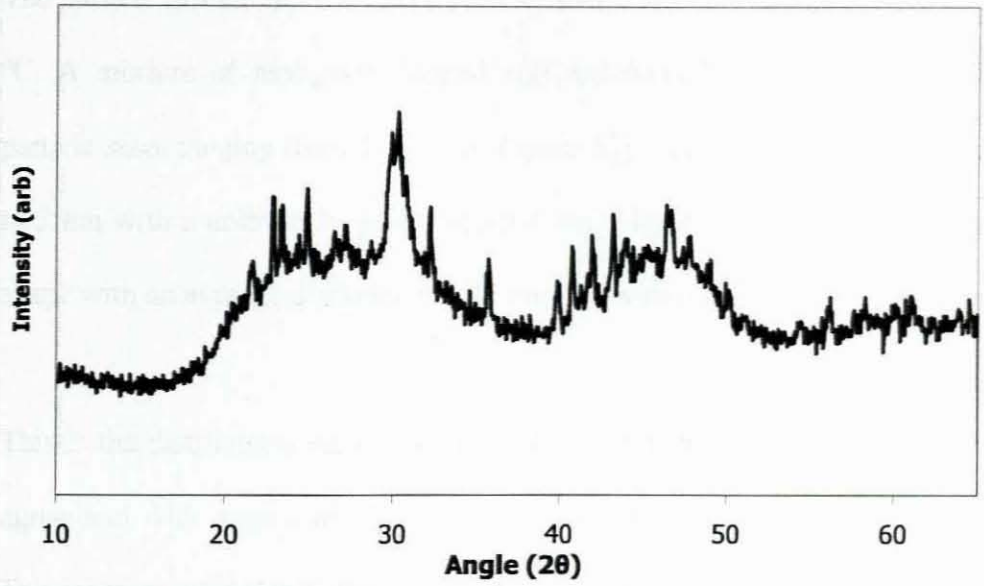

Figure 30: The XRD pattern of HDA-capped PbS nanoparticles from complex **V**.

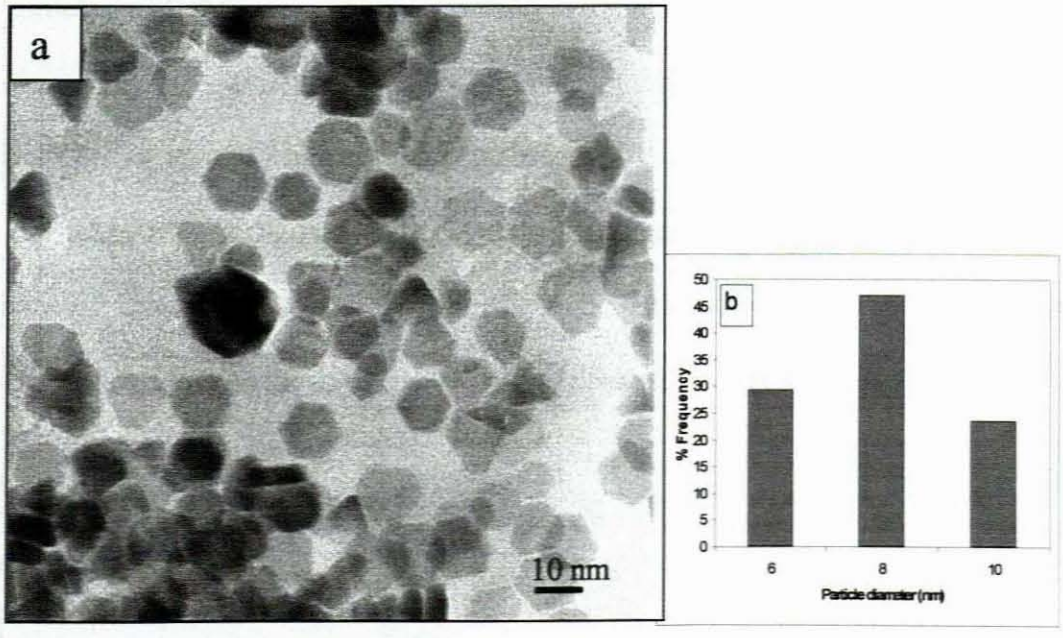

Figure 31: (a) TEM images of TOPO-capped PbS from complex **IV** at 200 °C and (b) corresponding particle size distribution histogram.

The particle growth in HDA gave even smaller diameters at temperature of about 200 °C. A mixture of hexagonal shaped and rod-shaped particles were obtained with particle sizes ranging from 2 to 4 nm (Figure 33). The rods have diameters of about 2 to 3 nm with a uniform length of about 4 nm. Majority of particles are hexagonal in shape with an average diameter of 2.25 nm and with a narrow size distribution.

This is the distribution indicative of highly monodispersed nanoparticles, which is in agreement with narrow band of the photoluminescence emission (that is < 100 nm). The presence of the rod shaped particles could explain the impurities obtained from the HDA-prepared PbS nanoparticles as evident from the XRD results (Figure 30). The absorption spectra of HDA-capped particles (Figure 27) gave evidence of smaller particles with the emergence of the band or shoulder at about 650 nm. The particle sizes show the expected trend with temperature. An increase from an average diameter of particles ranging from 8.0 nm to 10.8 nm as temperature increases from 200 to 250 °C in TOPO and the use of HDA as capping agent gave particles of average diameter 2.25 nm at 200 °C. Both optical properties and the structural characteristics conform to the particles in the nanosized region.

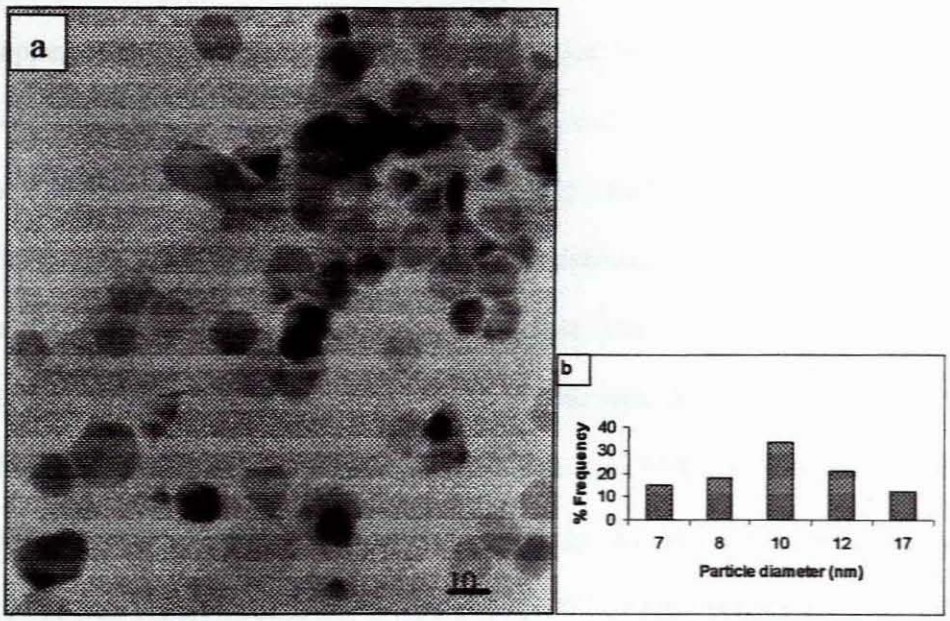

Figure 32: (a) TEM images of TOPO-capped PbS from complex **IV** at 250 °C and (b) corresponding particle size distribution histogram.

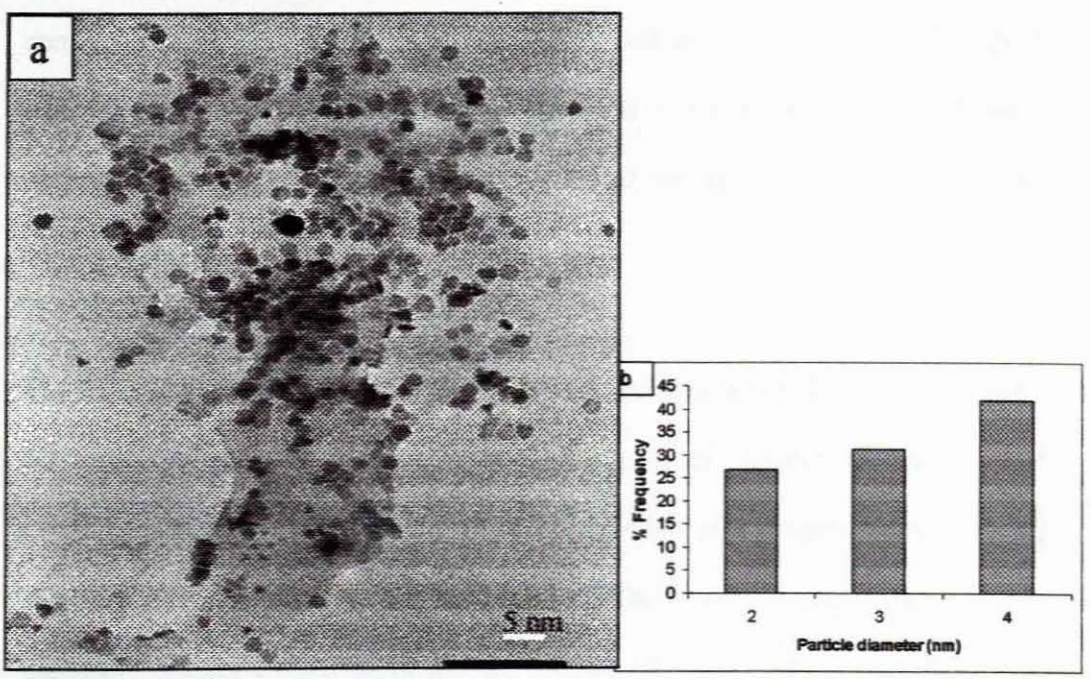

Figure 33: (a) TEM images of HDA-capped PbS from complex **V** at 200 °C and (b) corresponding particle size distribution histogram.

2.3.3. Synthesis of copper sulfide nanoparticles

Copper sulfide particles are very interesting due to their ability to form various stoichiometries. Their complex structure and valence state of copper sulphide result in some unique properties like green copper sulfide which shows a metal-like electrical conductivity. Following the successful use of dithiocarbamate copper complex as a single-source precursor to prepare copper sulfide nanoparticles,[288] efforts have been made to prepare similar complexes, with alkylthioureas being the source of sulphur. Thermolysis of copper complex of dithiocarbamate in TOPO gave comparatively low yields of the nanoparticles and a relatively large amount of the bulk material. No growth was observed at lower temperature (180 °C) and increasing temperature to about 200 °C produced large amount of product, which was proven to be bulk material by the XRD peaks obtained. Similar results were obtained with alkylthiourea complexes as precursors to preparing copper sulfide nanoparticles. Although the yields were high for the nanoparticles preparations, it was evidently bulk materials as observed from the XRD analysis of a mixture of various stoichiometries of copper sulfide particles.

The morphology of the particles in all synthesis was predominantly hexagonal, as was the phase from the XRD patterns. Rod-like shapes of particles of copper sulfide particles were observed from a microwave irradiation of a sodium dodecyl sulphate solution of copper nitrate and thioacetamide.[289] These were crystalline particles with diameters ranging from 5 to 10 nm and lengths of about 30-50 nm. Preparation of unique copper sulfide flakes in microemulsion under hydrothermal conditions was

reported by Zhang and Gao[290] in which much smaller hexagonal Cu_2S nanodisks formed with the pre-addition of n-dodecanethiol to the microemulsion. Table 14 outlines the conditions for the preparation of copper sulfide nanoparticles. This includes the variation of concentration using precursor and solvent as well as temperature.

Table 14: Conditions for the synthesis of copper sulphide nanoparticles using different precursors

Complex	Amount (g)	Temperature (°C)	Time (Min)	HDA (g)	TOPO (g)
VI	0.8	160	15	10	
	1.0	200	25	20	
	0.8	260	15	10	
VII	0.8	200	15	10	
	2.0	200	30		20

2.3.3.1. Optical properties

Copper sulfide is quite interesting in the sense that it has many stable phases from chalcocite (Cu_2S) to sulphur-rich covellite (CuS). Each stable phase has its own characteristic optical property e.g. covellite has a characteristic broad absorption band in the near infrared region (~920 nm) which decreases on increasing the sulfur content, that is from covellite to digenite ($Cu_{1.8}S$) to djulerite ($Cu_{1.96}S$). This absorption is completely absent in the chalcocite (Cu_2S) phase. As a result of these

observations and the optical features for the TOPO-capped copper sulfide from complex **VII** with an excitonic peak (480 nm) infers the chalcocite (Cu_2S) (Figure 34). This was evident from the absorption spectrum as the only excitonic feature observed for these nanoparticles. This is a large blue shift (near 2.58 eV) in relation to the bulk Cu_2S (1022 nm, 1.21 eV), from the near infrared region to the ultraviolet region. The absorption edge was broadening as observed when particles have a wider particle size distribution. Not only was the absorption edge broadened, but that lower yield of these particles was obtained using the method involving dissolving the precursor in TOP before thermolysis. A similar problem of lower yield of nanoparticles was reported[288] using the same method because of the formation of the bulk. The photoluminescence behaviour showed a red shift in relation to the excitonic absorption band (480 nm) with the emission maximum at about 527 nm. There are no observable additional features due to transitions associated to the surface defect states, presumably because of the uniform coverage of the surface of the small particles by the capping agent TOPO.

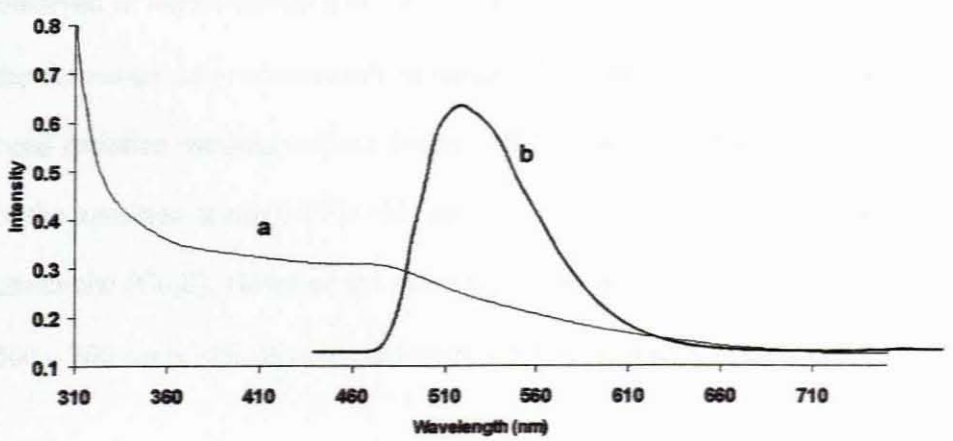

Figure 34: Absorption (a) and photoluminescence (b) spectra of TOPO-capped copper sulfide nanoparticles at 200 °C for complex **VII**.

The blue shifts indicate small size of the particles because nanosized semiconductor particles generally exhibit a threshold of energy in the optical absorption measurements. This is due to their size specific band gap structures, which is reflected by the blue shifting of the absorption edge (from near infrared to visible region) with decreasing particle size.

A mixture of copper sulphides were also confirmed from the optical spectra of some sample solutions which gave a broad band at about 650 – 900 nm in addition to the band edge typical of Cu_2S nanoparticles (in the range 488 nm). The broad band indicates the presence of particles associated with covellite (CuS) for the HDA-capped copper sulfide particles. The optical spectrum of HDA-capped copper sulfide particles also shows a blue shift in relation to the bulk. This was first observed from thermolysis of complex **VI** at temperatures 160, 200 and 260 °C (Figure 35). There are two major transitions observed with the first at about 370 nm (160 °C) and 380 (200 °C), whereas only the second broad transition in the region 550 – 800 nm was observed at higher temperature (260 °C). The second broad peak is associated with the formation of predominantly covellite (CuS) nanoparticles, which gives a broad band emission maximum about 586 nm. This is also confirmed by the disappearance of the transition at about 370 – 380 nm, which is associated with the predominance of chalcocite (Cu_2S). However the presence of the less intense broad band in the range 500 – 700 nm is indicative of chalcocite nanoparticles at 160 and 200 °C.

The optical properties are indicative of change from chalcocite to a more sulfur rich covellite as the temperature is increased. The TOPO-capped copper sulfide nanoparticles gave the major excitonic peaks at about 480 nm as compared to the additional band observed for particles observed for HDA-capped nanoparticles. This is more pronounced in the nanoparticles prepared from complex **VII** at 200 °C. The optical spectrum in Figure 38 indicates the emission band edge at about 453 nm with the photoluminescence spectrum showing the emission maximum at 460 nm.

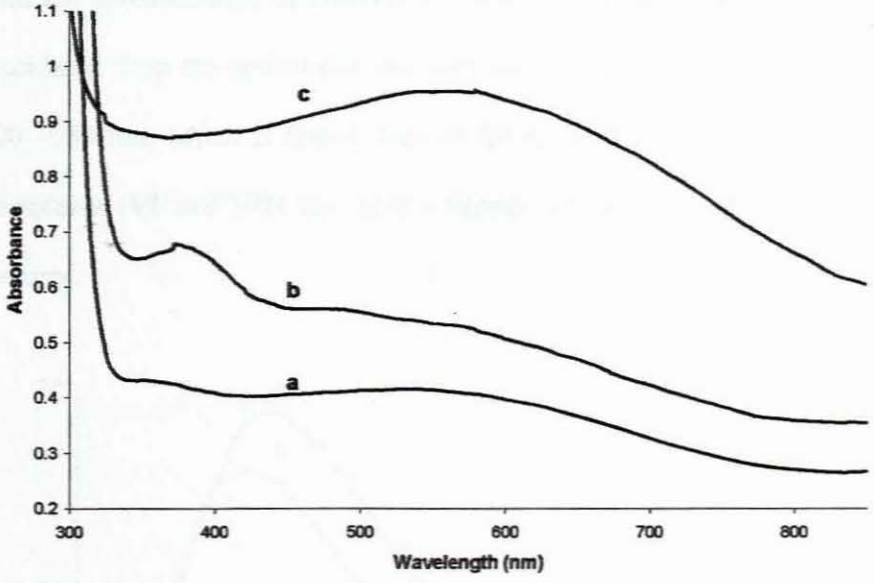

Figure 35: Absorption spectra of HDA-capped copper sulfide nanoparticles prepared from complex **VI** at (a) 160 °C, (b) 200 °C and (c) 260 °C.

This is a typical blue shift from the optical spectrum and red shift from the photoluminescence of nanoparticles. The second band which is broad is more pronounced and gave the maximum at 830 nm, which is lower than the expected band at about 920 nm for covellite (Figure 35). This indicates the formation of the sulphur rich covellite, which predominates over the other copper sulphides, which is further

supported by XRD analysis (Figure 38). The photoluminescence of the nanoparticles of complex **VI** shown in Figure 36 gave emission maxima at 439, 450 and 457 nm which corresponds to temperatures 160, 200 and 260 °C. The increased red shift of the photoluminescence behaviour appears to be the result of high temperatures presumably resulting in larger particles. However the mixture of Cu_2S and CuS might account for the observation of the red shift in photoluminescence behaviour. The variation of the capping agents from TOPO to HDA gave evidence of copper sulfide with the predominance of chalcocite (Cu_2S) and covellite (CuS) in HDA. This was elucidated from the optical features with the formation of a broad band in the region 800 –950 nm, which is known feature for covellite. Different alkylthiourea copper complexes (**VI** and **VII**) also give different optical and photoluminescence spectral features.

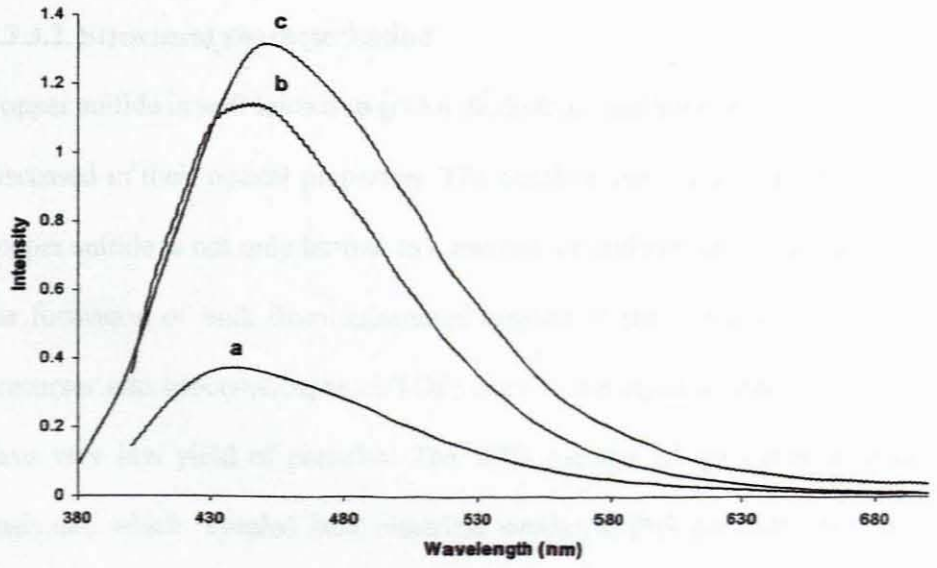

Figure 36: Photoluminescence spectra of HDA-capped copper sulfide nanoparticles prepared at (a) 160°C, (b) 200 °C and (c) 260 °C from complex **VI**.

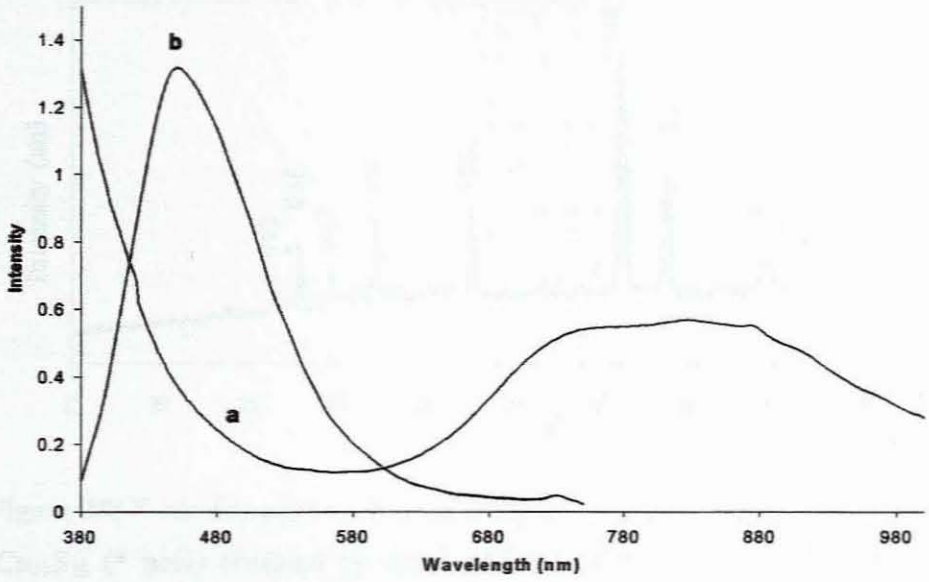

Figure 37: Absorption (a) and photoluminescence (b) spectra of HDA-capped copper sulfide nanoparticles prepared from complex **VII** at 200 °C.

2.3.3.2. Structural characterisation

Copper sulfide is well known to give a mixture of sulphides in different proportions as discussed in their optical properties. The problem associated with the preparation of copper sulfide is not only limited to a mixture of different stoichiometries, but also to the formation of bulk from substantial amount of the precursor. By dissolving the precursor into trioctylphosphine (TOP) prior to the injection into hot TOPO or HDA gave very low yield of particles. The XRD patterns of the material obtained were analyzed, which revealed bulk materials similar to PbS particles obtained from the corresponding alkylthiourea complex. The optical properties in solution and TEM showed predominance of the truncated octahedron for all the samples of copper sulfide particles.

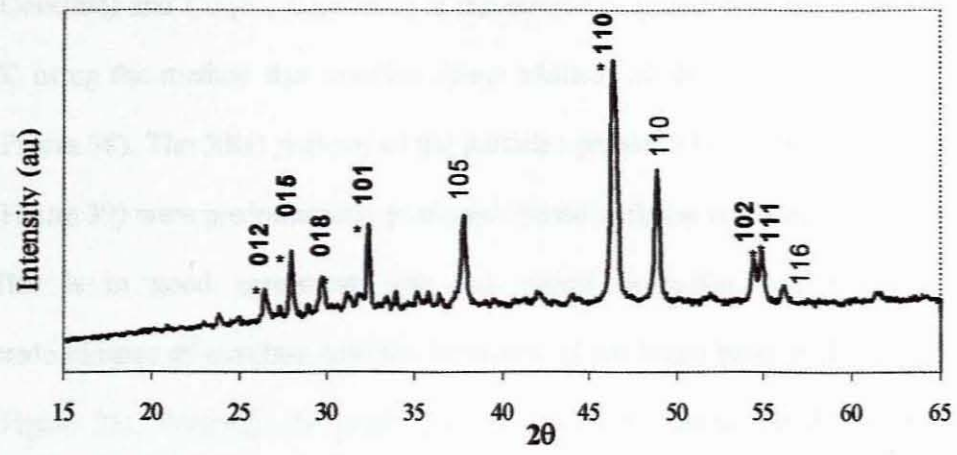

Figure 38: X-ray diffraction pattern of CuS_y showing a mixture of $Cu_{1.8}S$ and $Cu_{31}S_{16}$ (* bold) obtained by direct addition of the precursor in TOPO from the complex **VII** at 200 °C.

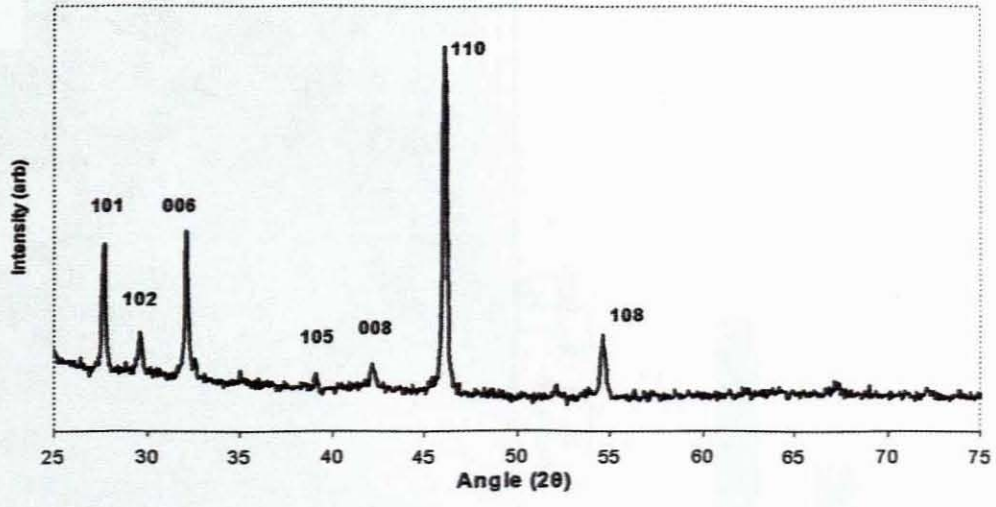

Figure 39: XRD patterns of copper sulphide particles prepared in HDA from complex **VI** at 200 °C.

The XRD patterns (Figure 38) were evident of a mixture of the sulphides, $Cu_{1.8}S$ (Covellite) and $Cu_{31}S_{16}$ (Djurleite) in the sample prepared from complex **VII** at 200 °C using the method that involves direct addition of the precursor into hot TOPO (Figure 38). The XRD patterns of the particles prepared from complex **VI** at 200 °C (Figure 39) were predominantly peaks associated with the crystalline covellite (CuS). This is in good agreement with the optical properties, which indicated the predominance of covellite with the formation of the broad band in the visible region (Figure 35). Although the peaks are very sharp indicating the formation of bulk material, the samples in solution from the optical study and TEM support the evidence of a predominantly hexagonal phase. This is conclusive of the same type of copper sulphide materials forming in both solution and bulk.

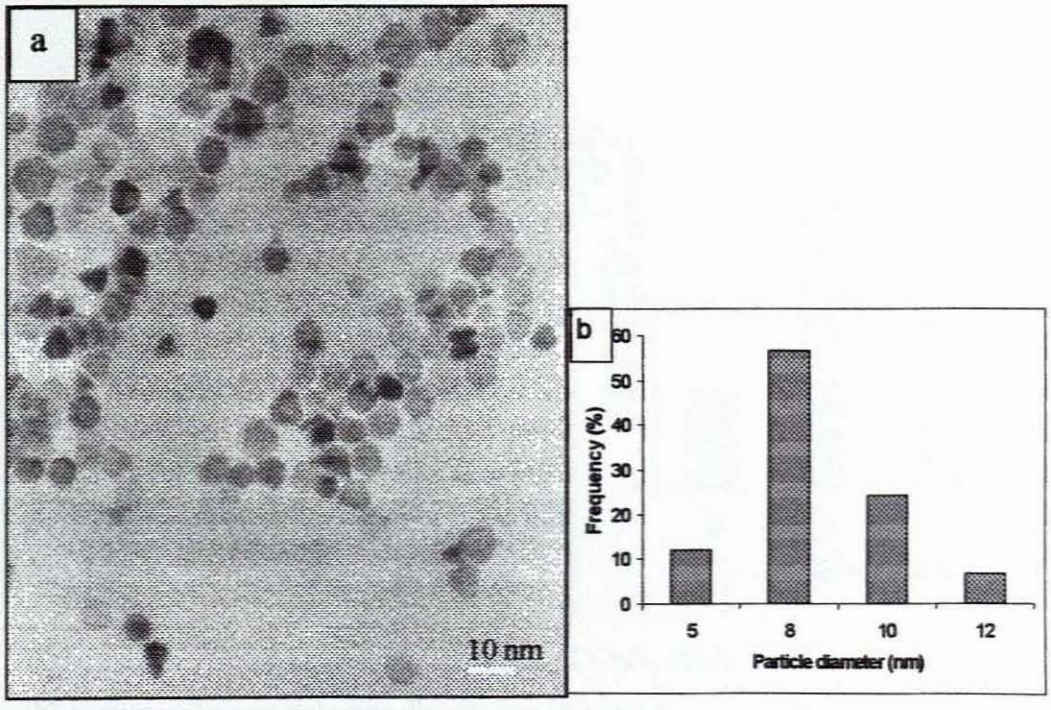

Figure 40: (a) TEM images of TOPO-capped CuS from complex **VII** at 200 °C and corresponding particle size distribution histogram.

The TEM images of copper sulfide nanoparticles show relative stability in that they show no signs of agglomeration and collapse of the particles compared to TOPO-capped CdS nanoparticles. This observation was irrespective of the capping agents, which were found to cover the surface of the particles uniformly and effectively. The particles prepared in both HDA and TOPO gave same morphology in truncated octahedron as in Figure 40. The particles were determined from these images and accounted for relatively narrow size distribution.

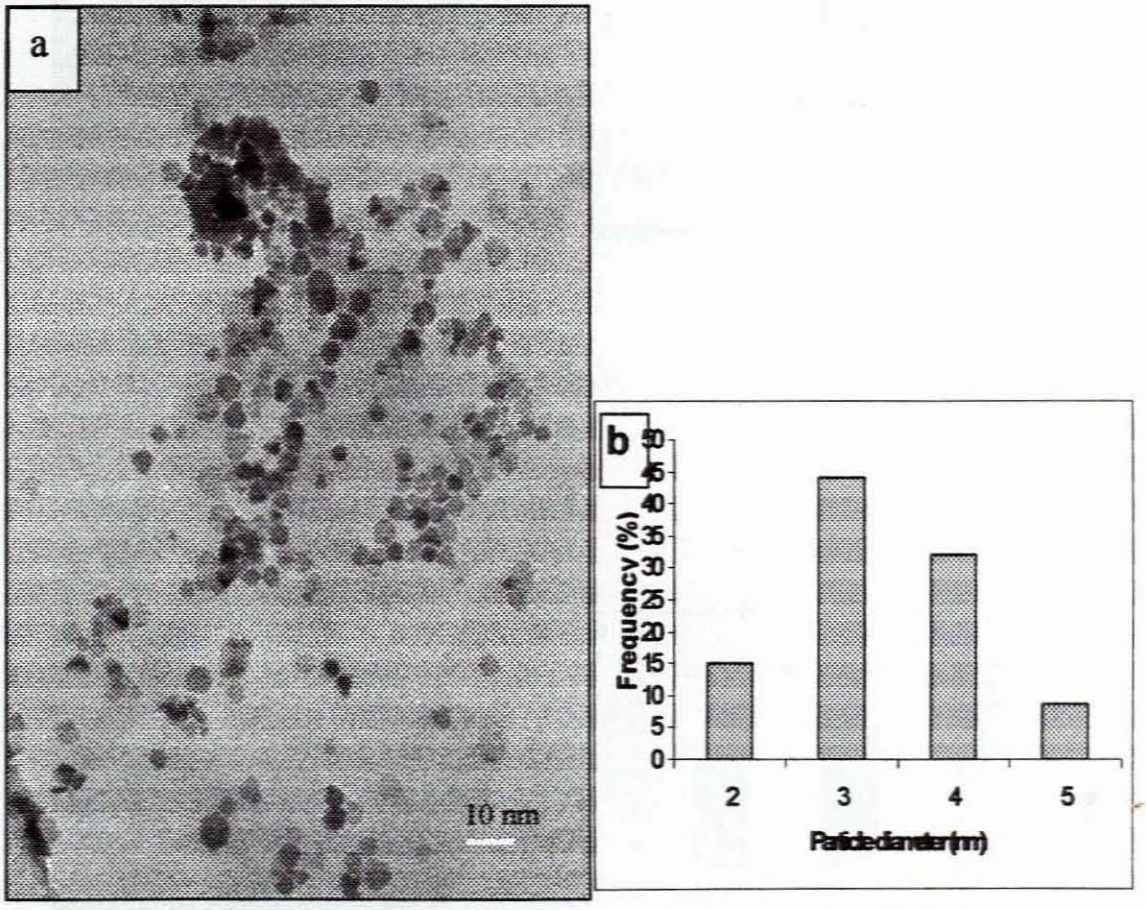

Figure 41: (a) TEM images of HDA-capped Cu_xS_y from complex **VI** at 160 °C and (b) corresponding particle size distribution histogram.

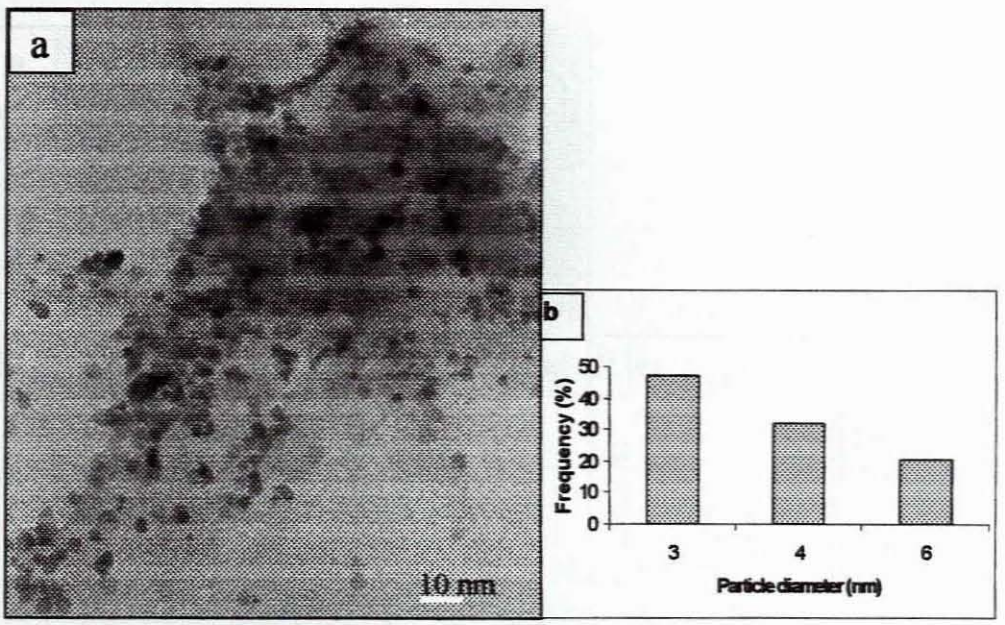

Figure 42: (a) TEM images of HDA-capped Cu_xS_y from complex **VI** at 200 °C and (b) corresponding particle size distribution histogram.

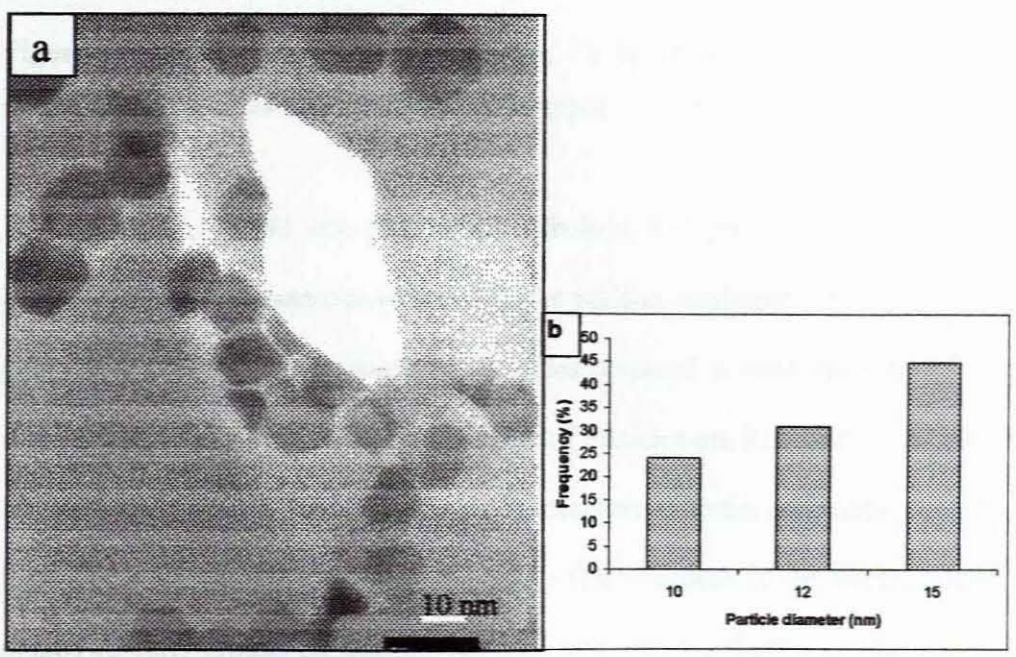

Figure 43: (a) TEM images of HDA-capped Cu_xS_y from complex **VI** at 260 °C and (b) corresponding particle size distribution histogram.

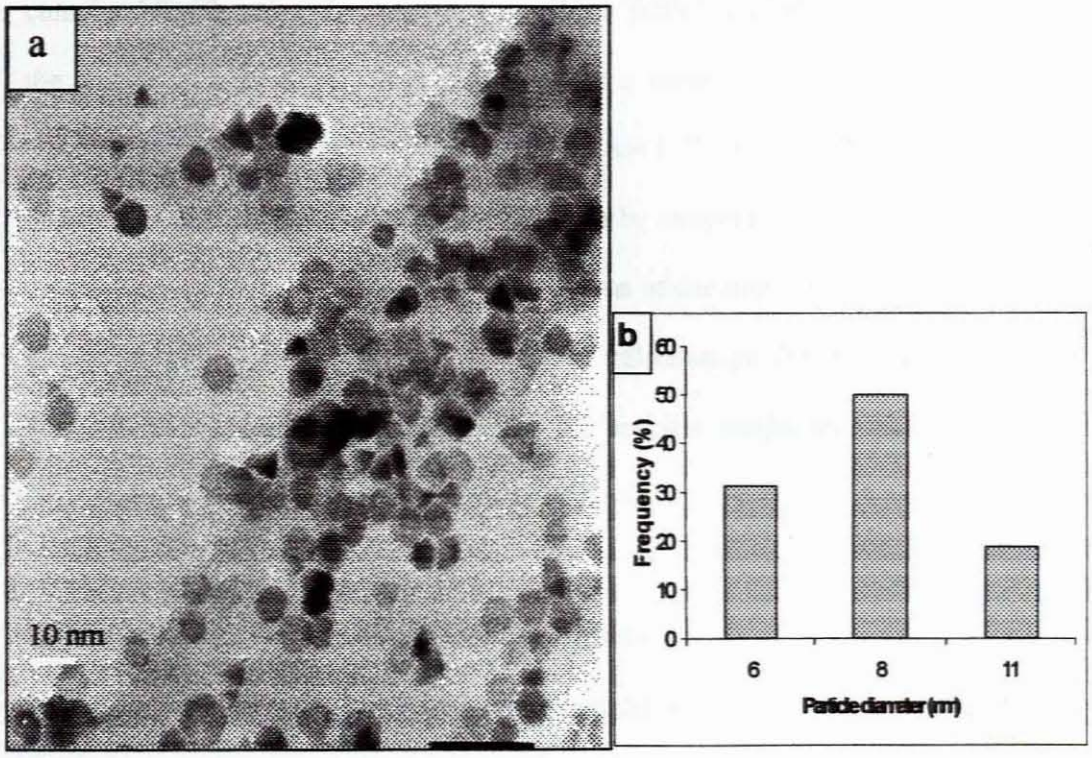

Figure 44: (a) TEM images of HDA-capped Cu_xS_y from complex **VII** at 200 °C (b) corresponding particle size distribution histogram.

Figures 40, 41, 42, 43 and 44 show morphology and particle size distribution of copper sulphide nanoparticles prepared under various conditions from complexes **VI** and **VII**. The temperature variation of samples prepared in HDA gave particles with narrow size distribution. Average diameters of particles are 3.5 nm (160 °C), 4.3 nm (200 °C) and 12.3 nm (260 °C) and this is consistent with the temperature as a factor influencing growth and size of nanoparticles. The variations of the alkyl groups from methyl to ethyl groups on the thiourea have significant influence on the size of the particles. This was observed by growth of copper sulfide at 200 °C in HDA, which

gave particles with average diameters 8.33 nm for complex **VII** and 4.33 nm for complex **VI**. Changing the capping group from TOPO to HDA resulted not only in the change of optical properties but also with a slight change in the diameters of particles (8.33 nm in HDA-capped (Figure 44) and 8.75 nm in TOPO-capped (Figure 40). In this case particle size is influenced more by temperature than the alkyl groups on the complex. It is known fact that the patterns of decomposition of precursors are greatly influenced by temperature, hence the reflection on the growth of particles. Hence it is most appropriate to choose the specific conditions suitable for size distribution or properties desired for the nanoparticles.

2.3.4. Attempted synthesis of zinc sulfide nanoparticles

Zinc sulfide an important semiconducting material which is commercially used as a phosphor and also in thin film electroluminescent devices.[291-293] ZnS also doped with various transition metal ions such as manganese is an efficient light emitting material. When such dopants are inserted into nanometre sized matrix, they exhibit interesting magneto-optical properties. ZnS nanoparticles have been studied in the form of colloids, with the main interest in their photocatalytic and photochemistry aspects.[294,295] Rosetti *et al.*[200] and Henglein *et al.*[296] have studied the evolution of the optical electronic properties of ZnS nanocrystallites with varying size. These colloids are however, stable only for a short duration of time, as they are prone to photo-corrosion and also agglomerate into larger particles.[142,297] There have been attempts to obtain free standing powders of ZnS nanocrystallites by using suitable surface passivating agents that binds to the surfaces of atoms of the nanocrystallites, making

them stable under normal atmospheric conditions.[298] However, most of the synthetic procedures yield crystallites having large size distribution. This is commonly evident from the optical absorption spectra, which in many reported cases, are broad and featureless. Good quality nanocrystallites are prepared by the thermolysis of elemental zinc and sulphur in a coordinating solvent.[299] The current use of ethylxanthate, N, N'-bis(thiocarbamoyl) hydrazine and N, N'-dioctylthiourea zinc complexes as single source precursors to prepare ZnS nanoparticles gave blue shifts in their optical absorption spectra.[272] However, the photoluminescence spectra show evidence of emission surface raps and the particles from the TEM images become poorly defined.

In this work attempts have been made to use the complex, $ZnCl_2(CS(NH_2)NHCH_3)_2$, prepared by refluxing zinc chloride and methylthiourea in ethanol. The complex is very stable and obtained in good yield, hence it was used in an attempt to prepare TOPO-capped ZnS nanoparticles by a single source precursor method. The TOPO capped nanoparticles were synthesised by the injection of the precursor dispersed in TOP into hot TOPO under an inert atmosphere of nitrogen gas. White particles were obtained which when analysed gave featureless UV-visible absorption and photoluminescence spectra, and also their EDAX elemental analysis of the TEM images giving only evidence of TOPO. By varying conditions such as amount of precursor, temperature and time gave no improvements on the analysis of these particles. These particles are extremely unstable similar to colloids prepared by

Rossetti *et al.*,[142] which were stable only for a short duration of time, as they are prone to photo-corrosion and also agglomerate into larger particles.

2.3.5. Attempts to deposit metal sulfide thin films by CVD.

The thermal decompositions of the cadmium complexes reported in this work were also studied by using thermogravimetric (TGA) methods under inert and air atmosphere. The decomposition start with a loss of weight in each compound around 200 °C and continue to about 400 °C where most of the organic part of the molecule and the chlorides has been lost. A period of slow loss of mass led to the formation of the metal sulphide, which was completed at about 500 – 600 °C. This conforms to the theoretical percentages of CdS expected to be formed the complexes.

This observation together with the colour of the residue indicated that these complexes yield predominantly metal sulfide independent of the atmospheric conditions. This may be due to the bonding of the thiourea ligand to the metal as sulfide source. We have not observed any exothermic process in our TGA curve in contrast to those observed for copper, zinc and tin thiourea complexes[136] in which cases the metal sulfides were converted to their metal oxides. No such conversion of cadmium, copper and lead sulfide into their oxides was observed during thermal decomposition of complexes reported in this work under air, which is usually accompanied by the slight increment of the curve at very high temperatures. Copper complexes thermally decompose to give black residues in which the TGA trends is similar to those of cadmium complexes. The onset of thermal decomposition for all

the copper complex ranges from about 200 to 230 °C and this correspond to their melting points region. This continues to about 400 °C where most of the organic parts of the molecule and the chlorides have been lost. A period of slow loss of mass led to the formation of sulfide, which was completed by about 500 – 600 °C. This conforms to the theoretical percentages of copper sulfide in the complexes. The zinc complex decomposes in a similar pattern to the corresponding cadmium and copper complexes with the onset at about 216 °C and this continues until the curve flattened when the entire residue left is only zinc sulfide. Mass loss continues to about 350 °C where most of the organic component of the precursor complex and the chlorides has been lost. A period of slow loss of mass led to the formation of the sulfide, which was completed by about 450 – 550 °C. The trends in decomposition of these complexes yielded products, which in colour correspond to the Cu, Pb and Cd sulphides. It follows from the detailed analysis of CdS from these residues that Cu and Pb would also be useful for preparing nanoparticles and for their potential for deposition of thin films. This sets good precedents for the use of these complexes as single-source precursors to the preparation of nanoparticles and thin films by chemical vapour deposition. The volatility of compounds is one of the primary requirements for the deposition of thin films.

Metal organic chemical vapour deposition (MOCVD) is the type of CVD technique for growing semiconductor films employing either a separate metal and chalcogenide source[300,301] for example CdS films prepared from $Cd(CH_3)_2$ and H_2S or single-source precursor method in which both the metal and sulfide are within a single molecule.

The dialkyldithiocarbamate metal complexes of Cd and Zn have been used to grow CdS, ZnS and Cd_x-$Zn_{1-x}S$ films.[302-305] The usefulness of single source precursors in MOCVD is based on the fact that they volatilise without decomposition and at higher temperatures they decompose to solid metal sulfide.[305,306] Two CVD techniques, i.e. low pressure (LPMOCVD) and aerosol assisted (AACVD), are composed of a reactor tube, graphite susceptor to hold the substrate, heating lamp (to control substrate temperature), furnace for heating the precursor, rotary pump and carrier gas as described elsewhere.[302,307] Both techniques are suited to grow good quality thin films using single-source molecular precursors.

In this work AACVD was used in an attempt to grow cadmium, lead and copper sulfide films. The precursor is first dissolved in a suitable solvent e.g. toluene or tetrahydrofuran to prepare an aerosol which was transported by nitrogen gas into the reactor tube. The substrate is kept in the tube, where the aerosol adsorbs and reacts to form a film and by-products. Aerosol delivery systems are suitable techniques where the precursor is thermally sensitive and slowly decompose if heated for extended period of time needed to elevate vapour pressure. Precursors are required to be non-toxic, stable at room temperature, need to produce high purity films and most importantly volatility. It was observed from the TGA decomposition curves that the complexes are involatile with the desirable lower melting pints. Temperatures ranging from 300 to 450 °C showed evident loss of organic components of the ligands from the precursor. These are temperatures employed for the film growth over a glass substrate. Various temperatures, amounts of precursor and growth times used,

produced either powdery or very thick black films, which upon analysis revealed substantial amount of carbon on the glass substrate. In some of the deposition processes especially with cadmium complexes produced no film. The growth of carbon films is attributed to the loss of organic components of the complexes and their involatile nature such that only carbon is deposited on the film substrate.

2.4. CONCLUSION

The single-source precursor method has provided one of the effective routes towards thermolysis of compounds to produce metal sulfide nanoparticles. Alkylthiourea metal complexes are very stable under normal conditions and decompose under inert atmosphere to metal sulfide particles upon thermolysis. By controlling the conditions for thermolysis such as temperature, time and alkyl group on thiourea ligands gave more insight into tailoring the size of nanoparticles with their electronic properties. A number of observable features were made by varying the metal sulphides and this includes cadmium, lead and copper sulfide with the band emission edges in the ultra-violet region of the spectrum. The blue shifts of the band edges are consistent with the quantum confinement of CdS particles in relation to the bulk. Lead sulfide gave two absorption features in the ultraviolet region, which are results of transitions of the surface modified PbS nanoparticles. Copper sulfide gave interesting optical features in that in TOPO chalcocite (Cu_2S) was more prevalent and HDA resulted in the features of covellite (CuS) particles.

The analysis of various forms of copper sulfide was supported by XRD patterns which indicated formation of a mixture of sulphides in TOPO whereas mainly peaks associated with covellite were observed for copper sulfide prepared in HDA. Cadmium and lead sulphides both gave XRD patterns, which show that the PbS and CdS particles are predominantly hexagonal in phase. Copper and lead sulphide gave very sharp peaks which are characteristic of bulk materials. This may be the result of large amount of the precursors of lead and copper decomposing into larger particles which settle in solution. The analysis was made from samples obtained as a result of an attempt to improve the yield of these particles by using an alternative route. The peaks observed for cadmium sulfide particles are broadened and increased broadening with decrease in particle size was also observed. The average particle size for CdS nanoparticles was determined from the broadened of peaks in their XRD using the Scherrer methods. These particle sizes were in good correlation to those determined from the emission band edges using the direct band gap method.

The TEM images revealed more crystallinity of CdS particles with the lattice fringes observed as well as from the selected area electron diffraction patterns. It was impossible to determine the particle sizes for CdS as they form agglomerates rapidly. Unlike CdS, sizes for copper and lead sulfide nanoparticles were determined from the TEM images, which also indicated similar morphology as truncated octahedron. The particle sizes were also monitored with temperature with larger particle sizes obtained at higher temperatures. The morphology of CdS nanoparticles was spherical to needle-like particles. The alkyl groups on the thiourea ligands have little influence on

the particle sizes but show potential influence on the morphology. The variation of methyl, ethyl and phenyl groups are usually overcome but factors such as temperature and time for preparation of nanoparticles. Hence the variation of these alkyl groups has not been extensively explored for the preparation of PbS and Cu_xS_y nanoparticles. Attempts to grow ZnS resulted in featureless optical properties and their photosensitive nature gave TEM images which only showed evidence of the capping agent. The involatile nature of the precursors gave poor or no film when employed in the growth of thin films by using AACVD technique.

2.5. FUTURE WORK

There are a number of problems associated with the nature of the precursors. This includes variations from the metal to the alkyl group on the thiourea ligands, which has been highlighted from these results. Cadmium precursors produced particles which agglomerate rapidly whereas copper and lead produced relatively stable but low yield of particles in solution. It would require further investigation as varying the capping group in CdS to make stable particles from these precursors. And second aspect is finding the best conditions to improve the yields of copper and lead sulfide nanoparticles from their precursors.

Bulk copper and lead sulfide show absorption spectra with the band gap lying in the visible region for coppers sulfide and near infrared region for lead sulfide. The incorporation of these stable nanoparticles into other metal chalcogenides to form core shell with interesting and intriguing electronic properties. The electronic

properties of metal sulfide vary from metals as well as the source of sulfide ion in the ligands attached to metals. Hence, long chain alkylthiourea ligands could be used as a probe for investigating the problems of lower yields and rapid agglomeration of particles. Henceforth the alkylthiourea complexes are very easy to prepare, inexpensive and very stable, which makes them good precursors. The use alkylthiourea as source of sulfide ions could be extended to alkylselenourea to prepare selenium analogous complexes which in turn would be thermolysed to give metal selenide nanoparticles. Some of the precursors could be used by other CVD techniques to grow thin films.

1.3.1.6. REFERENCES

1. S. E. Livingstone, Q. *Rev. Chem. Soc.*, **19** (1965) 386.
2. M. Nakamoto, *Infrared spectra of inorganic and coordination compounds* 2nd edn. Wiley-Interscience, NewYork (1970), 210.
3. R. B. Penland, S. Mizumisha, C. Curran, J. V. Quagliano, *J. Am. Chem.* **79** (1957), 1575.
4. A. Yamaguchi, R. B. Penland, S. Mizushima, T. J. Lane, C. Curran, J. T. Quagliano, *ibid.*, **80** (1958), 527.
5. M. Nardelli, *Gazz. Chim. Ital.* **87** (1957), 137.
6. M. Nardelli, I. Chierci, A. Braibantai, *ibid.*, **88** (1958), 37.
7. M. Nardelli, I. Chierci, *Ric. Sci.*, **29** (1959), 1733.
8. A. Yamaguchi; R. B. Penland, S. Mizushima, T. J. Lane, C. Curran, J. V. Quagliano, *J. Am. Chem. Soc.*, **80**, (1958), 527.
9. C. D. Flint and M. Goodgame, *J. Chem. Soc.* **A** (1966), 744.
10. J. V. Quagliano, L. Schubert, *Chem. Rev.*, **50** (1952), 201.
11. F. Basolo, R. G. Pearson, *Mechanisms of inorganic reactions, Wiley Interscience,* New York, (1958), 172.
12. N. S. Kurnakov, *J. Prakt. Chem.* **50** (1894), 483.
13. A. M. Giuliani,. *J. Chem. Soc. Dalton Trans.* (1975), 492 and 497.
14. T. H. Sidall III, W. E. Stewart, *J. Org. Chem.*, **32** (1967), 3261.
15. B. T. Brown, G. F. Katekar, *Tetrahedron letters*, **28** (1969), 2343.
16. H. Kessler, D. Leibfritz, *Tetrahedron letters*, **19** (1970), 595.

17. A. Yamaguchi; R. B. Penland, S. Mizushima, T. J. Lane, C. Curran, J. V. Quagliano, *J. Am. Chem. Soc.* **80** (1958), 527.

18. T. J. Lane, A. Yamaguchi, J. V. Quagliano, J. A. Ryan, S. Mizushima, *J. Am. Chem. Soc.* **81** (1959), 3824.

19. J. Dwarakanath, D. N. Sathyanarayana, *Bull. Chem. Soc. Jpn.* **52** (1979), 2084.

20. J. H. Bryden, *Acta Crystallogr.* **10** (1957), 714.

21. W. Walter, K. P. Rueβ, *Liebigs Ann. Chem.* **743** (1971), 167.

22. R. K. Gosavi, U. Agarwala, C. N. R. Rao, *J. Am. Chem. Soc.* **89** (1967), 235.

23. W. Walter, K. P. Rueβ, *Liebigs Ann. Chem.* **746** (1971), 54.

24. Y. Mido, T. Yamanaka, R. Awata, *Bull. Chem. Soc. Jpn.*, **50** (1977) 27.

25. B. Galabov, G. Vassilev, N. Neykova, A. Galabor, *J. Mol. Struct.* **44** (1978),15.

26. W. Walter, K. P. Rueβ, *Chem. Ber* **102** (1969), 2640.

27. G. Isaksson, J. Sandstrom, Acta Chem. Scand. **24** (1970), 2565.

28. Y. Mido, H. Okada, T. Itoh, *J. Mol. Struct.* **65** (1980), 35.

29. Y. Mido, *J. Mol. Struct.* **72** (1981), 3.

30. G. Vassilev, V. Koleva, M. Ilieva, B. Galabov, *J. Mol. Struct.*, **82** (1982), 35.

31. J. Kavalek, P. Fiedler, Z. Papouskova, O. Exner, *Collect. Czech. Chem. Commun.*, **47** (1982), 35.

32. Y. Mido, H. Okada, N. Fujita, H. Yoshida, H. Matsuura, *J. Mol. Struct.*, **415** (1997), 215.

33. A. Rosenheim, V. J. Meyer, *Z. Anorg. Chem.* **49** (1906), 13.

34. C. Pakawatchai, Y. Thanyasirikul, T. Saepae, S. Pansook, H. K. Fun, K. Chinnakali; *Acta Cryst.* **C54** (1998), 1750.

35. M. J. Cox, E. R. T. Tiekink, *Z. Kristallogr.* **214** (1999), 670.

36. Z. F. Sun, C. Y. Duan, X. Z. You, *Acta Cryst.* **C50** (1994), 1012.

37. E. H. Griffith, G. W. Hunt, E. L. Amma, *J. Chem. Soc. Chem. Commun.* (1976), 432.

38. R. C. Bott, G. A. Bowmaker, C. A. Davis, G. A. Hope, B. E. Jones, *Inorg. Chem.* **37** (1998), 651.

39. Y. Okaya, C. B. Knobler, *Acta Cryst.* **17** (1964), 928.

40. C. Marcos, J. M. Alia, V. Adovasio, M. Prieto, S. Garcia-Granda, *Acta Cryst.* **C54** (1998), 1225.

41. D. Gambino, J. Benitez, L. Otero, E. Kremer, E. J. Baran, O. E. Piro, *Polyhedron* **18** (1999), 2099.

42. V. T. Joy, T. K. K. Srinivasan, *Spectrochimica Acta* **A55** (1999), 2899.

43. T. Miyazawa, T. Shimanouchi, S. Mizushima, *J. Chem. Phys.* **24** (1956), 408; **29** (1958), 611.

44. D. J. Williams, R. L. Jones, P. H. Poor, *Inorg. Chim. Acta* **144** (1988), 237.

45. I. Wharf, T. Gramsted, R. Makhija, M. Onyszchuk, *Can. J. Chem.* **54** (1976), 3430.

46. M. Nardelli, G. Fava, *Acta Crystallogr.* **12** (1959), 727.

47. F. H. Herbstein, G. M. Reisner, *Z. Krystallogr.* **169** (1984), 83.

48. N. Kheddar, J. Protas, M. Le Baccon, R. Guglielmetti, J. D. Guerchais, *Bull. Chim. Soc. Fr.,* (1976), 803.

49. D. J. Williams, K. J. Wynne, *Inorg. Chem.* **17** (1978), 1108.

50. K. Nakamoto, *Infrared and Raman spectra of inorganic and coordination compounds,* **4th edn.**, Wiley Interscience, New York, (1986), 283.

51. M. Nardelli, G. Fava, *Proc. Chem. Soc.* (1959), 194.

52. M. Schaefer, C. Curran, *Inorg. Chem.* **5** (1966), 265.

53. Y. Mido, I. Kitagawa, M. Hashimoto, H. Matsuura, *Spectrochimica Acta,* **A55** (1999), 2623.

54. D. M. Adams, J. B. Cornell, *J. Chem. Soc.*, **A** (1967), 884.

55. R. Rivest, *Can. J. Chem.*, **40** (1962), 2234.

56. R. C. Bott, G. A. Bowmaker, C. A. Davis, G. A. Hope, B. E. Jones, *Inorg. Chem.*, **37** (1998), 651.

57. A. D. Baranyi, M. Onyszchuk, S. Fortier, G. Donnay, *J. Chem. Soc. Dalton Trans.* (1976), 2301.

58. M. Nardelli, A. Braibanti, G. Fava, *Gazz. Chim. Ital.,* **87** (1957), 1209.

59. G. Marcotrigiano, R. Battistuzzi, G. Peyronel, *Spectrochimica Acta* **A32** (1976), 291.

60. D. A. Berta, W. Spofford, P. Boldrini, E. L. Amma, *Inorg. Chem.*, **9** (1970), 136.

61. Y. G. Sakharova, V. N. Perov, *Zh. Neorg. Khim.*, **239** (1978), 2844.

62. T. Y. Ashikhmina, A. S. Karnankov, *Resp. Sb. Nauchn. Tr-Yarosl. Gos. Pedagog. Inst.*, **169** (1978) 34 (Chem. Abstr. **92** (1980), 51 196a).

63. F. H. Allen, W. D. S. Motherwell, *Acta Cryst.* **B58** (2002), 407, CSD version 5.23, April 2002.

64. W. A. Spofford III, E. L. Emma, *Acta Crystallogr.* **B26** (1970), 1474.

65. G. W. Hunt, N. W. Terry III, E. L. Emma, *Acta Crystallogr.* **B35** (1979), 1235

66. R. L. Girling, E. L. Amma, *Inorg. Chem.* **10** (1971), 335.

67. H. K. Fun, I. A. Razak, C. Pakawatchai, C. Khaokhong, S. Chantraproma, S. Saithong, *Acta Cryst.* **C54** (1998), 453.

68. W. A. Spofford III, E. L. Amma, *J. Chem. Soc. Chem. Commun.* (1968), 405.

69. Y. Okaya, C. Knobler, *Acta Cryst.* **17** (1964), 928.

70. L. P. Battaglia, A. B. Corradi, M. Nardelli, M. E. Vidoni Tani, *J. Chem. Soc. Dalton Trans.* (1976), 143.

71. Y. Okaya, C. B. Knobbler., *Acta Crystallogr.* **17** (1964), 928.

72. A. G. Gash, E. H. Griffith, W. A. Spofford, E. L. Amma, *J. Chem. Soc., Chem. Commun.* (1973), 256.

73. P. G. Eller, D. C. Bradley, M. B. Hursthouse, D. W. Meek, *Coord. Chem. Rev.* **24** (1977), 1.

74. N. R. Kunchur, M. R. Truter, *J. Chem. Soc.* (1958), 2551.

75. M. van Meerssche, R. Kamara, G. Germain, J. P. Declercq, *Bull. Soc. Chim. Belg.* **91** (1982), 553.

76. J. P. Declercq, R. Kamara, C. Moreaux, J. M. Dereppe, G. Germain, M. van Meerssche, *Acta Crystallogr.* **B34** (1978), 1036.

77. G. A. Bowmaker, C. Pakawatchai, B. W. Skelton, P. Thavornyutikara, Y. Wattanakanjana, A. H. White, *Aust. J. Chem.* **47** (1994), 15.

78. W. E. Stewart, T. H. Siddall III, *Chem. Rev.* **70** (1970), 517.

79. A. S. Tompa, R. D. Barefoot, E. Price, *J. Phys. Chem.*, **73** (1969) 435.

80. F. D. Rochon, J. Barinyanga, P. C. Kong, *Can. J. Chem.* **63** (1985), 2425.

81. G. Gadr; *Trans. Met. Chem.* **15** (1990) 116.

82. M. Krunks, J. Madarasz, L. Hiltunen, R. Mannonen, E. Mellikov, L. Niinisto, *Acta Chem. Scand.* **51** (1997), 294.

83. M. Krunks, T. Leskela, L. Niinisto, *Jpn. J. Appl. Phys.* **39** (2000), 181.

84. V. Golovanov, V. Smyntyna, G. Mattogno, V. Lanto, S. Kaciulis; *Sens. Actuators B: Chem.* **26** (1995), 108.

85. V. Lanto, V. Golovanov, *Sens. Actuators B: Chem.* **25** (1995), 614.

86. C. Nascu, I. Pop, V. Ionescu, I. Bratu, E. Indrea, *Mater. Lett.* **32** (1997), 73.

87. M. A. Martinez, C. J. Herrero, *Applied Surface Science,* **136** (1998), 8.

88. S. Bourne, K. R. Koch, *J. Chem. Soc., Dalton Trans.* (1993), 2071.

89. K. S. Kumar, S. K. Singh, S. N. Pandeya, *Bolletino Chimico Farmaceutico* **140(4)** (2001), 238.

90. I. Küçükgüzel, S. G. Küçükgüzel, S. Rollas, M. Kiras, *Bioorg. Med. Chem. Let.,* **11** (2001), 1703.

91. T. K. Venkatachalam, E. A. Sudbeck, F. M. Uckun, *Tetrahedron letters,* **42** (2001), 6629.

92. G. Vasilev, I. Tafrdzhiiski, N. P. Masher, *Dokl. Bolg. Akad. Nauk.,* **27(8)** (1974), 1121.

93. J. T. Wang, Y. F. Yuan, Y. M. Xu, Y. W. Zang, R. J. Wang, H. G. Wang, R. J. Zang, *J. Organomet. Chem.* **481** (1994), 211.

94. Z. Huang, L. Wu, J. Xiao, Q. Huang, Y. Liu, L. Gu, Youji Huaxue, *J. Organomet. Chem.* **15** (1995), 221.

95. X. Shen, X. Shi, B. Kang, Y. Liu, Y. Tong, H. Jiang, K. Chen, *Polyhedron,* **17** (1998), 4049.

96. F. A. French, E. J. Blanz, J. R. D. Amaraj, D. A. French, *J. Med. Chem.*, **13** (1970), 1117.

97. B. B. Mohapatra, S. Guru, B. K. Mohapatra, *J. Inorg. Nucl. Chem.*, **39** (1977), 2291.

98. W. Antholine, F. Taketa, *J. Inorg. Biochem.* **16** (1982), 145.

99. D. H. Petering, *Metal ions in Biological systems,* **Vol. 11 Chap. 4, Edn.** H. Siegel, Marcel Dekker, New York, (1980).

100. J. D. Ranford, P. J. Sadler, D. A. Tocher, *J. Chem. Soc. Dalton Trans.* (1993), 3393.

101. Z. Korolkiewiecz, E. Hac, L. Gagalo, P. Gorezyca, A. Lodzinska, *Agents Actions,* **26** (1989), 355 and references cited therein.

102. L. Beyer, J. J. Criado, E. Garcia, F. Leβmann, M. Medarde, R. Richter, E. Rodriquez, *Tetrahedron,* **52** (1996), 6233.

103. J. E. Fergusson, *The Heavy elements,: Chemistry, environmental Impact and Health effects,* (1990), 381.

104. P. J. Saddler, *Chem. Br.* **18** (1982), 112.

105. R. Campo, J. J. Criado, E. Garcia, M. Hermosa, A. Jimenez-Sanchez, J. L. Manzano, E. Monte, E. Rodriquez-Fernandez, F. Sanz, *J. Inorg. Biochem* **89** (2002), 74.

106. S. Jurisson, D. Berning, W. Jia, D. Ma, *Chem. Rev.* **93** (1993), 1137.

107. K. Hashimoto, K. Yoshihara, *Topics in current chemistry; in Technetium and Rhenium* **Vol. 176** Springer-Verlag, Berlin, Germany (1996), 275.

108. S. Srivastava, in S. J. Mather (Ed) *Current Directions in Radiopharmaceutical Research and Developments,* Kluwer Academic, Netherlands, (1996), 63.

109. G. Bandoli, U. Mazzi, H. Spies, R. Munze, E. Ludwig, E. Ulhermann, *Inorg. Chim. Acta* **132** (1987), 177.

110. M. J. Abrams, A. Davison, R. Faggiani, A. G. Jones, C. J. L. Lock, *Inorg. Chem.* **23** (1984), 3284.

111. M. Hashimoto, H. Wada, T. Omori, K. Yoshihara, *J. Radioanal. Nucl. Chem. Lett.* **153** (1991), 283.

112. K. Hashimoto, H. Kudo, T. Omori, K. Yoshihara, *Radiochim. Acta* **63** (1993), 167.

113. T. Omori; *Topics in current chemistry: Technetium and Rhenium* **Vol. 176** Springer-Verlag, Berlin, Germany (1996), 267.

114. F. Touchard, F. Fache, M. Lemaire, *Tetrahedron: Asymmetry* **8** (1997), 3319.

115. D. Cauzzi, M. Lanfranchi, G. Maezolini, G. Predieri, A. Tiripicchio, M. Costa, R. Zanoni, *J. Organomet. Chem.* **488** (1995), 115.

116. D. Cauzzi, M. Costa, L. Gonsalvi, M. A. Pellinghelli, G. Predieri, A. Tiripicchio, R. Zanoni, *J. Organomet. Chem.* **541** (1997), 377.

117. J. M. J. Breuzard, M. L. Tommasino, F. Touchard, M. Lemaire, M. C. Bonnet, *J. Mol. Cat. A: Chemical* **156** (2000), 223.

118. Enraf-Nonius CAD-4/PC Software. Version 1.5c (1992) Enraf-Nonius, Delft, The Netherlands.

119. K. Harms, *XCAD4. Program for data reduction.* (1996) Philipps-Universität, Marburg, Germany.

120. A. C. T. North, D. C. Phillips, F.S. Mathews, *Acta Crystallogr., Sect.* **A42** (1968), 351.

121. P. T. Beurskens, G. Beurskens, W. P. Bosman, R. de Gelder, S. Garcia-Granda, R. O. Gould, R. Israel, and J. M. M. Smits, (1996). The DIRDIF96 Program System, *Technical Report of the Crystallography Laboratory,* University of Nijmegen, The Netherlands.

122. G. M. Sheldrick, (1997) SHELX-97. *Program for solution and Refinement of Crystal Structures.* Univ. of Göttingen, Germany (f) L. J. Farrugia, *ORTEP-3 for Windows. J. Appl. Cryst.* **30** (1997), 565.

123. E. B. Sandell, *Colorimetric Determination of Trace Elements,* Interscience (1959), pp 199.

124. J. Kavalek, P. Fiedler, Z. Papouskova, O. Exner; *Collect. Czech. Chem. Commun.* **47** (1982), 35.

125. F. H. Herbstein, G. M. Reisner, *Z. Krystallogr.* **169** (1984), 83.

126. C. C. Lin, J. D. Swalen, *Rev. Mod. Phys.* **31** (1959), 841.

127. H. S. Gutowsky, C. H. Holm, *J. Chem. Phys.* **25** (1956), 1228.

128. R. C. Neuman Jr., L. B. Young, *ibid.*, **69** (1965), 2570.

129. R. C. Neuman Jr., D. N. Roark, V. Jonas V., *J. Amer. Chem. Soc.* **89** (1967), 3412.

130. A. Lowenstein, A. Melera, P. Rigny, W. Walter, *J. Phys. Chem.* **68** (1964), 1597.

131. F. H. Allen, O. Kennard, D. G. Watson, L. Brammer, A. G. Orpen, R. Taylor, *International Tables of Crystallography* Vol. C (1991), edited by Wilson A. J. C., pp. 685-706, Dordrecht, Kluwer publishers.

132. F. D. Rochon, R. Melanson, P. C. Kong, *Acta Cryst.* **C46** (1990), 571.

133. M. J. Moloto, M. A. Malik, M. Motevalli, P. O'Brien, G. A. Kolawole, *Polyhedron,* **22** (2003), 595.

134. F. H. Allen, O. Kennard, D. G. Watson, L. Brammer, A. G. Orpen, R. Taylor, *International Tables of Crystallography* Vol. C (1992), edited by Wilson A. J. C., pp. 685-706, Dordrecht, Kluwer publishers.

135. M. Okuya, S Kaneko, *Solid State Ionics* **141-142** (2001), 439.

136. A. J. Hoffman, H. Yee, G. Mills, M. R. Hoffman M. R., *J. Phys. Chem.* **96**, (1992), 5540.

137. V. L. Colvin, M. C. Schlamp, A. P. Alivisatos, *Nature* **370** (1994), 354.

138. F. Hakimi, M. G. Bawendi, R. Tumminelli, J. R. Haavisto, *US Patent* **5, 260** (1993), 957.

139. D. Duonghong, J. Ramsden, M. Gratzell, *J. Am. Chem. Soc.* **104** (1982), 2977.

140. H. Weller, *Adv. Mater.* **5**(1993), 88.

141. A. Hagfeldt, M. Gratzell, *Chem. Rev.* **95** (1995), 49.

142. R. Rosetti, J. L. Ellison, J. M. Gibson, L. E. Brus, *J. Chem. Phys.* **80** (1984), 4464.

143. A. Henglein, *Chem. Rev.* **89** (1989), 1861.

144. M. L. Steigerwald, L. E. Brus, *Acc. Chem. Res.* **23** (1990), 183.

145. Y. Wang, N. Herron, *J. Phys. Chem.* **95** (1991), 525.

146. T. Trindade, P. O'Brien, *Adv. Mater.* **8** (1996), 161.

147. T. Trindade, P. O'Brien, X. Zhang, *Chem. Mater.* **9** (1997), 523.

148. N. Revaprasadu, M. A. Malik, P. O'Brien, G. J. Wakefield, *J. Mater. Res.* **40(8)** (1999), 3237.

149. N. Revaprasadu, M. A. Malik, P. O'Brien, M. M. Zulu, G. J. Wakefield, *J. Mater. Chem.* **8(8)** (1998), 1885.

150. B. Ludolph, M. A. Malik, N. Revaprasadu, P. O'Brien, *J. Chem. Soc. Chem Commun.* (1998), 1849.

151. P. O'Brien, D. Otway, D. R. Walsh, *Adv. Mater. CVD* **3** (1997), 227.

152. M. A. Malik, N. Revaprasadu, P. O'Brien, *Chem. Mater.* **13** (2001), 913.

153. M. Chunggaze, J. McAleese, P. O'Brien, D. Otway, *J. Chem. Commun.* (1998), 833.

154. H. Weller, *Angew. Chem. Int. Ed. Eng.* **32** (1993), 41.

155. S. Schimtt-Rink, D. A. B. Miller, D. S. Chemla, *Phys. Rev.* **B 35** (1987), 8113.

156. L. Banyai, Y. Z. Hu, M. Lindberg, S. W. Koch, *Phys. Rev.* **B 38** (1988), 8142.

157. L. E. Brus, *Appl. Phys.* **A53** (1991), 465.

158. A. Henglein, *Top. Curr. Chem.*, **143** (1988), 113.

159. M. G. Bawendi, M. L. Steigerwald, L. E. Brus, *Annu. Rev. Phys. Chem.* **41** (1990), 477.

160. P. Roussignol, D. Ricard, C. Flytzanis, N. Neuroth, *Phys. Rev. Lett.* **62** (1989), 312.

161. A. P. Alivisatos, A. Harris, N. Levinos, M. L. Steigerwald, L. E. Brus, *J. Chem. Phys.* **89** (1989), 4001.

162. M. G. Bawendi, W. L. Wilson, L. Rothberg, P. J. Carroll, T. M. Jedju, M. L. Steigerwald, L. E. Brus, *Phys. Rev. Lett.* **65** (1990), 1623.

163. M. G. Bawendi, P. J. Carroll, W. L. Wilson, L. E. Brus, *J. Chem. Phys.* **96** (1992), 946.

164. A. P. Alivisatos, T. D. Harris, P. J. Carroll, M. L. Steigerwald, L. E. Brus, *J. Chem. Phys.* **90** (1989), 3463.

165. H. Haug, S. W. Koch, *Quantum theory of the optical and electronic properties of semiconductors;* World Scientific Publishing Co. Pty. Ltd.: (1990), 333.

166. L. E. Brus, *J. Chem. Phys.*, **79** (1983), 5566.

167. L. E. Brus, *J. Chem. Phys.* **80** (1984), 4403.

168. L. E. Brus, *J. Phys. Chem.* **90** (1986), 2555.

169. J. H. Fendler, F. C. Meldrum, *Adv. Mater.* **7** (1995), 607.

170. A. P. Alivisatos, *J. Phys. Chem.*, **100** (1996), 13226.

171. H. Weller, H. M. Schmidt, U. Koch, A. Fojtik, S. Baral, A. Henglein, W. Kunath, K. Weiss, E. Deiman, *Chem. Phys. Lett.* **124** (1986), 557.

172. H. M. Schmidt, H. Weller, *Chem. Phys. Lett.* **129** (1986), 615.

173. Y. Nosaka, *J. Phys. Chem.* **95** (1991), 5054.

174. P. E. Lippens, M. Lannoo, *Phys. Rev.* **B 39** (1989), 10935.

175. M. V. R. Krishna, R. A. Friesner, *J. Chem. Phys.* **95** (1991), 8309.

176. A. P. Alivisatos, *Science*, **271** (1996), 933.

177. M. C. Schlamp, X. G. Peng, A. P. Alivisatos, *J. Appl. Phys.* **82** (1997), 5837.

178. H. Mattoussi, L. H. Radzilowski, B. O. Dabbousi, E. L. Thomas, M. G. Bawendi, M. F. Rubner, *J. Appl. Phys.*, **83** (1998), 7965.

179. S. Coe, W. K. Woo, M. Bawendi, V. Bulovic, *Nature*, **420** (2002), 800.

180. W. Huynh, X. G. Peng, A. P. Alivisatos, *Adv. Mater.*, **11** (1999), 923.

181. W. Huynh, J. J. Dittmer, A. P. Alivisatos, *Science*, **295** (2002), 225.

182. M. Bruchez, M. Moronne, P. Gin, S. Weiss, A. P. Alivisatos, *Science*, **281** (1998), 2013.

183. W. C. Chan, S. M. Nie, *Science* **281** (1998), 2016.

184. T. S. Ahmadi, Z. L. Wang, T. C. Green, A. Henglein, M. A. Elsayed, *Science* **272** (1996), 1924.

185. P. V. Kamat, D. Meisel, *Eds. Semiconductor Nanoclusters, Studies in Surface Science and Catalysis*, Elsevier: Amsterdam, (1996), p103.

186. D. R. Lide, *CRC Handbook of Chemistry and Physics*, CRC Press, **73rd** student edn. Boca Raton, FL, (1993).

187. N. Chestnoy, T. D. Harris, R. Hull, L. E. Brus, *J. Phys. Chem.* **90** (1986), 3393.

188. T. Vossmeyer, L. Katiskas, M. Giersig, I. G. Popovic, K. Driesner, A. Chemseddne, A. Eychmuller, H. Weller, *J. Phys. Chem.* **98** (1994), 7665.

189. C. B. Murray, D. J. Norris, M. G. Bawendi, *J. Am. Chem. Soc.* **115** (1993), 8706.

190. A. L. Efros, M. Rosen, M. Kuno, M. Nirmal, D. J. Norris, M. G. Bawendi, *Phys. Rev.* **B54** (1996), 4843.

191. M. Nirmal, D. Norris, M. Kuno, M. G. Bawendi, A. L. Efros, M. Rosen, *Phys. Rev. Lett.* **75** (1995), 3728.

192. M. Nirmal, B. O. M. Daboussi, M. G. Bawendi, J. J. Macklin, J. K. Trautman, T. D. Harris, L. E. Brus, *Nature*, **383** (1996), 802.

193. U. Banin, M. Bruchez, A. P. Alivisatos, T. Ha, S. Weiss, D. S. Chemia, *J. Chem. Phys.* **110(2)**, (1999), 1195.

194. M. Brust, J. Fink, D. Bethel, D. J. Schriffren, M. Kiely, *J. Chem. Soc. Chem. Commun.* (1995), 1655.

195. J. Tanori, M. P. Pileni, *Adv. Mater.* **7** (1995), 862.

196. R. A. Andrievskii, *Russ. Chem. Rev.*, **63** (1994), 411.

197. A. Kornowski, M. Giersig, M. Vogel, A. Chemseddine, H. Weller, *Adv. Mater.* **5** (1993), 634.

198. A. Fojtik, A. Henglein, *Chem. Phys. Lett.* **221** (1994), 363.

199. A. Henglein, *Pure Appl. Phys.* **56** (1984), 1215.

200. R. Rossetti, R. Hull, J. M. Gibson, *J. Chem. Phys.* **82** (1985), 552.

201. J. H. Fendler, *Ed. Nanoparticles and Nanostructured Particles Preparation, Characterization and Applications,* Wiley Interscience, New York, (1998).

202. M. Green, P. O'Brien, *J. Chem. Soc. Chem. Commun.* (1998), 2459.

203. V. K. La Mer, R. H. Dinegar, *J. Am. Chem. Soc.* **69** (1950), 4847.

204. T. Johnson, V. K. La Mer, *J. Am. Chem. Soc.* **69** (1947), 1184.

205. R. J. Hunter, *Foundations of Colloid Science,* Oxford University Press, **6th ed.**, Oxford, (1993) **vol. 1**, pp. 13.

206. H. Weller, A. Fojtik, A. Hemglein, *Chem. Phys. Lett.* **117** (1985), 485.

207. M. Haase, H. Weller, A. Henglein, *Ber. Bunsen-Ges. Phys. Chem.* **92** (1988), 1103.

208. L. Spanhel, A. Henglein, H. Weller, *Ber. Bunsen-Ges. Phys. Chem.* **91** (1987), 1359.

209. A. Hasselbarth, A. Eychmuller, R. Eichberger, M. Giersi, A. Mews, H. Weller, *J. Phys. Chem.* **97** (1993), 5333.

210. H. S. Zhou, I. Honma, H. Komiyama, J. W. Haus, *J. Phys. Chem.* **97** (1993), 895.

211. H. S. Zhou, H. Sasahara, I. Honma, H. Komiyama, J. W. Haus, *Chem. Mater.* **6** (1994), 1534.

212. A. Eychmuller, A. Hasselbarth, H. Weller, *J. Lumin.* **53** (1992), 113.

213. A. R. Kortan, R. Hull, R. L. Opila, M. G. Bawendi, M. L. Steigerwald, P. J. Carrol, L. E. Brus, *J. Am. Chem. Soc.* **112** (1990), 1327.

214. C. F. Hoener, K. A. Allan, A. J. Bard, A. Champion, M. A. Fox, T. E. Mallouk, S. E. Webber, J. M. White, , *J. Phys. Chem,* **96** (1992), 3812.

215. D. V. Talapin, A. L. Rogach, A. Kornowski, M. Haase, H. Weller, *Nano. Lett.* **1** (2001), 207.

216. Y. Wang, N. Herron, *J. Phys. Chem.* **91** (1987), 257.

217. T. Cassagneau, G. B. Hix, D. J. Jones, P. Maireles-Torres, M. Rhomari, J. Roziere, *J. Mater. Chem.* **4** (1994), 189.

218. T. Abe, Y. Tichibana, T. Uematsu, M. Iwamoto, *J. Chem. Soc. Chem. Commun.* (1995), 1617.

219. M. E. Brenchley, M. T. Weller, *Angew. Chem. Int. Ed. Engl.***32** (1993), 1663.

220. G. Blasse, C. J. Dirksen, M. E. Brenchley, M. T. Weller, *Chem. Phys. Lett.* **234** (1995), 177.

221. H. J. Watzke, J. H. Fendler, *J. Phys. Chem* **91** (1997), 854.

222. C. Petit, T. K. Jain, F. Billoudet, M. P. Pileni, *Langmuir*, **10** (1994), 4446.

223. A. Khan-Lodhi, B. H. Robinson, T. Towey, C. Herrmann, W. Knoche, U. Thesing, *In The Structure, dynamics and equilibrium properties of colloidal systems;* D. M. Bloor, E. Wyn-Jones, Eds., London, (1990), 373.

224. T. F. Towey, A. Khan-Lodhi, B. H. Robinson, *J. Chem. Soc. Faraday Trans.* **86** (1990), 3757.

225. B. A. Korgel, G. Monbouquette, *J. Phys. Chem.* **100** (1996), 346.

226. K. M. Choi, K. J. Shea, *J. Phys. Chem.* **98** (1994), 3207.

227. K. M. Choi, K. J. Shea, *J. Am. Chem. Soc.* **116** (1994), 9052.

228. J. P. Carpenter, C. Lukehart, S. R. Stock, J. E. Wittig, *Chem. Mater.* **7** (1995), 201.

229. Y. Wang, A. Suna, W. Mahler, R. Kasowski, *J. Chem. Phys.* **87** (1987), 7315.

230. M. Gao, Y. Yang, B. Yang, F. Bian, J. Shen, *J. Chem. Soc. Chem. Commun.* (1994), 2779.

231. M. Nirmal, C. B. Murray, M. G. Bawendi, *Phys. Rev.* **B50** (1994), 2293.

232. R. Tassoni, R. R. Schrock, *Chem. Mater.* **6** (1994), 744.

233. M. Moffitt, A. Eisenberg, *Chem. Mater.* **7** (1995), 1178.

234. H. Shinojima, J. Yumoto, N. Uesugi, S. Omi, Y. Asahara, *Appl. Phys. Lett.* **55** (1989), 1519.

235. E. S. Brigham, C. S. Weisbecker, W. E. Rudzinski, T. E. Mallouk, *Chem. Mater.* **8** (1996), 2121.

236. G. Cao, L. K. Rabenberg, C. M. Nunn, T. E. Mallouk, *Chem. Mater.* **3** (1991), 149.

237. S. W Hagatta, X. Li, D. J. Cole-Hamilton, J. R. Fryer, *J. Mater. Chem.* **6** (1996), 1771.

238. S. W Hagatta, D. J. Cole-Hamilton, J. R. Fryer, *J. Mater. Chem.* **7** (1997), 1969

239. X. Li, J. R. Fryer, D. J. Cole-Hamilton, *J. Chem. Soc. Chem. Commun.* (1994), 1715.

240. J. E. McDougall, H. Eckert, G. D. Stucky, N. Herron, Y. Wang, K. Moeller, T. Bein, D. Cox, *J. Am. Chem. Soc.* **111** (1989), 8006.

241. M. L. Steigerwald, A. P. Alivisatos, J. M. Gibson, T. D. Harris, A. R. Kortan, A. J. Muller, A. M. Thayer, T. M. Duncan, D. C. Douglass, L. E. Brus, *J. Am. Chem. Soc.* **110** (1988), 3046.

242. T. Trindade, P. O'Brien, X. Zhang, M. Motevalli, *J. Mater. Chem.* **7** (1997), 1011.

243. T. Trindade, O. C. Monteiro, P. O'Brien, M. Motevalli, *Polyhedron* **18** (1999), 1171.

244. J. G. Brennin, T. Siegrist, P. J. Carrol, S. M. Stuczynski, L. E. Brus, M. Steigerwald, *J. Am. Chem. Soc.* **111** (1989), 4141.

245. T. Trindade, P. O'Brien, *J. Mater. Chem.* **6** (1996), 343.

246. A. A. Guzelian, J. E. B. Katari, A. V. Kadavanich, U. Banin, K. Hamad, E. Juban, A. P. Alivisatos, R. H. Wolters, C. C. Arnold, J. R. Heath, *J. Phys. Chem.* **100** (1996), 7212.

247. A. A. Guzelian, U. Banin, A. V. Kadavanich, X. Peng, A. P. Alivisatos, *Appl. Phys. Lett.* **69** (1996), 1432.

248. M. A. Olshavski, A. N. Goldstein, A. P. Alivisatos, *J. Am. Chem. Soc.* **112** (1990), 9438.

249. H. Uchida, C. J. Curtis, A. J. Nozik, *J. Phys. Chem.* **95** (1991), 5382.

250. E. K. Byrne, L. K. Parkanyi, H. Theopold, *Science* **241** (1988), 332.

251. T. Douglas, K. H. Teopold, *Inorg. Chem.* **30** (1991), 594.

252. S. C. Goel, M. Y. Chiang, W. E. Buhro, *J. Am. Chem. Soc.* **112** (1990), 5636

253. W. E. Buhro, *Polyhedron* **13** (1994), 1131.

254. M. A. Matchett, A. M. Viano, N. L. Adolphi, R. D. Stoddard, W. E. Buhro, M. S. Conradi, P. C. Gibbons, *Chem. Mater.* **4** (1992), 508.

255. P. O'Brien, J. R. Walsh, I. M. Watson, M. Motevalli, J. L. Henriken, *J. Chem. Soc. Dalton Trans.* (1996), 249.

256. M. B. Hursthouse, M. A. Malik, M. Motevalli, P. O'Brien, *Polyhedron* **11** (1992), 45.

257. M. Lazell, P. O'Brien, *Chem. Commun.* (1999), 2041.

258. N. Revaprasadu, M. A. Malik, P. O'Brien, G. Wakefield, *Chem. Commun.* (1999), 1573.

259. L. Spanhel, M. Haase, H. Weller, A. Henglein, *J. Am. Chem. Soc.* **109** (1987), 5649.

260. J. E. Katari, V. L. Colvin, A. P. Alivisatos,*J. Chem. Phys.* **98** (1994), 4109.

261. H. Noglik, W. J. Pietro, *Chem. Mater.* **6** (1994), 1593.

262. W. L. Wilson, P. F. Szajowsk, L. E. Brus, *Science* **262** (1993), 1242.

263. M. Danek, K. F. Jensen, C. B. Murray, M. G. Bawendi, *Chem. Mater.* **8** (1996), 173.

264. M. A. Hines, P. Guyot-Sionnest, *J. Phys. Chem.* **100** (1996), 468.

265. X. Peng, M. C. Schlamp, A. V. Kadavanich, A. P. Alivisatos, *J. Am. Chem. Soc.* **119** (1997), 7019.

266. Y. Tian, T. Newton, N. A. Kotov, D. M. Guldi, J. H. Fendler, *J. Phys. Chem.* **100** (1996), 8927.

267. P. S. Nair, T. Radhakrishnan, N. Revaprasadu, G. A. Kolawole, P. O'Brien, *Polyhedron*, **22** (2003), 3129.

268. P. S. Nair, T. Radhakrishnan, N. Revaprasadu, G. A. Kolawole, P. O'Brien, *J. Mater. Chem.*, **12** (2002), 1.

269. P. S. Nair, N. Revaprasadu, T. Radhakrishnan, G. A. Kolawole, *J. Mater. Chem.*, **11** (2001), 1555.

270. P. Sawant, E. Kovalev, J. T. Klug, S. Efrima, *Langmuir*, **18** (2001), 2913.

271. O. Tzhayik, P. Sawant, S. Efrima, E. Kovalev, J. T. Klug, *Langmuir*, **18** (2002), 3364.

272. P. S. Nair, PhD Dissertation, University of Zululand, Dept. of Chemistry, 2002.

273. X. Peng, L. Manna, W. Yang, J. Wickham, E. C. Scher, A. Kadavanich, A. P. Alivisatos, *Nature*, **404** (2000), 59.

274. L. Manna, E. C. Scher, A. P. Alivisatos, *J. Am. Chem. Soc.*, **122** (2000), 1270.

275. J. Yang, J. H. Zeng, S. H. Yu, L. Yang, G. Zhou, Y. Qian, *Chem. Mater.* **12** (2000), 3259.

276. Y. Li, X. Li, C. Yang, Y. Li, *J. Mater. Chem.*, **13** (2003), 2641.

277. J. I. Pankove, *Optical processes in semiconductors*, (Dover publications, New York), 1970.

278. M. G. Bawendi, A. R. Kortan, M. L. Steigerwald, L. E. Brus, *J. Chem. Phys.*, **91** (1989), 7282.

279. H. K. Schmid, *J. Am. Ceram. Soc.*, **70** (1987), 367.

280. H. P. Klug, L. E. Alexander, *X-Ray Diffraction Procedures*, (Wiley, New York) 1974.

281. J. Joo, T. Yu, J. H. M. Park, Y. W. Kim, F. Wu, J. Z. Zhang, T. Hyeon, *J. Am. Chem. Soc.*, **125** (2003), 6553.

282. X. Changqi, Z. Zhicheng, W. Hailong, Y. Qiang, *Mater. Sci. and Eng.*, **B104** (2003), 5.

283. W. W. Frank, *Acc. Chem. Res.*, **33** (2000), 773.

284. Y. Zhou, H. Itoh, T. Uemura, K. Naka, Y. Chujo, *Langmuir*, **18** (2002), 5287.

285. S. Wang, S. Yang, *Langmuir*, **16** (2000), 389.

286. S. Chen, L. A Traux, J. M. Sommers, *Chem. Mater.*, **12** (2000), 3864.

287. X. Ali, L. Guo, Y. Zhou, Q. Li, H. Zhu, *Mater. Lett.*, **38** (1999), 131.

288. N. Revaprasadu, M. A. Malik, P. O'Brien, *South African Journal of Science*, **57** (2004), 40.

289. X. H. Liao, N. Y. Chen, S. Xu, S. B. Yang, J. J. Zhu, *Journal of Crystal Growth*, **252** (2003), 593.

290. P. Zhang, L. Gao, *J. Mater. Chem.*, **13(8)** (2003), 2007.

291. G. F. J. Garlick, A. F. Gibson, *J. Opt. Soc. Am.* **39** (1949), 935.

292. M. Ohring, *The Materials Science of Thin Films,* Academic, San Diego, 1992.

293. I. P. MaClean, C. B. Thomas, *Semicond. Sci. Technol.* **7** (1992), 1394.

294. S. Yanagida, Y. Masahisa, T. Shiragami, C. Pac, *J. Phys. Chem.* **94** (1990), 3104.

295. D. E. Dunsyan, A. Hagfeldt, M. Almegren, H. O. G. Siegbahn, E. Mukhtar, *J. Phys. Chem.* **94** (1990), 6797.

296. A. Henglein, M. Gutierrez, *Ber. Bunsen-Ges Phys. Chem.*, **87** (1983), 852.

297. C. B. Murray, C. R. Kagan, M. G. Bawendi, *Science*, **70** (1995), 1335.

298. A. Y. Nakaoka, Y. Nosaka, *Lagmuir*, **13** (1997), 708.

299. Y. Li, Y. Ding, Y. Qian, Y Zhang, L. Yang, *Inorg. Chem.*, **37** (1998), 2844.

300. B. Cockayne, P. J. Wright, *J. Crystal Growth* **68** (1984), 223.

301. P. O'Brien, R. Nomura, *J. Mater. Chem.* **5** (1995), 1761.

302. P. O'Brien, J. R. Walsh, I. M. Watson, L. Hart, S. R. P. Silva, *J. Crystal Growth* **167** (1996), 133.

303. A. Saunders, A. Vecht, G. Tyrell, *Proc. 7th Int. Conf. on Ternary and Multinary compounds,* (Materials Research Society Pittsburg, (1987), pp. 213-218.

304. D. M. Frigo, O. F. Z. Khan, P. O'Brien, *J. Crystal Growth*, **96** (1989), 989.

305. R. D. Pike, H. Cui, R. Kershaw, K. Dwight, A. Wold, T. N. Blanton, A. A. Wernberg, H. J. Gysling, *Thin Solids Films* **224** (1993), 221.

306. P. O'Brien, S. Haggata, Adv. Mater. Opt. Electron. **5** (1994), 117.

307. M. A. Malik, P. O'Brien, *Adv. Mater. Opt. Electron.* **3** (1994), 171.